UNIVERSITÀ DEGLI STUDI DI TRIESTE

XVII CICLO DEL DOTTORATO DI RICERCA IN SCIENZE
DELL'INGEGNERIA - INDIRIZZO INGEGNERIA MECCANICA, NAVALE,
DELL'ENERGIA E DELLA PRODUZIONE

Electrocatalyst degradation in high temperature PEM fuel cells

Settore scientifico-disciplinare: ING-IND/09

Ph.D. Candidate
FRANCESCO VALLE

Ph.D. School Director
Prof DIEGO MICHELI

Thesis Supervisor
Prof RODOLFO TACCANI

Co-Supervisors
Prof HEINZ AMENITSCH
Dr BENEDETTA MARMIROLI

ANNO ACCADEMICO 2013 / 2014

A dissertation presented to the faculty of Università degli Studi di Trieste in candidacy for the degree of Doctor of Philosophy.

Recommended for acceptance by the Department of Engineering and Architecture.

Abstract

Durability and cost are the major limiting factors in current PEM fuel cells development and commercialization. Electrocatalyst materials are the main responsible of both cost of the entire fuel cell stack and its degradation during operation [1,2].

In this research durability and degradation have been investigated in high temperature PEM fuel cells (HT-PEMFCs). Specific diagnostic techniques have been studied and tested for the investigation of electrocatalyst structural properties. An experimental sensibility analysis has been carried out with the purpose to assess advantages and limitations of the use of cyclic voltammetry to determine the electrocatalyst ECSA in H_3PO_4/PBI high temperature PEM fuel cells. Small angle x-ray scattering (SAXS) has been used to obtain structural information of the electrocatalyst nanoparticles, such as size and distribution. A procedure to characterize HT-PEMFCs MEAs by means of SAXS has been developed and tested. Transmission electron microscopy (TEM) is a complementary technique to SAXS: it has been used to validate the diagnostic method and to compare the results. Electrocatalyst evolution during long-term operation has been studied and related with performance loss. Specific stress test protocols have been developed to accelerate electrocatalyst degradation in commercial HT-PEMFC MEAs operated in single cell configuration. Two MEAs have been subjected to load cycling and one to start/stop cycling. One of the two testing protocols based on load cycling included open circuit (OC) condition in each cycle with the purpose to study the effects of frequent and short OCs during

operation on MEA durability and electrocatalyst evolution. Specific start-up and shutdown procedures have been used in the start/stop test in order to limit other degradation mechanisms. Cell voltage and polarization curves have been recorded to monitor cell performance during the durability tests. The electrocatalyst structural evolution induced by load cycling has been characterized with SAXS and TEM.

The stress test protocols have been effective to accelerate performance and electrocatalyst degradation of the MEA. The voltage decay rate at 200 $mAcm^{-2}$ was higher than 25 μVh^{-1} in the samples subjected to load cycles. The start/stop cycling caused a performance degradation of 18 μV/cycle at 222 $mAcm^{-2}$ during the first 450 cycles of the test. Regarding the diagnostic techniques used to characterize the electrocatalyst, cyclic voltammetry (CV) seems not to be particularly reliable when performed at high temperatures (>100°C) due to the high dependence of the voltammogram shape to humidity conditions. SAXS, on the other hand, seems to be an effective tool to investigate structural properties of PEMFC electrocatalysts. SAXS analysis showed that after 100,000 load cycles the mean size of the platinum nanoparticles more than doubled. TEM results varied about 30% from the SAXS results: this divergence could be due to a very different population size of the nanoparticles that have been analysed in the two methods. Moreover, the preparation of the sample used in TEM may have strongly influenced the electrocatalyst structure. Finally, a visualization of the electrocatalyst structural evolution on large areas of the MEAs subjected to load cycling showed preferential directions of the particles growth that could be due to the position of the channels on the flow-field plates of the fuel cell.

Acknowledgments

This research has been supported by the Italian Ministry of Education, Universities and Research (MIUR).

I wish to thank my adviser Prof Rodolfo Taccani, Dr Benedetta Marmiroli and Prof Heinz Amenitsch from the Austro SAXS beamline at Elettra for the collaboration during the experimental activity and data elaboration, Dr Emanuela Negro from TU Delft for the TEM measurements, Prof Joachim Scholta and Dr Roswitha Zeis from the Zentrum für Sonnenenergie- und Wasserstoff-Forschung (ZSW) Baden-Württemberg for the valuable discussions on cyclic voltammetry measurements on HT-PEMFCs.

List of Tables

Appendix

List of Figures

Appendix

Contents

List of Abbreviations

ABPBI	Acid-Based Polybenzimidazole
CL	Catalyst Layer
CSD	Crystallite Size Distribution
CV	Cyclic Voltammetry
DHE	Dynamic Hydrogen Electrode
DMFC	Direct Methanol Fuel Cell
ECSA	Electro-Chemical Surface Area
ED	Electron Diffraction
EDX / EDS	Energy Dispersive X-Ray Spectroscopy
EIS	Electrochemical Impedance Spectroscopy
FCTESTNET	Fuel Cell Testing and Standardization Network
GDL	Gas Diffusion Layer
GUI	Graphical User Interface
GISAXS	Grazing-Incidence Small-Angle X-ray Scattering
HFR	High-Frequency Resistance
HOR	Hydrogen Oxidation Reaction
HRTEM	High-Resolution Transmission Electron Microscopy
HT-PEMFC	High Temperature PEM Fuel Cell
JRC	Joint Research Centre
LSV	Linear Sweep Voltammetry
LT-PEMFC	Low Temperature PEM Fuel Cell

MEA	Membrane Electrode Assembly
MPL	Micro Porous Layer
OC	Open Circuit
OCV	Open Circuit Voltage
ORR	Oxygen Reduction Reaction
PAFC	Phosphoric Acid Fuel Cell
PBI	Polybenzimidazole
PDDF	Pair Distance Distribution Function
PEM	Polymeric Electrolyte Membrane
PEMFC	Polymeric Electrolyte Membrane Fuel Cells
PFSA	Perfluorinated Sulfonic Acid
PIXE	Proton-Induced X-ray Emission
RH	Relative Humidity
RHE	Reversible Hydrogen Electrode
SAXS	Small-Angle X-ray Scattering
SEM	Scanning Electron Microscopy
SHE	Standard Hydrogen Potential
TEM	Transmission Electron Microscopy
TPB	Triple-Phase Boundary
U. S. DOE	United States Department Of Energy
UVPS	UV-induced Photoelectron Spectroscopy
WAXS	Wide-Angle X-ray Scattering
XPS	X-ray Photoelectron Spectroscopy
XRD	X-Ray Diffraction
XRE	X-Ray Emission
XRF	X-Ray Fluorescence
ZSW	Zentrum für Sonnenenergie- und Wasserstoff-Forschung Baden-Württemberg

List of Symbols

A	scattering amplitude of a sphere of radius r
α	parameter defining the range of the inter-particle potential
c	constant of the diffuse scattering
c_p	Porod constant
d	lattice spacing
E^0	standard electrode potential of the reaction
f_R	distribution function of the particles size
I	scattering intensity
I_0	fitting constant for the scattering intensity of the particles
I_{air}	scattering intensity of air (setup without the sample)
I_s	normalized and corrected scattering intensity
$\bar{I}_{s+air}$	scattering intensity normalized with respect to air
I_{s+air}	scattering intensity of the sample in air environment
J_{air}	transmission signal of air (setup without the sample)
J_{s+air}	transmission signal of the sample in air environment
k_1	vector of the incoming wave
k_2	vector of the diffracted wave
k_3	vector of the transmitted wave
l_c	correlation length
n	integer number
p	Porod exponent

P	form factor
$\tilde{P}$	form factor averaged on all the particles
p	pair distance distribution function (PDDF)
q	small-angle scattering vector
Q	integral scattering or invariant
r	radial coordinate
R	mean radius of the particles
R_g	radius of gyration
R_{hs}	hard sphere radius
S	structure factor
T_{s+air}	transmission factor of the sample in air environment
U	inter-particle potential
V_f	volume fraction of the particles surrounding every single particle
V_{max}	maximum value of the voltage sweep in a cyclic voltammogram
V_{min}	minimum value of the voltage sweep in a cyclic voltammogram
V_P	volume of the single particle
Z	width parameter of the size distribution
Γ	gamma function
$\Delta\rho$	electron density contrast
ε	depth of the attractive inter-particle potential
θ	half-value of the diffraction angle
λ	air-to-fuel ratio
λ_x	radiation wavelength
ρ	electron density
ρ_1	solvent electron density
ρ_2	solute electron density
σ_R	root mean square deviation of the particle radius

1

Introduction

1.1 Context

Polymer electrolyte membrane (PEM) fuel cells are a class of energy-converting systems characterized by high efficiency, high energy density and low or zero pollutant emissions. They have, indeed, the potential to contribute to a clean energy supply, as an alternative power system to combustion engines. Fuel cells are electrochemical devices able to convert the chemical energy present in a fuel directly to electricity, without the need of intermediate energy conversion steps. This feature makes fuel cells more efficient in the conversion of chemical energy to electrical energy than any other present technology [2]. When fuel cells are supplied with hydrogen derived from renewable energy sources, they can be a clean and reliable power source. Moreover, the employment of hydrogen from renewable sources can avoid the economic dependence on fossil fuels and increase energy security. PEM fuel cells are considered an effective electrical power source for stationary, transport and portable applications [3]. At present, however, the widespread use of this technology is strongly limited by cost and durability.

The causes of the gradual decline in fuel cell performance are still not completely understood, but it is supposed that different degradation mechanisms affecting the different components contribute together. During operation, the components of a PEM fuel cell are subjected to an aggressive environment due to the combination of strong oxidizing conditions, liquid water, strongly acidic conditions, high temperature, high electrochemical potentials and gradients, high electric currents, reactive intermediate reaction products and a chemically reducing atmosphere at the anode [2]. Fuel cell operative conditions can also affect its performance and durability. Dynamic operations such as start/stop and load cycling induce transient operative conditions that can strongly reduce fuel cell lifetime [2,4]. In order to design more durable fuel cells it is important to understand the various mechanisms of degradation of each single component. The degradation of the electrocatalyst and its support is one of the main factors that limit fuel cell durability. The involved degrading mechanisms are surface area and activity loss due to catalyst dissolution, catalyst particle growth and agglomeration, activity loss due to catalyst support corrosion, and catalyst performance loss due to contamination [2,5,6]. The cost of fuel cell systems is another limiting factor in their commercialization and the electrocatalyst plays a central role in this issue as well. It has been estimated that, for high volume productions, nearly half of the cost of a fuel cell stack is due to catalyst and catalyst ink application, while approximately a quarter of the cost is due to bipolar plates and approximately a tenth to the electrolytic membrane [7].

Durability and cost are thus the main current issues in the development of fuel cell systems. Moreover, they are strongly interrelated on each other and with cell performance, even if the latter almost reached the targets (see *Appendix A1*). Indeed, the optimization of one of those parameters often leads to negatively influence the others. The real challenge is thus to meet simultaneously the targets for durability and cost, without lowering

current fuel cell performance. A possible solution to this problem could lie in the employment of innovative materials and in the development of specific operative procedures to mitigate degradation. The first step in this direction, however, is the identification of the factors that determine PEMFCs lifetime and to study the degradation mechanisms.

1.2 Aim and approach of the research

The purpose of the present research is to study and develop methodologies for the analysis of the performance degradation of the MEA in high temperature PEM fuel cells. In particular, techniques for the nano-morphological characterization of the electrocatalyst have been considered. The research question of this thesis is: what are the effects of operative conditions on HT-PEMFC performance and electrocatalyst nanostructure? Performance and evolution of the electrocatalyst structure have been observed during specific ageing tests designed to accelerate electrocatalyst degradation. Electrocatalyst degradation is intended as the modification of the initial catalytic properties owned by the electrocatalyst. Fuel cell performance has been evaluated through polarization curves that have been periodically recorded during the tests. Electrocatalyst structural evolution has been investigated measuring the mean nanoparticle size and distribution. Different diagnostic techniques for the electrocatalyst characterization have been tested and compared. Cyclic voltammetry (CV), small angle x-ray scattering (SAXS) and transmission electron microscopy (TEM) have been used to characterize the structural properties of the electrocatalyst. A sensibility analysis on CV measurements in high temperature PEMFCs has been carried out in order to show its experimental limitations to characterize the electrocatalyst degradation at high temperature. A method to characterize HT-

PEMFCs electrocatalysts with SAXS has been developed and tested with the purpose to determine its effectiveness and compare this diagnostic technique with common alternatives. The effect of cyclic open circuit (OC) condition during long-term fuel cell operation has been investigated in order to understand if even very short times in OCV are significant in terms of performance loss and catalyst degradation. Moreover, electrocatalyst structural changes due to operation have been studied on a large area of the MEA by means of a specifically developed mapping method.

A better knowledge of the relation between electrocatalyst properties, fuel cell performance and operative conditions could be very helpful to solve some of the current problems related to PEM fuel cells durability.

1.3 Plan of the thesis

The present thesis is organized in two main sections: scientific background and experimental.

The scientific background (*Chapter 2*) includes a brief description on PEMFC membrane electrode assemblies (*Paragraph 2.1*), the fundamentals of catalyst layer degradation (*Paragraph 2.2*), a discussion on the influence of operative conditions on catalyst layer degradation (*Paragraph 2.3*), a review of the state of the art in electrode materials (*Paragraph 2.4*), and an introduction to some of the main diagnostic techniques currently used to characterize PEMFC electrocatalysts (*Paragraph 2.5*).

The experimental section (*Chapter 3*) presents the research activity that has been carried out by the author on electrocatalyst characterization in HT-PEMFCs. The materials that have been used in the experiments are described in *Paragraph 3.1*. The comparison of two standardized procedures for the acquisition of polarization

curves is discussed in *Paragraph 3.2*. *Paragraph 3.3* includes a sensibility analysis of cyclic voltammetry measurements on HT-PEMFCs. A method for the characterization of HT-PEMFC MEAs with small angle x-ray scattering (SAXS) is presented and discussed in *Paragraph 3.4*. *Paragraph 3.5* describes the design of a test bench for long-term testing of HT-PEMFCs, including the implementation of specific testing procedures. Methodology, results and discussion of long term durability tests based on load cycling are presented *Paragraph 3.6*. *Paragraph 3.7* describes the methodology of a start/stop long-term test and includes the discussion of the results.

Conclusions and final remarks are discussed in *Chapter 4*.

2

Scientific background

2.1 Membrane electrode assembly

In order to provide a clear context for the following discussions related with degradation, structure and components of membrane electrode assemblies (MEAs) of PEM fuel cells will be briefly presented in this paragraph. A single PEM fuel cell consists of an anode, a cathode and an electrolyte in the middle. In PEMFCs the electrolyte is a polymeric membrane. Both cathode and anode are made up of a catalyst layer (CL) and a gas diffusion layer (GDL). The catalyst layer can be attached to either the electrolytic membrane or to the GDL. A schematic cross section of a typical PEM fuel cell is shown in *Figure 1*.

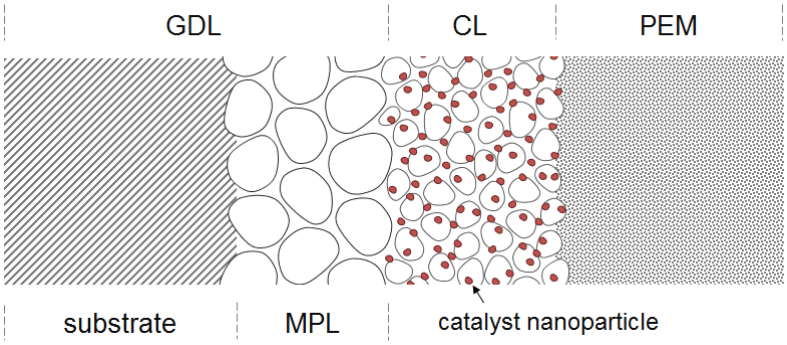

***Figure 1**. Schematic cross-section of a typical PEM fuel cell: gas diffusion layer (GDL), catalyst layer (CL) and polymer electrolyte membrane (PEM). GDL is constituted by a macro-porous substrate and a micro-porous layer (MPL).*

The task of the gas diffusion layer is to distribute uniformly the reactants on the catalyst layer area, to provide conducting paths for electrons and facilitate the water removal from the MEA to the flow channels. GDL typically consists of two layers, a macro-porous substrate and a micro-porous layer (MPL) or diffusion layer. The macro-porous substrate is made of a carbon fibre matrix with a large void volume, while the micro-porous layer consists of carbon black mixed with fluoropolymer. The catalyst layer or active layer is constituted by catalyst nanoparticles of platinum or platinum alloys deposited on a high-surface-area carbon support. The electrocatalyst usually is in the form of nanoparticles of about 3 nm in order to maximize the active catalytic surface area per unit mass of platinum [1]. Particles size is normally not further decreased because smaller platinum particles start to be significantly unstable. The stability of platinum, platinum alloys, carbon support and the interaction between platinum nanoparticles and carbon support strongly affect PEM fuel cells durability [2]. The polymeric electrolytic membrane (PEM) is made of polymeric material with sulfonic-acid side chains and a fluorocarbon or hydrocarbon backbone. The standard electrolytic membrane material is Nafion®, a perfluorinated sulfonic acid-based ionomer (PFSA), trademark of DuPont. The set of a polymeric electrolyte membrane (PEM) sandwiched between an anode and a cathode constituted by a gas

diffusion layer (GDL) and a catalyst layer (CL) is called membrane electrode assembly (MEA). The MEA is the central part of a PEM fuel cell since there electrochemical reactions that drive the fuel cell take place. The voltage produced by a single PEM fuel cell with a specific current of 1 Acm^{-2} is about 0.6 V [1]. In order to obtain a higher voltage, many individual cells are assembled in a fuel cell stack. The single cells are electrically connected in series by bipolar plates and properly compressed by special end plates. The function of bipolar plates is to distribute reactants on the MEA surface and remove the product water through their flow channels, provide conducting paths for electrons, remove excess heat by means of their cooling channels, provide structural integrity to the stack and avoid gas transport between different cells. Bipolar plates have thus to be electrically conductive, impermeable to gases, easy to manufacture, resistant to mechanical and thermal stresses and stable in the typical operative environment of a PEM fuel cell. Bipolar plates are usually made of graphite composite based materials or metal alloys coated with anti-corrosion materials.

2.1.1 MEAs for HT-PEMFCs

One of the approaches to overcome some of the problems related to traditional low temperature PEMFCs, such as CO poisoning, slow reaction kinetics, water and heat management is to increase the operational temperature above 90°C. High temperature PEM fuel cells (HT-PEMFCs) are a specific class of PEM fuel cells designed to operate at temperatures higher than 100°C. High temperature operation presents several advantages such as enhanced electrochemical kinetics, higher tolerance to carbon monoxide in the fuel, an easier water management due to its presence in the vapour phase only, a better heat management that is possible because of the higher temperature gradient between the fuel cell and the environment. The latter advantage makes HT-PEMFCs particularly suitable for cogeneration since the heat produced from fuel cell

operation can be effectively used for further applications, reaching very high efficiency levels. The possibility to operate with higher CO content is another significant advantage compared to low temperature PEMFCs because it allows the use of reformated hydrogen as a fuel, extending considerably their range of applications [8]. On the other hand, however, the higher operative temperature favours most of the degradation mechanisms of PEM fuel cells, included the degradation of the electrocatalyst and its support. In high temperature PEM fuel cells (HT-PEMFCs) the structure of the MEA is very similar to the one of low temperature PEMFCs, even if the materials of some components are different. The polymeric electrolyte membrane (MEA) consists of a polymeric backbone with side-chains possessing acid-based groups that have the function to promote the proton conductivity through the membrane. The proton carrier can be either water or an ionic medium such as phosphoric acid (H_3PO_4) or an ionic liquid such as 1-butyl-3-methylimidazolium tetrafluoroborate ($BuMeImBF_4$) [9]. The catalyst layer is made by nanoparticles of electrocatalitic material, such as Pt or Pt alloy, supported by a conductive material, usually carbon, similarly to PEMFCs. GDL materials are usually the same of those used in low temperature PEMFCs (Toray H-120, SGL GDLs, ELAT woven GDLs, Carbon cloth). Bipolar plates are commonly made by graphite due to its chemical stability and high conductivity. Metallic plates sometimes are preferred in order to reduce the cost, increase the volumetric power density and enhance the mechanical strength [10]. The operation at high temperature allows the use of a wide range of flow field designs because the problem of water management is reduced by the absence of liquid water in the fuel cell [11].

2.2 Catalyst layer degradation

Catalyst layer in PEM fuel cells is composed by a mix of an electrocatalyst, usually in form of nanoparticles, and a support [1]. In this paragraph the fundamentals of catalyst layer degradation in PEMFCs are described and discussed.

2.2.1 Electrocatalyst degradation

The common electrocatalysts in PEMFC electrodes consist in Pt or Pt-alloy nanoparticles with a 3-5 nm size that can provide fuel cell active areas of 25-40 m^2g^{-1} [2]. Platinum is the available catalytic material with the highest activity, but its cost is the main limitation on a large scale PEMFC production. Moreover, the durability of the catalytic properties is a determining factor in the useful lifetime of a PEM fuel cell. One of the main causes of performance loss during fuel cell operation has been considered the reduction of the electrochemical active surface area (ECSA) of the electrocatalyst [5,6,12]. ECSA loss is mainly attributed to three different phenomena related to the electrocatalyst: agglomeration, isolation and dissolution [1].

Catalyst particles agglomeration is supposed to be driven by three different mechanisms: coalescence, re-precipitation and Ostwald ripening. Particle coalescence occurs when Pt particles are in close proximity and sinter together to form larger particles. Re-precipitation consists in the Pt dissolution in the ionomer phase within the cathode and in its precipitation as newly formed Pt particles. During Ostwald ripening process small particles dissolve in the ionomer phase, diffuse and then redeposit on larger particles. The driving force in the Ostwald ripening mechanism is the minimization of the surface energy, leading to reduced Pt particle surface. Ostwald ripening and re-precipitation are quite similar processes, the main difference is that in Ostwald ripening the

nucleation site for platinum deposition is a previously existing platinum particle, while in re-precipitation, the nucleation site is a particle or a defect that previously was not a platinum site [2]. The knowledge of the crystallite size distribution (CSD) statistics could be very helpful in the determination of the particle coarsening mechanism, since dissolution and re-precipitation produce very different CSDs compared to Ostwald ripening. Ascarelli et al. [13] proposed a method to distinguish coalescence and Oswald ripening. The coalescence process leads to log-normal particle size distributions, with a maximum shifted towards the small-particles side and a tail on the large-particles side. The Ostwald ripening process, instead, is characterized by a tail towards the small-particle side, while the maximum is shifted on the large-particle side. In the case of Pt dissolution and re-precipitation, which may also be associated with Pt particle coalescence, the dissolved Pt species nucleate both in the ionomer phase and on the carbon support surface. The resulting distribution of particles sizes depends on the localized Pt concentrations within the ionomer and on the Pt-Pt nucleating particle distances. The CDS profile of the Pt particle size distribution changes when Pt re-deposition mechanism is coupled with particle coalescence. In this case the distribution is characterized by a bimodal particle size distribution, where some fractions of small Pt particles are maintained in the cathode while others grow larger. The particle size distribution became broader due to the nucleation of small and highly separated Pt particles within the ionomer that in part nucleate together into larger particles via coalescence. Ostwald ripening of Pt particles consists in the dissolution of the smaller Pt particles in the ionomer phase and their re-deposition on larger ones, resulting in the disappearance of small particles and the growth of larger ones. This process is due to the chemical potential difference of differently sized particles at high operating potentials typical of the cathode side. Pt ions move through the ionomer, while the electrons through the conductive carbon support. Electronic conductivity between the particles

involved in the Ostwald ripening process is thus necessary. Re-deposition and coalescence growth by aggregation of small particles maintains thus a log-normal distribution during the increase in average particle size, while Ostwald ripening causes an increase in the percentage of large particles with a decrease in the relative fraction of small particles [2]. More et al. [14] observed changes in the Pt particle size distribution during potential cycling between 0.1 and 1.2 V, shifting towards a bimodal distribution with increasing potential. This behaviour suggests that Ostwald ripening is not the only Pt particles agglomeration mechanism, because in that case the Pt size distributions should just be shifted to larger particle size ranges during the cycling test. Instead, the size distribution gets broader since a fraction of the very small Pt particles remains after the potential cycling even if the number of larger particles increases. The Pt particles growth behaviour can thus be described by a combination of Pt particle coalescence and Pt dissolution/re-precipitation within the ionomer [2]. Ferreira et al. [12] investigated the Pt particles size distribution in PEMFCs and found that nanoscale Ostwald ripening was dominant at the GDL interface on the cathodic side, since the mean particle size was larger and the Gaussian size distribution wider, due to the limited hydrogen crossover for Pt ion deposition. In the area close to the electrolytic membrane the particle distribution profile was bimodal, because of the hydrogen crossover reduction of the Pt ions. The different Pt size distributions in different areas of the catalyst layer may thus be caused by differences in the potential distribution within the ionomer instead of H_2 concentration differences. A Pt band could form where hydrogen and oxygen diffused through the membrane react with each other and provoke a high local potential [15]. There is also to take into account a Pt ion concentration gradient in the cathode due to the tendency of Pt ions to diffuse into the membrane from cathode to anode. Pt mass distribution within the cathode is thus not uniform and larger Pt particles may be formed in the area close to the electrolyte [2].

Catalytic ECSA can also be reduced by the loss of the triple-phase boundary (TPB). TPB is the simultaneous presence of the conductive material for the electronic network, the polymer electrolyte for the pathway of protons and the presence of reactants. Electrocatalyst sites are active when they are in the TPB condition [6]. Finally, electrocatalyst can also dissolve in the ionomer phase and be physically removed from the catalyst layer and be transported out of the fuel cell by the products or be re-deposited in areas of the MEA where the triple-phase boundary is not available, such as in the GDL or in the electrolyte. Platinum dissolution is larger in the cathode, where potentials are higher [2,16,17]. The deposition of the dissolved Pt on existing Pt particles consists in the re-precipitation process described before. Ferreira et al. [12] made a distinction between the coarsened spherical particles still in contact with the carbon support and the non-spherical ones removed from the carbon support. Both processes include Pt dissolution, but in the former the agglomeration is driven by the Ostwald ripening mechanism, since the particles are in contact with the carbon support that acts as conductive material, while in the latter the agglomeration results from the deposition in the ionomer by dissolved hydrogen. Pt solubility in aqueous electrolyte is governed by the chemical state of the platinum surface and the Pt species in solution and it is influenced by the electrolyte materials, solvent, pH, temperature and potential [2]. Pt in the form of nanoparticles showed a higher solubility than in the bulk form [2]. Moreover, it has been found that Pt solubility increases with temperature following the Arrhenius relationship, indicating that the dissolution reaction is endothermic. The dissolution reaction seems to be more dependent on the oxidation-reduction cycles rather than on the length of the cycle or time at oxidizing potentials [2].

Moreover, when Pt in aqueous electrolyte is subjected to potentials in the range between 0.7 and 1.5 V, the formation and reduction of a multilayer, multivalent Pt oxide film occurs. This phenomenon has also been observed in the voltammetry of the electrode layer in a

PEMFC membrane electrode assembly in the absence of gas-phase reactants, when anode and cathode are both purged with an inert gas [2]. The increasing charge under the oxide reduction peak in the voltammogram of the cathode of a PEMFC suggests that Pt is slowly oxidized during operation at high potential (0.85-0.95 V) [2]. The presence of gas-phase oxygen accelerates the oxidation and at high constant potentials, fuel cell performance can be halved in just 1 h of operation. The loss has been attributed to the blocking of Pt surface sites to take part in the oxygen reduction reaction by the formation of platinum oxide [18]. The performance loss due to Pt oxidation, however, is completely recoverable with a short excursion of the cathode potential to a value lower than 0.5 V that trigs the reduction of the oxide layer formed at the higher cathode potentials [19].

In phosphoric acid fuel cells (PAFCs) Pt degradation is expected to be higher than in PEMFCs, because of more corrosive conditions due to the electrolyte materials and higher operative temperatures [2]. The degradation mechanisms are the same described above. PAFCs ECSA loss has been mainly attributed to Pt dissolution at the cathode when operating at potentials higher than 0.8 V, re-deposition of Pt to form larger particles via Ostwald ripening mechanisms and Pt loss into the electrolyte with migration toward the anode. The analysis of the Pt distribution on the cross-section of operated PAFCs showed a large amount of Pt dissolved and migrated from the cathode into the electrolytic membrane [2].

Many factors affect the particle growth rates and the involved mechanisms can change depending on the electrode potential, cell voltage cycling conditions, current density, state of hydration of the membrane and operating temperature [2]. The influence of operating conditions on electrocatalyst degradation will be discussed in *Paragraph 2.3*.

2.2.2 Carbon support degradation

Within the catalyst layer, carbon support has the function to anchor the catalyst nanoparticles and to provide electrical conductivity to the gas diffusion layer and the bipolar plates. The electrochemical corrosion of the carbon support materials causes electrical insulation of the catalyst particles when they are break away from the support or aggregation of the catalyst particles when the support feature is lacking due to carbon corrosion. Both these processes lead to a decrease of the catalytic electrochemical surface area and to an increase in the hydrophilicity of the catalyst layer surface, which can in turn result in a decrease of the gas permeability since the liquid water fill the pores of the carbon structure and obstruct the gas transport [2]. The corrosion reaction of carbon material in aqueous acid electrolytes, PEM included, can be generalized [20] as

$$C + 2\,H_2O \rightarrow CO_2 + 4\,H^+ + 4\,e^- \qquad E^0 = 0.207\,V$$

Even if the standard electrode potential of the reaction E^0 is in the range of the normal fuel cell operation, the reaction is believed to be very slow in that potential range and at the lower operative temperatures of PEMFCs. This corrosion is considered negligible in the short time-scale for potentials lower than 0.8 V, while in long-term operation it can affect the durability of the fuel cell [2]. In PAFC the corrosion of the carbon support start to be significant after 0.9 V even for a cell that has uniform hydrogen coverage on the anode. Carbon corrosion current is dependent to the potential, material, temperature and time. Its dependence with the potential follows the Taefel behaviour, while the dependence with the temperature follows the Arrhenius behaviour. Moreover, there is a linear relation between the corrosion current and time in log-log plots. During a transient operation of the fuel cell, such as start-up and shutdown,

hydrogen-rich regions and hydrogen-starved regions coexist in the anode chamber and provoke local corrosion at the cathode areas corresponding to the fuel-starved areas in the anode (see *Paragraph 2.3.4*). This process, called "reverse-current mechanism", induces a potential that is high enough for oxygen evolution and carbon corrosion. It is supposed that oxygen crossover rate from cathode to anode is enough to support the reverse-current mechanism [2].

PEMFCs and PAFCs catalyst layers have a similar structure and materials, even if the catalyst support is usually graphitized carbon in PAFCs to enhance the carbon stability in high-temperature acid environments [5]. In PEMFC fully graphitized carbons are usually not used for the catalyst layer, because carbon is more stable in low-temperature environment [2]. At operating temperatures higher than 160°C carbon corrosion currents can be quite large: currents of 1-10 mA/mg_{carbon} have been observed for Vulcan XC-72 at 180°C and 1.0 V [20–22]. A mechanism of local cathode corrosion similar to the reverse-current mechanism in PEMFCs has been proposed for PAFCs [23]. Common methods to characterize the carbon corrosion are corrosion-curve evaluation, weight loss, CO_2 generation, cyclic voltammetry (CV), X-ray photoelectron spectroscopy (XPS), scanning and transmission electron microscope (SEM and TEM) [2].

2.3 Influence of operating conditions on degradation

Fuel cell durability is highly dependent on operating conditions [1,2,5]. In this chapter, the effects of operative conditions such as presence of impurities, load cycling, fuel starvation, start/stop cycling and operative temperatures on the degradation of the electrocatalyst and its support are discussed.

2.3.1 Impurities

Impurities have a negative impact on fuel cell performance and durability. They can be present in reactants or result from some fuel cell component degradation and can induce several mechanisms that decrease fuel cell performance. The electrode charge-transfer process can be hampered by the absorption of impurities on the electrocatalyst surface, with the result of interfacial overpotential losses. Performance losses due to impurities can be permanent and irreversible or temporary and reversible. For some kind of impurities, the performance loss can be recovered by the interruption of the impurity supply or after performing specific procedures [24]. In most of the applications hydrogen is currently produced by reforming of hydrocarbon fuels such as natural gas, methanol, propane, gasoline and diesel. The reformate gas is the first product of a reforming reaction and is constituted by different gases in different percentages, depending on the original fuel and the reforming method. The reforming process leaves some impurities in the hydrogen in an amount that depends on the type of process, the fuel used and eventual post-treatments of the reformate gas. The presence of CO_2 is in general considered as a dilution of the fuel, but it can react via the reverse water-gas-shift reaction and produce CO that is a more severe impurity for PEMFCs. CO forms a strong bond by chemisorption on the Pt surface, blocking the adsorption of hydrogen on the active catalytic sites for the hydrogen electro-oxidation (HOR). This poisoning of the catalyst reduces the electro-oxidation rates and enhances the electrode overpotentials, leading to performance loss [2]. CO concentrations as low as few tens of ppm causes significant losses in fuel cell performance [1]. Fuel cell operation at higher temperatures (>120°C) allows significantly higher CO tolerances in fuels. For example, Celtec®-P MEAs operated at temperatures between 120 and 180°C can tolerate CO concentrations in the fuel up to 3% [25].

Natural gas may contain large amounts of hydrogen sulphide (H_2S), depending on the geographic region of extraction, while other fossil fuels such as gasoline contain some sulphur-containing compounds that are converted in H_2S during the reforming process for H_2 production. Hydrogen sulphide has a strong degradation effect on Pt catalysts, related with H_2S concentration and time of exposure [2]. The U. S. FreedomCAR Fuel Cell Technology Team [26] compared the performance of a fuel cell with traces of impurities (H_2S, CO, CO_2 and NH_3) in the hydrogen with one fed with neat hydrogen on a 1,000 h steady-state test. They observed a performance loss of 100 mV for the cell operated with the impurities and attributed it to the presence of NH_3 and H_2S. 40 % of the Pt catalyst surface was poisoned by H_2S. Impurities can also be present on the air side of the fuel cell. Sulphur dioxide (SO_2) can be present in high concentrations in urban areas of in close proximity to some chemical plants. The effects of SO_2 at the cathode are similar to those of H_2S in the anode. Performance degradation is due to a strong chemisorption of SO_2 on the Pt catalyst surface and is not reversible just by normal operation with SO_2-free air [26]. Sodium chloride (NaCl) is another impurity that may contaminate the cathode via the air supply. The electrocatalyst can be affected by the presence of NaCl, since it has a strong effect on oxygen reduction kinetics at the cathode [2].

2.3.2 Load cycling

In many PEM fuel cells applications dynamic operation is required. First at all, automotive applications may need rapid changes in load during all fuel cell lifetime. The operative voltage range of a PEM fuel cell is between 0.6 and 1.0 V. This range varies for high temperature PEM fuel cells, where the operative range is slightly lower (between 0.5 and 0.9 V). Proprieties of electrodes materials such as degree of oxide coverage of catalyst and carbon support change when they are subjected to potential variations. Moreover, during the operation at high cathode potentials, platinum can dissolve very fast until the

formation of a protective oxide layer on the platinum surface [2]. Bi et al. [15] observed deposition of platinum in Nafion membrane after 3,000 potential cycles under H_2/air conditions. After the cycling test, approximately the 13% of the platinum initially present in the cathode was transported into the membrane and a Pt band was formed in the ionomer. Shao et al. [27] investigated the degradation of Pt/C electrocatalysts under potential-static holding conditions (at 1.2 and 1.4 V vs. RHE) and under potential step conditions (between 1.4 V and 0.85-0.60 V). They found that Pt/C degrades under the test with the lower potential limit of 0.85 V mainly through the coalescence process of Pt nanoparticles due to the corrosion of carbon support, which was similar to that under potential-static holding conditions. Moreover, they observed that Pt/C degrades mainly through the dissolution/loss and dissolution/re-deposition process if stressed under the test with the lower potential limit of 0.60 V. The difference in the degradation mechanisms has been attributed to the chemical states of Pt nanoparticles: Pt dissolution can be alleviated by the protective oxide layer under the test with a higher lower potential limit and the potential-static holding conditions.

2.3.3 High potentials

As above mentioned, fuel cell operation at high potentials (>0.8 V) and in particular at open circuit (OC) condition have also been identified as a cause of degradation for both the electrocatalyst and its carbon support [2]. Open circuit voltage (OCV) can accelerate the decay rate because voltages higher than 1 V strongly favour oxidation processes [1]. High voltage operation and OC condition can occur during transient operations such as start-ups and shutdowns. Zhang et al. [28] studied the effect of OC conditions on a PEMFC MEA during a 250 h durability test. The decline in performance during the test was attributed mainly to the structural changes in the electrolytic membrane and the catalyst layer. The

catalyst degradation due to Pt oxidation or catalyst contamination, however, was partially recovered by a subsequent potential cycling process. Qi and Buelte [29] analysed the impact of OCV on performance and degradation of H_3PO_4/PBI fuel cells operated at 180°C. OCV showed a quick increase in the first minutes, followed by a much slower increase and a peak at about 35 min. Then an exponential voltage decline began with proportional effects on the fuel cell performance. OCV and fuel cell performance was temporarily boosted by operation at 0.2 Acm^{-2}, even if it was not possible to permanently recover the performance. Cathode Pt crystallite size increased by over 400% after 245 h at OCV, while at the anode no significant changes have been observed. Moreover, significant increase in kinetic and mass transport resistance has been observed during the test. The mass transport increase was attributed to the oxidation of the carbon support of the catalyst. Wu et al. [30] investigated the performance degradation of a PEM fuel cell under close to OC conditions, where only idle auxiliary load power was drawn from the power supply with a relatively high fuel cell potential of around 0.9 V. A 6-cells PEMFC stack was operated under close to OC conditions in a 1,200 h durability test. After 800 h the fuel cell performance significantly decreased, probably because of membrane failure, while in the previous period the degradation was attributed to catalyst decay.

2.3.4 Fuel starvation

Single fuel cells with large active areas and stacks experience different operative conditions in different points of the MEA. Non-uniform distribution of reactants, local blockages and imperfections in the single components manufacture may lead to non-uniform distributions of current on the active surface area of the fuel cell. This condition is particularly critical in fuel cell stacks, where the cells are arranged in series and often experience different flows of reactants and coolant due to imperfect manifolding, even if they are

forced to carry the same current of the neighbouring cells. These non-uniform reactants distribution may cause starvation in some localized areas of the MEA. In particular situations of diffused starvation, anode potential increases, carbon support oxidizes instead of the absent fuel and cell voltage can become negative [31,32]. During the potential reversal provoked by fuel starvation carbon is oxidized to form carbon dioxide at the anode and the result is a permanent damage of the anode catalyst layer. This phenomenon can also occur during localized fuel starvations and can induce local potentials on the cathode higher than 1 V that corrode the carbon support and result in permanent loss of electrochemically active area. Localized fuel starvations take place quite often during transient conditions, especially during load cycling and start-stop operation. In the regions of the cell where fuel is present at the anode, the cell behaves normally and the potential stay close to equilibrium, delivering high currents until hydrogen is consumed. In the regions of the cell where fuel is not present, potential increases since it cannot be more stabilized by proton or electron transport. Electrodes potentials thus increase significantly in order to maintain the potential difference imposed by the active part of the cell and a reverse current is established. The reverse current is sustained in the fuel-starved region by oxygen evolution and carbon corrosion on the positive electrode and by oxygen reduction from crossover on the negative electrode [1]. Yousfi-Steiner et al. [33] reviewed the PEMFC degradation under starvation condition, analysing causes, consequences and proposing procedures for its mitigation. They considered the loss of catalyst ECSA one of the main causes of performance decrease during long-term operation.

2.3.5 Start-ups and shutdowns

Start-ups and shutdowns induce complex transient phenomena that can cause significant degradation to the catalyst layer of the fuel cell.

During a prolonged shutdown without reactants supply and purging procedures, hydrogen crossover from anode to cathode may empty the anode chamber that may be then filled by air. Restarting the fuel cell from this condition, the fuel flow will induce a transient condition in which fuel is present at the inlet while the outlet is still fuel-starved. This condition can lead to local potentials on cathode up to 1.8 V vs. SHE [2] and cause corrosion of the carbon support. Specific operative procedures for start-ups and shutdowns can reduce the effects of some of those mechanisms [34,35]. Park et al. [36] investigated carbon support corrosion in PEMFCs during simulated start/stop cycling. The results showed a severe decrease of ECSA, mass activity and fuel cell performance that was attributed to the detachment of Pt particles from the carbon support due to carbon corrosion, structural collapse and Ostwald ripening. Liu et al. [37] performed a drive cycle protocol that simulates start/stops in real automotive applications. The damage of the catalyst layer micro-structure was considered decisive for the performance degradation after 900 h of durability test. Dillet et al. [38] developed specific testing protocols in order to separate the effect of fuel cell start-up and shutdown on performance degradation (see *Paragraph A2.1.2*). The results showed that stat-ups are significantly more damaging than shutdowns in terms of CO_2 evolution, catalyst ECSA decrease and performance losses. Schmidt et al. [39] investigated the properties of commercial high temperature PEM fuel cells under start/stop operation mode and observed significantly increased cathodic mass transport overpotentials as a result of enhanced corrosion of the cathode catalyst support.

2.3.6 Temperature and relative humidity

Transitions between different power levels may provoke significant changes in temperature and relative humidity of the fuel cell. For an operation with fixed stoichiometric ratios, the cell is in general relatively cool and wet at low currents and hotter and drier at

higher currents [2]. Since the ionomer swells with the water uptake, changes in RH conditions can lead to compressive stresses in the membrane that increases in water uptake when exposed to high RH conditions and then yields tensile residual stresses when it is drying due to lower RH conditions. Frequent changes in RH conditions could significantly contribute to the mechanical failure of the membrane. Both temperature and relative humidity have been shown to affect the rate of platinum particles growth, and thus the rate of catalyst electrochemically active surface area loss [40].

Cai et al. [41] simulated the degradation processes of carbon corrosion and platinum ECSA loss by means of an accelerated thermal sintering protocol and compared thermal with electrochemical degradation. Catalyst ECSA loss after 10 h of thermal degradation was found to be equivalent to more than 500 load cycles between 0 and 1.2 V. Stevens et al. [42] tested carbon-supported catalysts at elevated temperatures under dry air conditions. The amount of carbon that was lost after extended oven exposure at constant temperature was shown to depend on both the temperature and platinum loading. Oono et al. [43] investigated the influence of operating temperature on cell performance in high temperature PEM fuel cells. Higher operative temperatures resulted in higher cell voltage, but also in lower fuel cells lifetime. The early stage degradation was attributed to aggregation of the electrocatalyst particles. Vengatesan et al. [44] studied the MEA degradation under accelerated relative humidity cycling and observed a strong dependence of degradation with respect to relative humidity. A decrease in ECSA was noted during the test. Wang et al. [24] investigated the recoverable degradation in PEMFCs operated under drive cycles and different humidities. The cell performance of a single fuel cell decreased after 5 h operation and recovered after one night rest at high humidities (100%, 75% and 50% RH), while it decreased continuously at lower humidity (35% RH). They found that water content is one of the main contributors to performance degradation, affecting also the catalyst utilization.

Wu et al. [45] studied the effect of RH cycling and load cycling in PEM fuel cells and observed Pt agglomeration and carbon corrosion.

Start-stop cycling from subfreezing temperatures may lead to a decrease in fuel cell performance and structural changes to the catalyst and gas diffusion layer. A reduction in the cathode electrochemical surface area of the electrocatalyst and an increase in the membrane high-frequency resistance (HFR) have been attributed to the formation of ice in the electrodes [31]. When fuel cell is operated at sub-zero temperatures, the water generated at the cathode tends to form ice. In order to reduce the degradation during start-stop operation at subfreezing temperatures some mitigation strategies have been developed to prevent ice formation. Those procedures include keeping the fuel cell warm, drying the fuel cell or replacing the water with a non-freezing liquid and providing external heat. Even if these strategies are technically effective, they add complexity to the fuel cell system and are not able to respect the energy targets [2].

2.4 State of the art in electrode materials

Novel materials for PEM fuel cells electrodes are currently investigated with the purpose to decrease cost and enhance durability. Catalysts made of carbon-supported Pt nanoparticles of 2-3 nm in averaged particle size offer the highest oxygen reduction reaction (ORR) activity per unit mass. Further attempts to obtain stable Pt nanoparticles of smaller sizes are limited by the decrease in the catalytic activity of platinum or Pt-alloy catalysts. Moreover, smaller nanoparticles are prone to increase the performance losses associated with catalyst morphology changes [2]. Alternative catalysts to pure Pt particles are currently investigated by many research groups. Platinum alloys have been used in both PEMFCs and PAFCs in order to improve the oxygen reduction reaction [5].

Several platinum alloys on high-surface-area carbon in acid electrolytes show high degrees of crystallinity and exchange current densities that are 2-3 times enhanced in comparison with Pt/C. Even if the metals which are co-alloyed with platinum would tend to be less stable than pure metals and platinum, the alloy produces higher mass activity and has a higher stability to cycling and resistance to dissolution, despite with a lower metal surface area compared to Pt/C. It is still not clear if this improvement in stability is due to improved thermodynamic stability or to differences of the kinetics of platinum dissolution or in passivating oxide formation [1]. The replacement of platinum with non-platinum catalysts is another approach that has been followed. The problem of cost is however not solved when the alternatives are precious metals that recently had similar or even greater increases in price than platinum had. Moreover, the catalyst activity of other noble-metals is lower if compared to platinum. The non-platinum catalysts are usually based on Pd or Ru [2]. Non-precious Pt-free catalysts, on the other hand, started to become always more attractive for the oxygen reduction reaction (ORR) in PEM fuel cells. Many non-precious metal catalysts exhibit both good oxygen reduction activity and significant performance durability in alkaline and neutral media. However, all the non-precious metal catalysts developed in these years showed low activity and poor stability in the acidic environment of PEMFC cathode [2]. Moreover, information on the long-term performance of non-precious oxygen reduction catalysts is scarce, especially during fuel cell operating conditions. The ORR activity and the long-term performance durability of the currently developed non-precious catalysts are thus insufficient to match the technical requirements to operate in PEMFCs [2]. The employment of Pt shell on non-Pt core is an advanced method to decrease the platinum loading while keeping a high catalytic surface area [2,46].

Many alternatives to the common carbon nanoparticles have been studied in order to get a better stability and long term durability of the catalyst layer. Carbon nanotubes performance is higher in

comparison to other catalyst supports, but their durability has still to be deeply studied in order to prove real advantages of these materials in PEMFCs applications [1]. Some studies [2,47] suggest that nanotubes and similar structures are more oxidant resistant than carbon blacks and that they reduce the catalyst ECSA loss, but this improvement may not be sufficient to provide the needed benefits for a large-scale commercialization, first at all due to their much higher cost. Silicon-based fuel cells can be manufactured using electronic fabrication techniques: a silicon substrate with flow channels can be made with photolithography or similar techniques. These fuel cell systems are currently intended for micro-power application and their employment on larger scales is excluded due to cost limitations. Moreover, even if some performance advantages have been showed, data on their durability is still scarce. Electronically conductive polymers have been widely studied for many electronic and electrochemical applications, but applications in fuel cells are still limited. The polymeric material increases Pt dispersion and utilization, but the stability of this support may be an issue, particularly at the cathode side. Conductive diamond can be obtained doping diamond with boron in order to obtain electronic conductivity. It is more resistant to corrosion and electrochemically stable compared to carbon. However, the employment of conductive diamond as catalyst support may not be better than carbon in limiting the mobility or dissolution of platinum nanoparticles, unless the particles are quite large or entrapped in the support structure. Moreover, Pt utilization may be low for fuel cell applications. The use of porous honeycomb diamond with larger Pt particles results in high surface areas. Even if the resistance to corrosion of boron-doped diamond is very high, its application as fuel cell material for catalyst support may thus be limited due to the low Pt utilization and rough factor. Nano-conductive whiskers are an unique class of nano-structured organic catalyst support materials developed by 3M [48]. Differently than most of the alternative catalyst supports for fuel cells applications, these whisker structures are non-

conductive. Pt is sputtered on the high surface area of the whiskers in order to obtain electronic conduction and catalytic activity. The whiskers have thus the function to provide structure and large surface area to the deposited catalyst. The deposited Pt particles tend to have larger sizes than those on carbon support in order to improve electronic conductivity and catalyst activity. The near bulk-like Pt activity and high surface utilizations of non-conductive whiskers allow a comparable or better fuel cell performance respect to conventional supports, even if their low active area is lower. The main advantage of these structures is that they are not affected by the fuel cell environment: catalyst degradation induced by support corrosion is thus limited and consequently the catalyst layer durability is expected to be higher. Two disadvantages of the nonconductive whiskers structure are that they can be prone to contaminants due to the lower active areas and to flooding [2].

2.5 Diagnostics techniques

The polymeric electrolyte membrane (PEM) fuel cell is a complex electrochemical power system. Most of the components of a PEMFC are made by composite materials, porous materials for gas and water transport, or nano-materials in order to achieve high electrochemical activity. Moreover, many complicated processes such as the electrochemical reactions, electron transfer, proton transfer, reactants transport, product water and vapour transport as well as heat transfer, take place within the fuel cell. Transport phenomena may occur across multiple boundaries and involve multiphase flows while the electrode reaction takes place at a multiphase boundary. The characterization of these processes and materials became thus often difficult since many complicated phenomena happen simultaneously at very different spatial scales. Three-dimensional analysis is also particularly important for

performance and durability of fuel cell stacks, because they are very sensitive to local conditions. Finally, severe operating conditions such as high potentials, temperatures, pressures, gas flows and humidification may contribute to make *in situ* measurements more difficult. Since fuel cells are electrochemical systems, electrode processes play a central role in their performance and durability. For this reason, common electrochemical techniques, such as polarization curves, cyclic voltammetry (CV), linear sweep voltammetry (LSV), CO stripping voltammetry and electrochemical impedance spectroscopy (EIS) have become standard methods for fuel cells characterization. Information of electrocatalyst performance and structural properties can be obtained from electrochemical methods. However, due to the mentioned complexity of those systems, electrochemical methods may be subjected to limitations and other diagnostic tools are often necessary.

Physical-chemical methods are used to investigate PEMFC electrocatalysts in order to obtain information on their structure, composition and interaction with other materials. The analysis of electrocatalyst structure composition and phase can be performed by techniques like x-ray diffraction (XRD), electron diffraction (ED), x-ray fluorescence (XRF), x-ray emission (XRE) and proton-induced x-ray emission (PIXE). Other structural information such as size, shape and distribution of the electrocatalyst can be determined with small angle x-ray scattering (SAXS). A morphological characterization can be carried out with electron microscopy techniques such as scanning electron microscopy (SEM) and transmission electron microscopy (TEM). Surface information on the electrocatalyst structure and composition can be obtained with x-ray photoelectron spectroscopy (XPS), UV-induced photoelectron spectroscopy (UVPS) and energy dispersive spectroscopy (EDS).

In the following paragraph, only the diagnostic techniques that have been used in this research will be presented and discussed.

2.5.1 Polarization curves

The polarization curve is a standard technique in fuel cell testing and consists in the plot of the cell voltage versus the current density. A typical PEM fuel cell polarization curve is shown in *Figure 2*. It is usually performed in a quasi-steady-state in which the current is held at specified points until the voltage stabilizes, but it can also be obtained changing linearly the current [49–51].

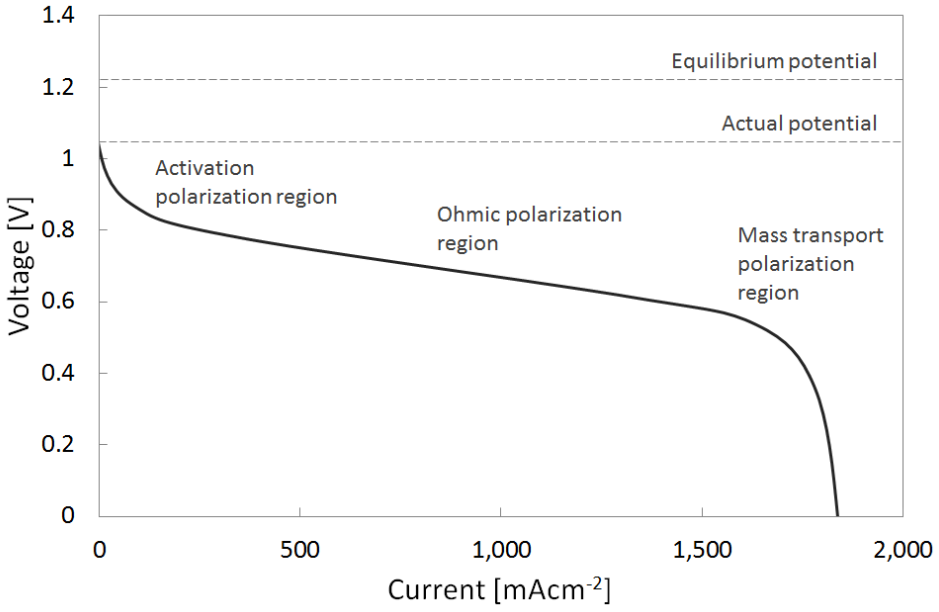

***Figure 2**. Typical polarization curve for PEM fuel cells. Activation, ohmic and mass transport polarization regions have been indicated in the graph.*

Polarization curves can be performed increasing or decreasing the current, or even following random values. Typically it is performed with increasing points, then decreasing points and the results are averaged for each measuring point. Polarization curves are a versatile diagnostic technique for the evaluation of fuel cell performance and the effect of changes in particular operating parameters. From a polarization curve it is possible to distinguish between kinetic, ohmic and mass transport losses [49]. The

activation polarization region is this first part of a polarization curve, where current densities are low. In this part of the curve the cell potential drops significantly due to the slow kinetics of the ORR. At higher current densities the curve follows a linear decrease for the largest part of the plot. This is the region of ohmic polarization: the voltage loss is mainly caused by ohmic resistances and the voltage drop is proportional with the current density. The ohmic resistance that affects this region of the curve regards both the electronic transport through the electrodes and the protonic one through the electrolyte. The third part of the polarization curve (high current densities) is dominated by mass transport and it is called region of concentration polarization. In this region a drastic decrease of the cell performance is provoked by the transport limit of the reactants gases through the pore structure of the GDL and catalyst layer. The gap between the actual cell potential and the equilibrium potential (or Nerst potential) results from crossover of fuel and oxidizer through the electrolyte or internal short circuits in the cell [52]. It is possible to obtain the power density versus current density plot from the polarization curve by multiplying the potential by the current density at each point. The information provided by a polarization curve regards the fuel cell performance as a whole and the performance of individual components within the cell or different mechanisms are often not distinguishable. Polarization curves cannot be performed during normal fuel cell operation and a significant time is necessary to perform the measurement. This limitation could affect the characterization of some time-dependent processes occurring in a fuel cell [49]. Standard procedures for polarization curves have been developed by European Commission JRC (Joint Research Centre) for single fuel cells [51] and stacks [53].

Polarization curves have been widely used to investigate the effects of different catalysts and their degradation on fuel cell performance. Even if it is not possible to obtain direct information on the electrocatalyst from the polarization curve, it is a very useful tool to

assess the general status of the fuel cell. For this purpose PCs are often measured and compared before and after the test. For example Aricò et al. [54] used polarization curves to compare performance and degradation of different Pt/C and PtCo catalysts in high temperature PEM fuel cells after specific accelerated degradation tests. Wu et al. [30] recorded polarization curves during a long-term test of a 6-cells PEMFC stack to monitor performance degradation. The difference in OCV observed in the curves was supposed to be caused by the mixed potential of the Pt/PtO catalyst surface and hydrogen crossover. Hu et al. [55] used polarization curves to monitor the performance of a PBI/H_3PO_4 high-temperature PEMFC during a 500 h continuous aging life test. They concluded that the performance loss during the test was caused by membrane degradation and catalyst degradation in high temperature operation. Matsutani et al. [56] investigated the durability of Pt and PtCo catalysts with different particle sizes under load cycling operation by means of polarization curves before and after cycling.

2.5.2 Cyclic voltammetry

Cyclic voltammetry is a standard electrochemical technique for the study of electro-active species and electrode surfaces. Cyclic voltammetry is mainly used to obtain qualitative information of electrochemical reactions, search of redox couples, study reaction intermediates, and obtain stability in reaction products [49]. The potential relative to a reference electrode is scanned at a working electrode between two predetermined potential limits, increasing and decreasing linearly the potential, while the resulting current flowing through a counter electrode is monitored. The current response is then plotted as a function of the applied potential. This curve, called cyclic voltammogram, gives information about reactions and processes occurring on the surface of the working electrode [57]. A typical cyclic voltammogram recorded for a Pt-black/nafion electrode is shown in *Figure 3*.

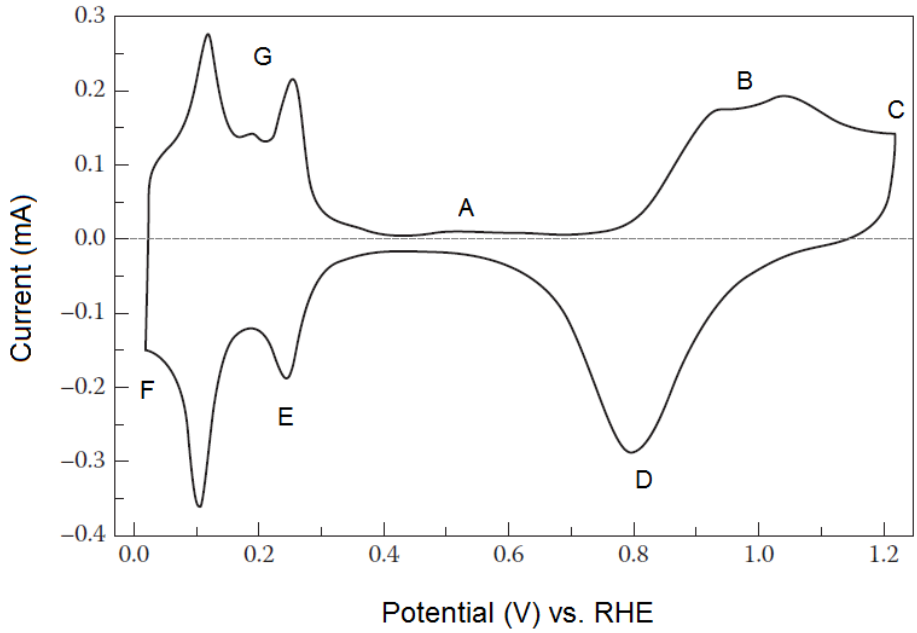

***Figure 3**. Typical fuel cell cyclic voltammogram of Pt-black/Nafion electrode* [49]*. The letters indicate the main processes taking place in the electrochemical system during the potential sweep, as explained in the text.*

Different intrinsic reaction mechanisms of the electrochemical system can cause several cathodic and anodic peaks during the potential sweep in a cyclic voltammogram. Increasing the potential from the point "A", almost no current is flowing in the system. Only a small capacitive current is present due to the charging up of the double layer. Increasing the potential to "B" after about 0.80 V Pt oxide surface is being created. In order to avoid the formation of oxygen gas, the potential is limited to 1.20 V and the direction of the potential sweep is reversed at point "C". A negative current is flowing at point "D", where the surface oxide created during the positive sweep at "B" is being reduced in the opposite reactions. At "E" a hydrogen layer is being adsorbed on the surface. A negative current is thus generated and two separated peaks are visible since hydrogen adsorbs on the electrode surface through two separated processes. Hydrogen is first adsorbing at a higher potential (about

275 mV) onto the Pt(100) sites and then at a lower potential (about 100 mV) onto the Pt(110) sites during the negative potential scan. At point “F” the second process is completed and a full hydrogen layer is created. The direction of the potential sweep is then changed again in order to avoid a further hydrogen gas evolution. Increasing the potential from point “F” the hydrogen layer is desorbed in two steps, at “G”, following the opposite reactions to the ones described after “E” [57]. Position and height of the peaks in the voltammogram can provide useful information about adsorption, desorption, diffusion and coupled homogeneous electrochemical reaction mechanisms [49]. The position of the peaks is dependent to the rate of the electron transfer at the electrode surface: when it is fast enough, compared to other processes, such as diffusion, the peak of one reaction has the maximum current at the same potential of the reverse reaction. In this case the reaction is considered reversible and the positions of the oxidation a reduction peaks are independent to the potential sweep rate, while the height of the peaks is proportional to the square root of the potential sweep rate. If on the contrary the reaction is also controlled by the rate of diffusion, the position of the reduction and oxidation peaks is separated and their distance increases with the sweep rate. In this case the reaction is considered irreversible. The electrochemical reversibility of a reaction is thus a relative condition, related to the potential sweep rate. The contribution of the charging up of the double layer is another mechanism dependent to the potential sweep rate [49,57].

It is possible to control the potential difference between the working and the reference electrodes varying the resistance of the resistor within the potentiostat. The voltage difference between the reference and the working electrodes is measured by an electrometer with very high-input impedance in order to minimize the current flowing through the reference electrode, avoiding its polarization and keeping constant its potential. The potential sweep cycle is normally repeated several times in order to obtain a stable

and reliable measure. This operation indeed activates the electro-active Pt surface and removes possible impurities [57]. The first voltammograms are thus usually not considered in the data elaboration. The sweep rate can vary from few mVs^{-1} to hundreds of Vs^{-1}, depending on the experimental conditions. Cyclic voltammetry can be performed both in *ex situ* and *in situ* experiments. In *ex situ* experiments (half-cell experiments) the properties of the catalyst are investigated using a standard three-electrode configuration, where the working electrode consists in a catalyst-coated glass carbon disk electrode while the counter electrode is usually a Pt wire, graphite, Au or other highly conductive materials with good resistance to redox environments. Cyclic voltammetry performed in half-cell experiments with a three-electrode configuration is often used to evaluate the relative activities of different electrocatalysts with the same reaction or the activity of one single electrocatalyst in different reactions. This experimental setup is not suitable to evaluate fuel cell electrodes under operating conditions. *In situ* cyclic voltammetry experiments normally employ a two-electrode configuration in which the working electrode is the electrode of interest and the other serves as both a counter electrode and a pseudo-reference electrode [49]. When the experiment is performed to investigate the properties of the cathodic electrode, the fuel cell anode is used as the counter/reference electrode, with the assumption that its polarization is small in comparison with the one imposed on the fuel cell cathode (working electrode). In this configuration, H_2 is fed at the anode that acts as a dynamic hydrogen electrode (DHE). Cathode is fed with inert gas (N_2 or Ar) and acts as working electrode. It is preferable to limit the maximum of the potential sweep to 1 V (vs. DHE) in order to avoid carbon oxidation. During the investigation of carbon supported catalysts by mean of cyclic voltammetry, carbon oxidation features can cover the H_2 adsorption and desorption characteristics.

2.5.2.1 ECSA determination

Both *in situ* and *ex situ* experimental setups are often employed to determine ECSA and catalyst utilization of PEM fuel cell electrodes [1]. Since not all the catalyst present in a fuel cell electrode is able to participate in the electrochemical reaction, because of lack of the triple boundary condition, the determination of the catalytic ECSA is particularly important in the electrocatalyst characterization. *In situ* cyclic voltammetry has been proven to be a valid technique for this purpose. From a cyclic voltammogram it is possible to obtain the charge needed to remove a monolayer of adsorbed hydrogen on the electrode and the total number of active sites. From this information, the ECSA can be determined. The charge needed to remove a monolayer of adsorbed hydrogen on the electrode surface can be calculated integrating the current of the hydrogen adsorption/desorption region of the cyclic voltammogram, both in the cathodic or in the anodic scan. The hydrogen adsorption charge on a smooth Pt electrode has been measured to be 210 $\mu C/cm^2$ of Pt loading in the catalyst layer. The ECSA of the electrode can thus be calculated using the following formula

$$ECSA = \frac{charge}{210 \times catalyst\ loading} \qquad (1)$$

where the resulting ECSA is expressed in cm^2_{Pt}/g_{Pt}, the charge in $\mu C/cm^2$ and the catalyst loading in g_{Pt}/cm^2.

As mentioned in *Paragraph 2.3.1*, CO strongly adsorb on the platinum surface, reducing its catalytic activity. The ECSA of a PEM fuel cell can also be determined with a method based on the oxidation of adsorbed CO at room temperature, under the same principle of the hydrogen adsorption/desorption method. This technique is called CO stripping voltammetry and the ECSA determined with this method is normally comparable with the one

measured with the hydrogen adsorption/desorption method. According to Pozio et al. [58] and Chaparro et al. [59] the relative error is less than 10%. One of the main limitations of CO stripping voltammetry is the uncertainty of the types of CO bonding that take place on the catalyst surface and thus of the number of CO atoms per metal atom.

Modestov et al. [60] evaluated the Pt particles growth in a HT-PEMFC PBI-H_3PO_4 MEA during a life test. A sample of the catalyst has been removed after the test and analysed in a solution of 0.5 M H_2SO_4 at room temperature with cyclic voltammetry. The average Pt particle size was 3.8 nm for pristine catalyst and increased to 7.8 nm after the durability test. Galbiati et al. [61] carried out a 6,000 h parametric investigation on PA-doped high temperature PEM fuel cells. They performed cyclic voltammetry in order to estimate the catalyst active area of the cathode electrode during the operation of the MEA. The potential of the working electrode has been swept constantly between 0.05 and 0.5 V with a speed rate of 100 mVs^{-1}. The evolution of the cyclic voltammograms with time of operation showed a distortion of the peaks in the voltage region included between 0.15 and 9.20 V. This change has been supposed to be caused by the interaction of phosphate anions with the catalyst. The hydrogen desorption peaks have been observed to decrease with time, because of a consistent ECSA reduction. The cathode catalyst active area mainly decreased within the first 4,296 h of fuel cell operation and then stabilized. In this period almost 50% of the initial ECSA has been lost.

2.5.3 Small angle x-ray scattering

Small-angle x-ray scattering (SAXS) is a technique that employs the elastic scattering produced by the interaction between x-rays and the sample to get structural information in the nm-range . The sample is invested by a monocromated and collimated x-ray beam

and the resulting scattering is recorded in the range between 0.1° and 10°. A schematic of the experimental setup is shown in *Figure 4*.

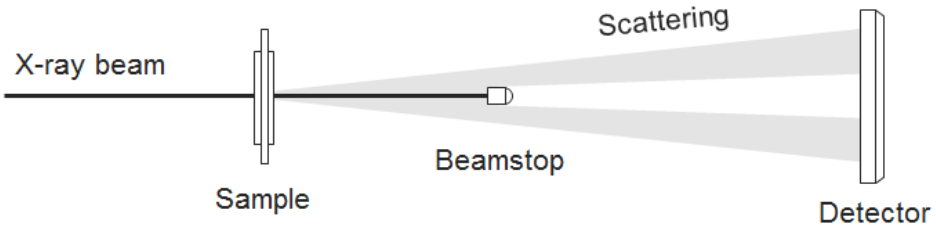

***Figure 4**. Schematic of a generic SAXS experimental setup.*

After the interaction with the sample, part of the parallel x-ray beam deviates from its path and photons scatters in other directions. The scattering is detected at small angles. The scattering patterns in the small-angle region contain structural information such as size, shape and distribution of small objects in the nm-range. SAXS patterns are formed as a consequence of the principle of wave interference. The theory employed to correlate the scattering patterns with the nanometric structure of the sample usually assumes pure elastic scattering, photon absorption and inelastic scattering are neglected. Shape and intensity of the scattering patterns are due to inhomogeneties of the electron density within the sample. SAXS is thus a technique able to detect the electron density contrast in the sample. The scattering emitted from polydisperse systems is more sensitive to large objects than to small ones because the scattering intensity is directly proportional to the square of the objects' volume. As any other scattering process, SAXS is characterized by a reciprocity law which gives an inverse relationship between the size of the object detected and the scattering angle employed. The relation between the x-ray wavelength λ_x, the half-value of the diffraction angle θ, and the lattice spacing d is defined by Bragg's law

$$n\lambda_x = 2d \sin\theta \qquad (2)$$

where n is an integer number. From *Equation (2)* it is possible to note that the larger the scattering angle the lower is the dimension measured. The dimensions in the scattering patterns (inverse space) are thus inversely proportional to the dimensions in the sample (real space). It is possible to convert the information measured in the inverse space into the real space by means of the Fourier transform. It is not possible to derive uniquely the electron density distribution in the real space from the scattering pattern because only the intensity of the scattering is measured while the phase information is lost. This information loss complicates the data analysis and allows different possible interpretation of the scattering patterns [62]. That is why complementary techniques like TEM are useful to give information that helps solving the structure obtained by SAXS.

2.5.3.1 Theory and data analysis

The scattering intensity curve is the plot of the scattering intensity against the scattering angle or the scattering vector magnitude. The small-angle scattering vector $\boldsymbol{q}$ is defined as the vectorial difference between the incident wave vector and the scattered wave vector, as shown in *Figure 5* and its magnitude can be defined [63] as

$$q = \frac{4\pi \sin(\theta)}{\lambda_x} \qquad (3)$$

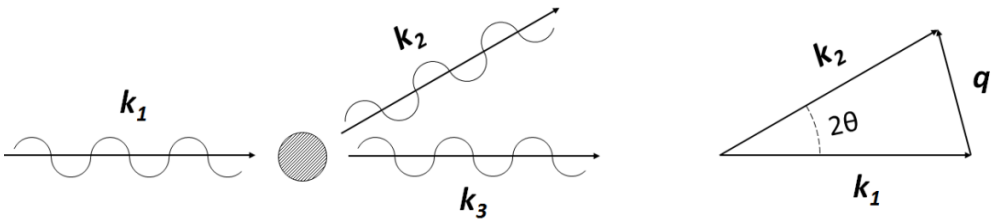

Figure 5. *Vectorial representation of the scattering vector* ***q****.* $\mathbf{k_1}$ *is the vector of the incoming wave,* k_2 *is the vector of the diffracted wave and* $\mathbf{k_3}$ *is the vector of the transmitted wave.*

The scattering intensity curve can be calculated for a given particle shape. If the particle is anisotropic, the resulting scattering can be calculated as the averaged scattering in all the directions. In order to separate the information of the single particle and the information of the presence of a multitude of particles, the scattering intensity curve may be formulated as

$$I(q) = P(q) \cdot S(q) \qquad (4)$$

where *P(q)* is called form factor and *S(q)* structure factor. The form factor is the scattering intensity of a single particle and describes its shape and size. It can be calculated by the Fourier transformation of the electron density *ρ(r)*. The structure factor represents the scattering interference of a multitude of different particles and describes their distribution and interaction. A sample with a very low concentration of particles (typically 1 mg/ml) can be approximated to an extreme condition in which the dilution is infinite and thus the structure factor is equal to 1. In this case the scattering intensity curve coincides with the form factor [63].

An alternative method to calculate the scattering intensity curve employs the pair distance distribution function (PDDF) *p(r)* that is function of the radial coordinate *r* and can be derived from geometrical considerations. The scattering intensity curve *I(q)*,

function of q, can be calculated from the Fourier inversion of the pair distance distribution function $p(r)$

$$I(q) = 4\pi \int p(r) \frac{\sin(qr)}{qr} dr \qquad (5)$$

The scattering amplitude of the particles only is proportional to their electron density ρ. Considering a more realistic case in which the particles are dissolved in a solvent, the scattering amplitude of the particles is proportional to the difference between the solute electron density ρ_2 and the solvent electron density ρ_1, while the scattering intensity is proportional to $(\rho_2 - \rho_1)^2$. For particles dispersed in a sufficiently dilute solution, the total scattering intensity can be calculated as the sum of the scattering intensities of the individual particles.

The scattering intensity curve contains the information of averaged particle size, shape, mass and electron density distribution. The analysis of the small-angle scattering intensity curve obtained from a SAXS experiment leads to the determination on these parameters. This analysis is based on the fitting between the experimental scattering intensity curve and a parametric intensity curve derived from a proper analytical model that describes the colloidal system of the sample. The development of a suitable scattering model could be challenging, since it needs complex calculations that sometimes can only be numerical. This process could also be very time consuming because a trial and error procedure could be necessary in order to find the appropriate model. The experimental scattering curve, however, possesses many useful parameters that can be quickly determined with a fitting on a limited part of the intensity curve. The radius of gyration R_g corresponds in mechanics to the radius of inertia and in a Guinier plot ($\ln I$ versus $(2\theta)^2$) it is proportional to the square root of the scattering intensity curve gradient when 2θ

tends to 0. The radius of gyration is the root-mean square of the distances of all electrons from their centre of gravity and can be used to have an intuitive measure of the particles spatial extension. A particularly useful relation for electrocatalyst analysis, where spherical particles are assumed, is the one between the radius of gyration R_g and the mean radius of the particles R

$$R_g = \sqrt{\frac{3}{5}R} \qquad (6)$$

The volume fraction of the scattering elements V_f is another useful parameter that can be calculated directly from the experimental scattering curve. It is proportional to the integral scattering Q, or invariant, which is the degree of dispersion of the scattering elements

$$V_f \propto \frac{Q}{\Delta\rho^2} \qquad (7)$$

$\Delta\rho$ is the electron density contrast. The invariant can be extrapolated from the following formula

$$Q = \int I(q) \cdot q^2 \, dq \qquad (8)$$

The pair distance distribution function *p(r)* can also be calculated from the experimental scattering curve by Fourier inversion

$$p(r) = \frac{1}{2\pi^2}\int_0^\infty I(q)\cdot qr\cdot \sin(qr)\,dq \qquad (9)$$

Another useful parameter that can be obtained before the fitting is the correlation length l_c. It can be calculated from the following formula

$$l_c = \pi\frac{\int q\,I(q)\,dq}{Q} \qquad (10)$$

From the correlation length it is possible to get information on the size of colloids. This feature may be very useful in PEMFC electrocatalyst characterization, where, for spherical particles the averaged radius of the particles can be directly obtained from the correlation length [64] as

$$R = \frac{2}{3}l_c \qquad (11)$$

From these parameters and specific scattering curves calculated for numerous three-axial objects it is possible to determinate size and shape of many macromolecules with a reasonable approximation [63]. When the particle shape is known, a size distribution may be fitted to the scattering intensity. In the SAXS analysis of PEMFC electrocatalysts spherical particles are usually assumed. This assumption is usually proven by means of a TEM experiment that is often complementary to the SAXS measurement [63].

2.5.3.2 SAXS characterization of PEMFC electrocatalysts

SAXS is an emerging technique for the nano-morphological characterization of PEM fuel cell electrocatalysts and the current literature on SAXS catalyst analysis applied to PEM and especially HT-PEM fuel cells is scarce. The fundamental difference between XRD and SAXS in PEM fuel cell electrocatalysts characterization is that XRD is able to determine size and distribution of crystallites [29,54,65–68], while SAXS offers size and distribution the entire nanoparticles.

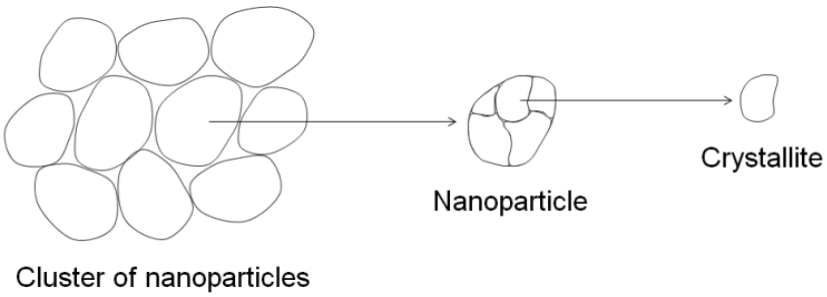

***Figure 6**. Schematic showing the difference between cluster, particle and crystallite.*

The complementary use of SAXS, XRD and transmission electron microscopy (TEM) allows a deep analysis of the electrocatalyst state and its evolution with operation, since each of those techniques offers different specific information [69]. Stevens et al. [70] employed laboratory SAXS to determine the average Pt particle size in samples of carbon-supported platinum electrocatalysts for PEM fuel cells applications. The base carbon has been fitted with a random pore model and the resulting fitting curve has been compared with the SAXS intensity scattering curves of different Pt loadings on Vulcan XC-72 with the purpose to highlight the changes in the scattering profiles due to the presence of Pt. Tsao et al. [71] used SAXS to investigate the Pt electrocatalyst structure in DMFCs with high Pt mass loading at various hot pressures. The SAXS analysis allowed the determination of size, shape, specific surface

and structure of both the primary Pt particles and the aggregates. They moreover calculated the surface-to-volume ratio for the primary Pt particles and the aggregates, showing a 40% loss due to the formation of aggregates. Speder et al. [72] investigated the influence of the Pt-to-carbon ratio on the degradation of Pt based PEMFC electrocatalysts. The effect of Pt loading on ECSA loss has been evaluated applying accelerated stress tests based on load cycling and start-stop. No clear influence of the Pt loading on the ECSA loss has been observed during load cycling, while it significantly increased with increasing Pt loading during start-stop operation. The use of synchrotron radiation to perform SAXS may overcome some limits of conventional laboratory instrumentation, since the brightness of x-ray radiation is 10^{12} times higher. In particular, beam quality can be improved by means of additional devices, even if those absorb part of the incoming radiation, and both time and space resolved measures can be performed since the exposure time can be significantly reduced. Smith et al. [73] carried out an in situ SAXS experiment on custom made fuel cells Pt-based catalysts. Pt samples with a 0.4 mg/cm^2 load of 20 wt%Pt and 40 wt%Pt have been investigated. An ageing test protocol based on potential cycling between 0.4 and 1.4 V with a sweep rate of 10 mVs^{-1} and a potentiostatic hold of 30 s every 50 mV has been used to accelerate the degradation. The particle size of the pristine samples was about 2.2 nm and 3.2 nm for the 20 wt%$_{Pt}$ and 40 wt%$_{Pt}$ samples, respectively. During potential cycling the authors observed a rapid increase of the particle size for 20 wt%$_{Pt}$ samples over the first 8 h before reaching slower growth at about 3.2 nm, while in 40 wt%$_{Pt}$ samples the particles size exhibited a steady growth during the entire test, reaching more than 4 nm after 14 h of testing. A progressive particle size increase and a slight broadening of the size distribution have been observed in both the tested samples. Hong et al. [69] observed with *in situ* synchrotron SAXS the size growth of Cu-ZnO nanoparticles encapsulated in the carbon shell during temperature-programmed carbonization. SAXS patterns have been

measured during the formation of the Cu-ZnO@C nanoparticles through a carbonization process. Before the carbonization the grains had rough surfaces in the nanometric scale and the formation of nanoparticles was absent at this stage. As the temperature increased from 70°C to 250°C in the carbonization process, small nanoparticles began to form. Ruiz-Camacho et al. [74] investigated the ORR on Pt-TiO_2-C catalysts and employed synchrotron SAXS to determinate the particle size and distribution of the electrocatalyst and its support. They recognized two regions in the scattering intensities curves: one related to the supporting carbon material (0.2-0.9 nm^{-1}) and one related with catalyst materials (0.9-4.5 nm^{-1}).

2.5.4 Transmission electron microscopy

Electron microscopes employ a beam of highly energetic electrons to provide information at micro- and nano-metric scale. These techniques allow morphological investigations of the samples as well as the analysis of their composition [1]. Transmission electron microscopy (TEM) can achieve resolutions of more than 1 nm and magnifications up to 10^7×. TEM is able to examine the nanometric structure, composition and other properties of a specimen. Objects in the order of few Angstroms can be observed. In TEM the electron beam is passed through the sample and the transmitted electrons are detected. The interaction between the electron beam and the atoms of the sample emits several types of radiation, including secondary electrons coming from the sample itself, backscattered electrons of the beam that bounce off the nuclei of atoms in the sample, beam electrons that are transmitted through the sample, X-rays, light and heat. X-rays are emitted when an electron from the core level of an atom leaves a vacancy that can be filled by an electron from a higher energy level. This radiation can be used to investigate the composition of the volume penetrated by the electron beam since the energy gap between electron levels is specific of a particular atom. Energy dispersive x-ray analysis (EDX)

can determine the composition of the sample surface by means of a special detector that detects this radiation and is often installed in combination with SEM or TEM [1]. There is a limitation on the sample thickness in the TEM experimental setup, since it has to be lower than 300 Å and even lower than 50 Å for the high-resolution transmission electron microscopy (HRTEM) [49]. The interaction between the electron beam and the atomic structure of the sample results in a phase contrast from which it is possible to assemble the image. The transmitted electrons are deflected by proper electromagnetic lenses that deviates their trajectories converging them in a single focus point. The resulting image is obtained by differential contrast between the electrons investing the sample and the transmitted electrons focused on the detector.

TEM has been widely used to investigate PEM fuel cell electrocatalysts since it enables a very detailed observation of nanoparticles. Liu et al. [75] used TEM, SEM and EDX before and after a 600 h steady-state life test of a PA-based high temperature PEMFC at a current density of 714 $mAcm^{-2}$ (for the first 510 h) and 300 $mAcm^{-2}$ (for the last 90 h). TEM indicated an increase of the Pt/C nanoparticles from 3.72 nm in the pristine sample to 7.40 nm in anode and 8.39 nm in cathode. SEM images of the cross-section showed a thinning of the electrolytic membrane after the aging test. EDS analysis revealed leaching of phosphoric acid from the PBI membrane. The authors concluded that the degradation of the electrolytic membrane, the phosphoric acid leaching and the electrocatalyst agglomeration were responsible for the performance decay during the durability test. Zhai et al. [67] investigated the stability of Pt/C catalyst in a single H_3PO_4/PBI PEMFC operated at high temperature. TEM has been used to observe the electrocatalyst sintering at the cathode. Electrocatalyst ECSA decreased fast in the first 300 h of intermittent operation (constant current of 700 $mAcm^{-2}$ for 12 h followed by 12 h shutdown) and showed only a small decrease in the following 210 h. The mean particle size was 4.02 nm for the pristine sample and 5.73 nm, 8.30 nm and 8.95 nm after 100

h, 300 h and 520 h, respectively. The results suggested that Pt particles agglomeration occurred via coalescence mechanism on carbon. EDX analysis showed that no Pt was found in the tested electrolytic membranes, suggesting that Pt dissolution probably had not occurred. Oono et al. [43] investigated the effect of operating temperature on cell performance and durability in HT-PEMFCs. Single H_3PO_4/PBI HT-PEMFCs have been subjected to long-term ageing tests at different temperatures (150°C, 170°C and 190°C). TEM analysis of the electrocatalysts after 1,000 h testing showed a growth of mean particle size from 3.8 nm, for the fresh sample, to 4.1 nm and 6.0 nm for the samples operated at 150°C and 190°C, respectively, confirming the significant influence of operating temperature on catalyst degradation. They also used TEM to study the electrocatalyst degradation mechanisms during long-term operation for periods of up to 17,860 h at 0.2 Acm^{-2} and 150°C [76].

3

Experimental

The research that has been carried out by the author on the characterization of HT-PEMFCs MEAs is presented and discussed in this Chapter.

3.1 Materials

Commercial high-temperature PEM membrane electrode assemblies (MEAs) have been tested in single fuel cells. The MEAs used in this research are Celtec®-P 1000, a series of commercial H_3PO_4/PBI MEAs for high temperature PEM fuel cells produced by BASF Fuel Cell [77]. The carbon support in the catalyst layer is Vulcan XC-72, while the electrocatalyst material is Pt-alloy (0.75 $mg_{Pt}cm^{-2}$) at the cathode and Pt (1 $mg_{Pt}cm^{-2}$) at the anode [39]. The MEAs have an active area of 45.16 cm^2 and they have been operated in single fuel cells fed with pure hydrogen and air. Graphite based plates with serpentine flow fields have been used to distribute the reactants on the MEA surfaces. The same hardware has been employed in all the experiments, except in the CV sensibility analysis discussed in *Paragraph 3.3*, where a slightly different setup has been used. PTFE

gaskets of 320 μm (anode side) and 345 μm (cathode side) have been used to assemble the MEAs in the fuel cell hardware that has been subjected to a compression given by six screws tighten at 7 Nm in order to obtain a reduction of 20% of the gaskets original thickness, as suggested by the producer [77].

3.2 Polarization curve procedures

Polarization curves have been used during the durability tests presented in *Paragraph 3.6* and *Paragraph 3.7* to assess the performance of the fuel cell. The common procedure to record polarization curves in PEMFC testing is based on the acquisition of cell voltage for a series of fixed current points, as described in *Paragraph 2.5.1*. The method that has been standardized by EU JRC for polarization curves at fixed current points for PEMFC requests long times of fixed operation on each current point. This is necessary in order to stabilize the voltage and get reliable points of the curve. There are two disadvantages of the use of this method for durability test in which the cell degradation has to be characterized. The first is the measuring time necessary to get one single curve. The second one is the effects of the measure itself on fuel cell degradation. During the acquisition of the polarization points at low currents, the cell voltage is very high and this condition has to be kept for a long time in order to obtain reliable results. This condition is significantly harmful for fuel cell electrodes, enhancing in particular the corrosion of carbon support, as discussed in *Paragraph 2.2.2*. This method has been tested following the FCTESTNET procedure [51] and it has been observed that a very long time was necessary to stabilize cell voltage in our experimental setup. EU JRC proposed an alternative standardized method to acquire polarization curves based on a variable current sweep with different rates [51]. In the variable current method the current

density is increased at fixed rates. The rate can change for different current density ranges in order to obtain different resolutions, accuracies and measuring times. In the FCTESTNET protocol it is suggested to keep a lower sweep rate in the first part of the curve (8 $mAcm^{-2}min^{-1}$ for currents lower than 100 $mAcm^{-2}$), in order to take into account the logarithmic behaviour of the activation overpotential, and to increase it in the second part of the curve (40 $mAcm^{-2}min^{-1}$ for currents higher than 100 $mAcm^{-2}$), with the purpose to reduce the testing time. It has been observed that for a polarization curve measured in the range between 0 and 500 $mAcm^{-2}$ the fixed current density method requires a measuring time of more than 1 h, while following the variable current method with those two different rates less than 23 min are enough. The measuring time of the fixed current densities method could also get longer during the test, depending on the time necessary for the voltage to stabilize for each current density with oscillations lower than ±5 mV. The comparison of the polarization curves obtained with these two methods in our experimental setup is shown in *Figure 7*. It is possible to note some differences in the results obtained with the two methods. First at all, the OCV value in the polarization curve obtained with the variable current method is lower, probably because voltage had not enough time to reach a stable value in this condition. Moreover, at the current density of 100 $mAcm^{-2}$, the instantaneous change of the current sweep rate from 8 $mAcm^{-2}min^{-1}$ to 40 $mAcm^{-2}min^{-1}$ caused a slight step in the curve. Finally, the temperature oscillation during the measurement, that in this case had amplitude of about 3°C, provoked oscillations in the values of the voltage during the acquisition. This effect is particularly evident in the region of faster current sweep rate and particularly for high current densities.

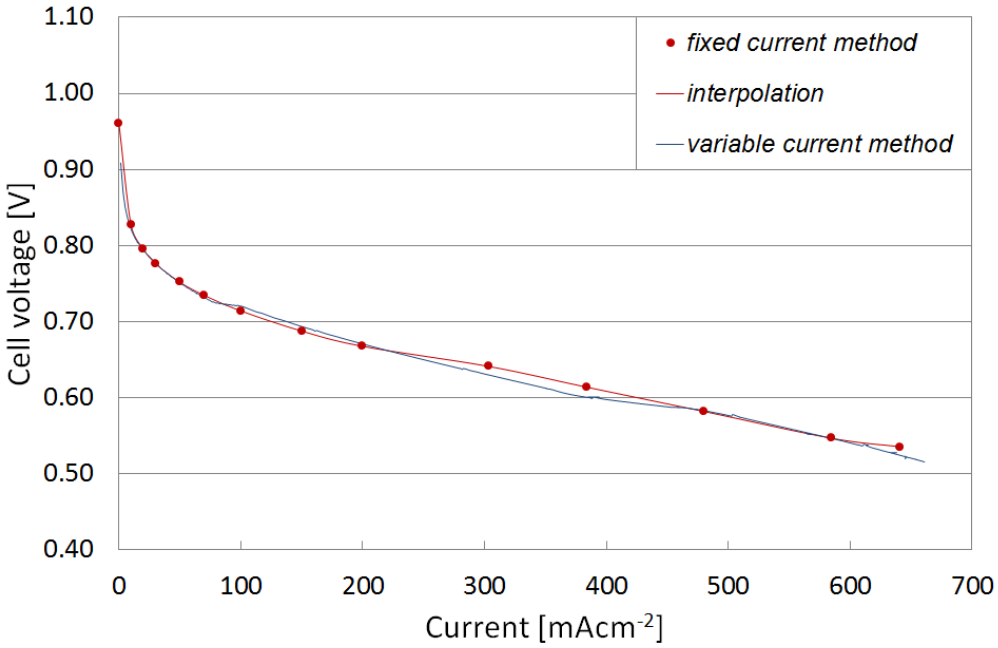

***Figure 7**. Comparison of the polarization curves acquired with the fixed current method and with the variable current method. The points measured with the fixed current method are indicated in the graph with thick red dots, while the red line is their interpolation curve. The result of the variable current method is represented by the blue curve. The followed methods are standard procedures proposed by EU JRC FCTESTNET [51].*

Despite these observations, the variable current method has been preferred to the traditional method based on fixed current steps for performance characterization during the durability tests. This choice has been done taking into account the purpose of this measure in the tests and the priorities of the experiment. This method has been preferred in order to limit the measuring time and the effects of the measure itself on the degradation of the electrode materials. During the test, however, some drawbacks related to this method emerged. First at all, the oscillations on the curve due to temperature made sometimes difficult the comparison of the curves. It has been possible to compare only the curves with the same phase in the temperature oscillation during the measurement. Moreover, the presence of the step in all the curves at 100 $mAcm^{-2}$ limited the possibility to compare these curves with other curves obtained for

the same MEAs in other works. In order to reduce the oscillations in the high-currents region of the curve, temperature variations could be reduced by a more precise control system, while the step caused by the sudden change in current sweep rate could be avoided keeping the current sweep rate constant during the measure or by changing it progressively.

3.3 Cyclic voltammetry in HT-PEMFCs

An experimental sensibility analysis has been carried out with the purpose to assess advantages and limitations of the use of cyclic voltammetry for the investigation of the electrocatalyst degradation in H_3PO_4/PBI high temperature PEM fuel cells. Cyclic voltammograms have been obtained in different voltage ranges and at different temperatures in order to understand the reproducibility of the measurements and determine a testing procedure for high temperature PEM fuel cells. The purpose of the measurements was the calculation of the electrocatalyst ECSA (as described in *Paragraph 2.5.2.1*) from the analysis of the hydrogen adsorption peak of the voltammogram.

3.3.1 Methodology

The MEAs used in this experiment are BASF Celtec®-P 2100 of 100 cm^2. The measurement has been performed feeding the anode with dry hydrogen (0.60 slpm) and the cathode with dry nitrogen (0.42 slpm). The anode has been taken as reference electrode and the cathode as working electrode. The sweep rate was 20 mVs^{-1} in all the measurements, while the scanning potential range and the operative temperature varied. A *Zahner Electrochemical Workstation IM6* has been used to perform the experiments and the *Thales Zennium-CV-software* [78] has been used to control the potentiostat, acquire the experimental data and save the results. The cyclic

voltammograms have then been analysed by means of an automatic procedure developed in *Excel®* by the Zentrum für Sonnenenergie- und Wasserstoff-Forschung Baden-Württemberg (ZSW). This procedure calculates the integral of the hydrogen adsorption peak of the cyclic voltammogram and then the electrocatalyst ECSA by means of *Equation (1)*, as described in *Paragraph 2.5.2.1*. For the ECSA calculation it has been assumed that the cathode catalyst is covered by a monolayer of hydrogen with a charge density of 210 $\mu C/cm^2$. The area obtained from the integration of the hydrogen desorption peak of a generic cyclic voltammogram is shown in *Figure 8*.

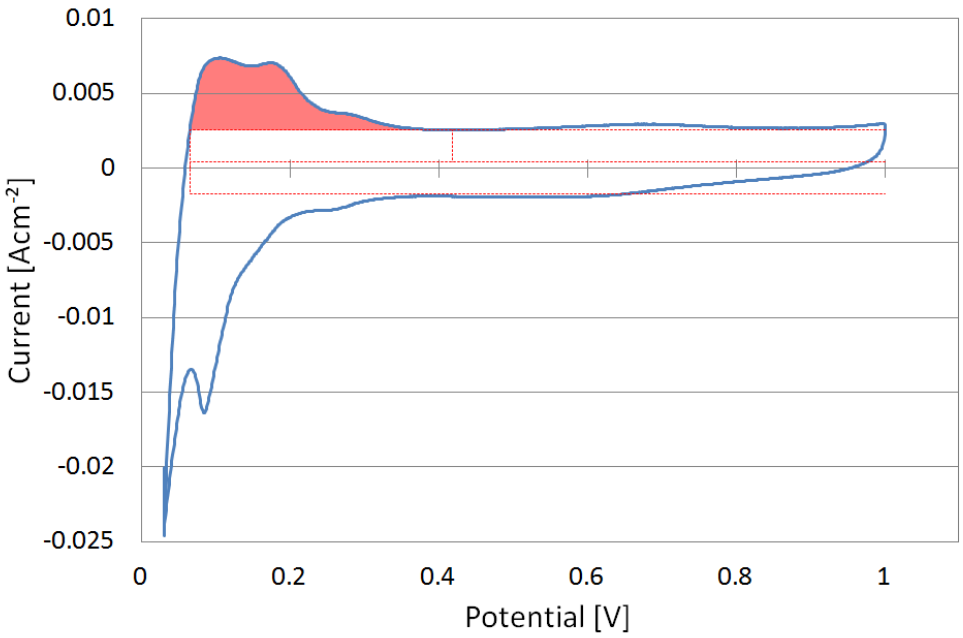

***Figure 8**. Integration of the hydrogen desorption peak by means of the Excel procedure used to obtain the ECSA from the cyclic voltammograms. The integrated area is evidenced in red on the graph.*

3.3.2 Influence of voltage sweep range

The shape of the cyclic voltammogram is strongly influenced by the range of the potential sweep that is used to perform the measurement. Moreover, for different ranges of the potential sweep different information on the electrochemical system can be obtained. The sweep rate has also a significant influence on the obtainable results, but this parameter has not been investigated in this research. The extremes of the voltage sweep have been varied in order to observe the effects on the shape of the hydrogen adsorption and desorption peaks. *Figure 9* shows the cyclic voltammograms for different minimum values of the voltage sweep, while the ECSA values calculated for these cyclic voltammograms are included in *Table 1*. V_{min} and V_{max} are, respectively, the minimum and the maximum value of the voltage sweep.

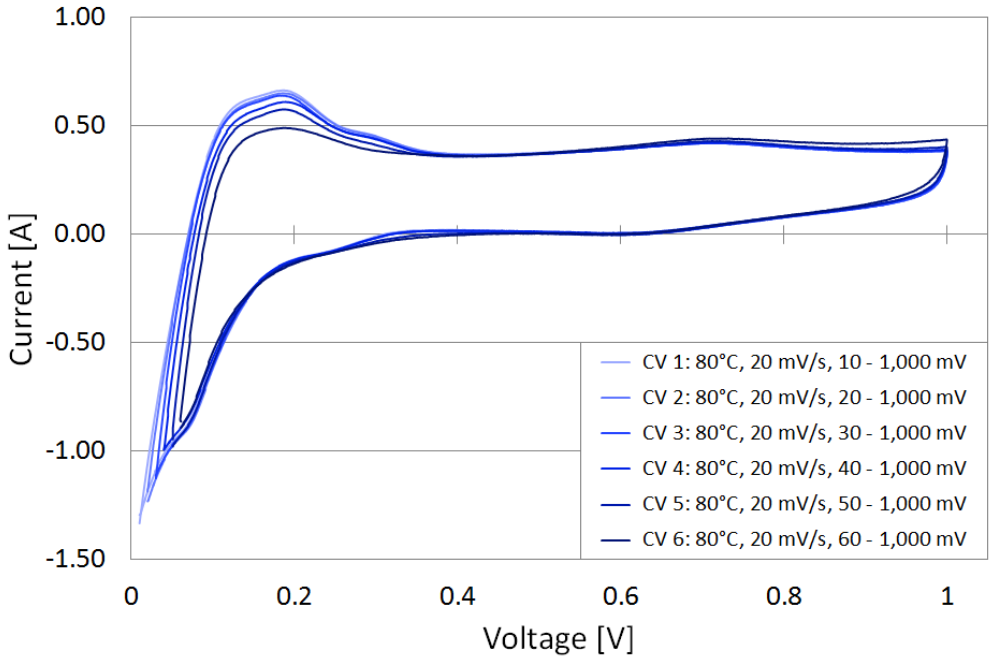

***Figure 9**. Cyclic voltammograms recorded for different minimum values of the voltage sweep range. The cell temperature is 80°C, the maximum voltage of the sweep is 1 V and the sweep rate is 20 mVs^{-1} in all the measurements.*

***Table 1**. ECSA values calculated for the cyclic voltammograms showed in Figure 9.*

Curve	**Temperature** [°C]	**Sweep rate** [mVs^{-1}]	**V_{min}** [mV]	**V_{max}** [mV]	**ECSA** [$cm_{Pt}^2 cm^{-2}$]
CV 1	80	20	10	1,000	103.0
CV 2	80	20	20	1,000	99.0
CV 3	80	20	30	1,000	95.0
CV 4	80	20	40	1,000	84.2
CV 5	80	20	50	1,000	68.4
CV 6	80	20	60	1,000	38.4

From *Figure 9* it is possible to observe that decreasing the minimum voltage of the sweep, desorption and adsorption peaks are more pronounced. The rest of the cyclic voltammogram seems to be almost unaffected by this parameter. For minimum values of the voltage sweep lower than 30 mV the shape of the hydrogen desorption peak is almost the same and the ECSA calculated from it just slightly changes. ECSA however decreases increasing the minimum value of the voltage sweep after this value.

In *Figure 10* cyclic voltammograms for different maximum values of the voltage sweep are shown. In *Table 2* the ECSA values calculated for these cyclic voltammograms are reported. In the series of cyclic voltammograms plotted in *Figure 10*, the secondary peaks for hydrogen desorption and adsorption are more pronounced compared to the series of voltammograms of *Figure 9*. The hydrogen adsorption peaks are the only part of the cyclic voltammograms that showed significant changes for different maximum values of the voltage sweep. The rest of the curve is almost unaffected by this parameter and the ECSAs calculated from the hydrogen desorption peak in each voltammogram are very similar, as shown in *Table 2*. The standard deviation of all the ECSAs calculated from the series of cyclic voltammograms plotted in *Figure 10* is just 3.38 $cm^2_{Pt}cm^{-2}$ for an average value of 173.97 $cm^2_{Pt}cm^{-2}$.

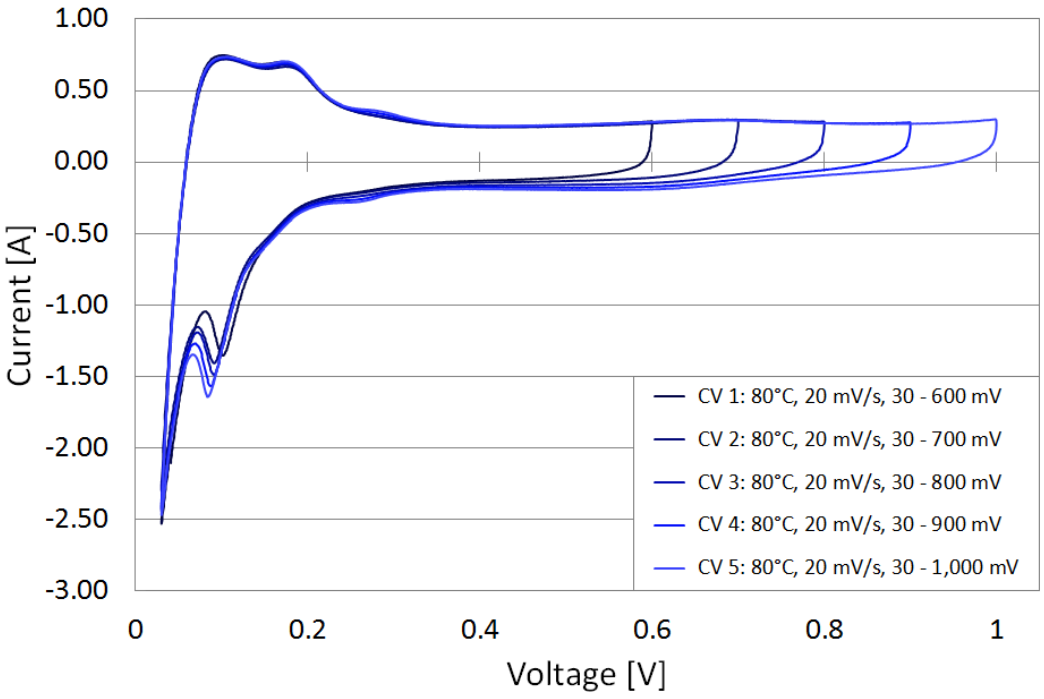

***Figure 10**. Cyclic voltammograms recorded for different maximum values of the voltage sweep range. The cell temperature is 80°C, the sweep starting potential is 30 mV and the sweep rate is 20mVs^{-1} in all the measurements.*

***Table 2**. ECSA values calculated for the cyclic voltammograms showed in Figure 10.*

Curve	**Temperature** [°C]	**Sweep rate** [mVs^{-1}]	**V_{min}** [mV]	**V_{max}** [mV]	**ECSA** [$cm_{Pt}^2 cm^{-2}$]
CV 1	80	20	30	600	175.2
CV 2	80	20	30	700	170.1
CV 3	80	20	30	800	171.2
CV 4	80	20	30	900	175.1
CV 5	80	20	30	1,000	178.4

3.3.3 Influence of cell temperature

The series of cyclic voltammograms showed in *Figure 11* have been recorded keeping constant the voltage sweep range to 50 - 600 mV and varying the cell temperature between 80°C and 150°C. Since the maximum value in the voltage sweep does not influence the hydrogen desorption peak, according to the analysis showed in *Figure 10*, the maximum voltage in the sweep has been limited to 600 mV in order to minimize carbon corrosion during the measurement. The minimum value of the sweep voltage has been set to 50 mV because at high temperatures the potentiostat was not able to perform the measurements with lower values, since the induced currents were too high. The temperature range (80°C - 150°C) in which the cyclic voltammograms have been recorded has been chosen to assess the effect of liquid water on the shape of the hydrogen adsorption and desorption peaks. The ECSA values have been calculated for all the cyclic voltammograms showed in *Figure 11* and have been reported in *Table 3*. As visible in *Figure 11*, increasing the cell temperature the area included in the voltammogram increases. In particular, the hydrogen desorption peak is higher and the hydrogen adsorption peak is much lower. The latter seems thus to be much more sensitive to temperature changes. At high temperatures a very high negative current is obtained. Moreover, at higher cell temperatures, the secondary peak is visible both in the adsorption and desorption regions, while it almost disappears below 120°C. As a consequence of higher hydrogen desorption peaks, ECSA increases with cell temperature. At 150°C ECSA is almost four times the one at 80°C.

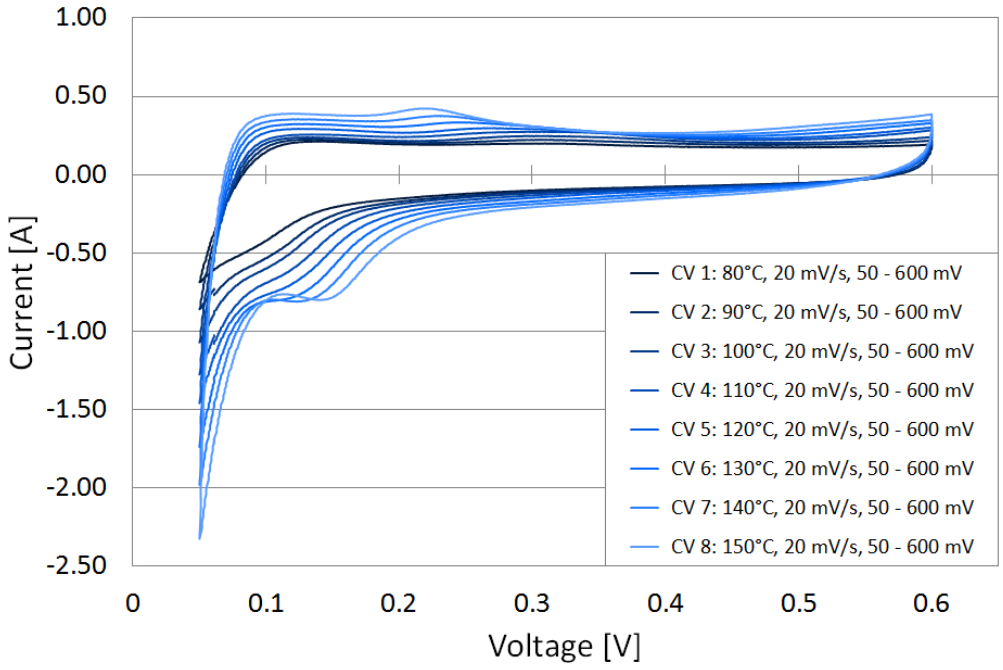

***Figure 11**. Cyclic voltammograms recorded at different cell temperatures in the range between 80°C and 150°C. The potential sweep range is between 50 and 600 mV and the sweep rate is 20 mVs^{-1} for all the measurements.*

***Table 3**. ECSA values calculated for the cyclic voltammograms showed in Figure 11.*

Curve	**Temperature** [°C]	**Sweep rate** [mVs^{-1}]	**V_{min}** [mV]	**V_{max}** [mV]	**ECSA** [$cm_{Pt}^2 cm^{-2}$]
CV 1	80	20	50	600	15.8
CV 2	90	20	50	600	16.7
CV 3	100	20	50	600	21.2
CV 4	110	20	50	600	25.4
CV 5	120	20	50	600	35.0
CV 6	130	20	50	600	43.8
CV 7	140	20	50	600	52.7
CV 8	150	20	50	600	60.1

3.3.4 Discussion of the results

From these results it is possible to conclude that cell temperature and extreme values of the voltage sweep have a significant influence on both desorption and adsorption peaks of hydrogen, while the hydrogen desorption peak seems to be unaffected by different maximum values of the sweep potential. The latter result is very important when performing cyclic voltammetry in HT-PEMFCs because at high temperatures potentials higher than 0.8 V could significantly speed up the corrosion of the carbon support. If the electrocatalyst ECSA is calculated from the hydrogen desorption peak, cyclic voltammograms can thus also be obtained sweeping the potential below 0.7 V without significant changes in the results. The minimum value of the sweep voltage, on the contrary, is a significant parameter in order to obtain well defined hydrogen desorption peaks. Minimum values of the sweep potential lower than 30 mV lead to larger peaks and below this value the changes are insignificant. For higher temperatures it could be difficult to reduce the minimum value of the sweep potential because high negative currents could be generated in order to keep very low potentials. The significant influence of temperature on cyclic voltammograms suggests the importance to keep during the measurement, when it is possible, the conditions that the fuel cell experiences during normal operation in order to obtain representative results. Performing cyclic voltammetry at 160°C, however, will imply a limitation in the choice of the minimum value of the voltage sweep, due to the high sensibility of the hydrogen adsorption current generated at low potentials.

Comparing the series of cyclic voltammograms showed in *Figure 9*, *Figure 10* and *Figure 11*, it is possible to note a substantial difference in the shape of the cyclic voltammogram. Moreover, the cyclic voltammogram *CV 5* of *Figure 10* and *CV 3* of *Figure 9* have been acquired with the same testing parameters, but the shape is anyhow quite different. As previously observed, voltammograms of *Figure 10*

have secondary peaks for hydrogen adsorption and desorption that are not visible in *Figure 9*. The reason of this difference is thus not only ascribable to the different testing parameters. The different shape of the cyclic voltammograms in the different series of measurements could be caused by different humidity conditions of the MEA during the measurements. The conditions of the MEA during the measurement seem to be very influenced by the previous state of the fuel cell. The MEAs for HT-PEMFCs used in this research are operated with non-humidified reactants and the humidification of the MEA during operation is given only by the H_20 produced from the oxygen reduction reaction (ORR). In the case of normal operation of these MEAs, the H_20 produced is in vapour state, since the operative temperature is 160°C. In order to perform the measurement in similar conditions to normal fuel cell operation, even cyclic voltammetry should be performed at 160°C and with non-humidified gases. The cyclic voltammograms presented in this research have been acquired one after the other in each series of measurements. Consequently, the humidification condition of the first measurement was very different to the last one. Also the temperature at which the measurement has been performed had an influence on the MEA humidification state. Before the acquisition of the voltammograms showed in *Figure 9*, the cell operated at 160°C and 200 $mAcm^{-2}$. Then the reactants have been switched off and the fuel cell has been cooled down to 80°C. At that point anode and cathode have been fed with dry hydrogen and nitrogen, respectively. The water produced during operation at 160°C probably was still present in the MEA and in liquid form due of the low temperature. Thus, even if the gases employed for the test were non-humidified, the MEA may have been highly humidified due to the residual water. This event probably didn't happen in the test showed in *Figure 11* because the measurements have been performed after a long flowing of dry gases and without fuel cell operation. Moreover, even if the fuel cell was not operating before the measurement, the presence of non-humidified gases could dry the MEA. At low

temperatures and without the flowing of non-humidified gases, the MEA could adsorb water from air due to the hydrophilic properties of the PBI-based polymeric electrolyte.

The influence of relative humidity on the shape of the hydrogen adsorption and desorption peaks could thus be the main limitation in cyclic voltammetry for high temperature PEM fuel cells because it is very difficult to manage during the tests. A solution could be to perform all the tests with the same procedure during the test and to use the results just to have a trend during the test instead of reliable absolute values. In this case, consecutive measurements have to be avoided. Even in this case, however, changes in the humidification state of the MEA that could be caused by degradation of other components could also result in different cyclic voltammograms. Another possible solution to this problem could be to humidify the gases during the test. This operation could help to get better defined peaks, but the measuring environment will be different than the one in which the fuel cell really operates. Cyclic voltammetry seems thus to be advantageous to monitor the ECSA evolution during durability tests only under particular conditions. Other techniques such as TEM and SAXS could bring additional information like nanoparticle size and shape, but they are not able to determine the ECSA. Cyclic voltammetry remain thus a fundamental diagnostic technique for the investigation of electrocatalysts, even if more research in needed in order to develop proper procedures for reliable measurements on HT-PEMFCs.

3.4 SAXS characterization of HT-PEMFC MEAs

Small angle x-ray scattering (SAXS) has been used in this research to characterize the electrocatalyst structural properties in HT-PEMFCs and its evolution during long-term operation. As discussed in *Paragraph 2.5.3.2*, this technique has been already used to

investigate PEMFC electrocatalysts [70–74]. The purpose of this work was to develop a non-intrusive method to characterize HT-PEMFCs MEAs. The methodological results presented in the following paragraphs, however, could also be partially extended to low-temperature PEMFC materials.

3.4.1 Methodology

Small angle x-ray scattering experiments have been carried out at the synchrotron radiation source Elettra in Trieste, Italy, at the Austrian SAXS beamline [79]. A picture of the beamline is shown in *Figure 12*.

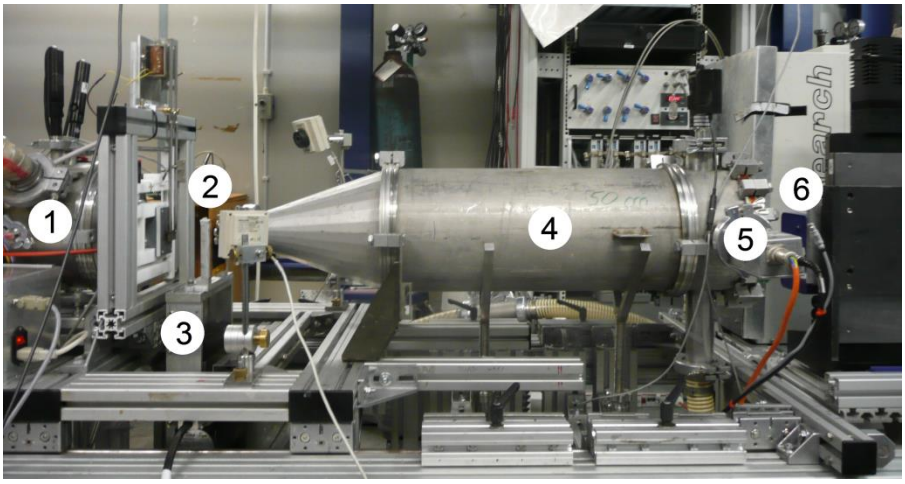

***Figure 12**. Austrian SAXS beamline at Elettra, Trieste. (1) is the ionization chamber, (2) the sample holder, (3) the sample support, (4) the vacuum tube, (5) the beamstop with diode, (6) the detector.*

The x-ray beam has been operated by transmission through the samples. The dimension of the x-ray beam used in the experiments was 1.0×0.5 mm, the wavelength was 1.54 Å and the typical exposure time was 3 s. A *Pilatus 100K* 2D detector by *Dectris Ltd. Swiss* has been used to collect the SAXS patterns that have been integrated over the azimuthal angle with the software *FIT2D* [80] in

order to obtain the experimental scattering intensity with respect to the scattering vector magnitude q. The experimental setup has been calibrated in order to determine the proper sample-to-detector distance and to define the relation between the scattering vector magnitude q and the spatial coordinates of the detector. A capillary containing silver behenate has been used for this purpose, since the scattering peaks of this material are sharp and well known. A sample-to-detector distance of 80 cm has been set up in order to resolve a q-range from 0.1 to 4.0 nm^{-1}.

The scattering intensity curves have been normalized to the same primary intensity and corrected for the sample adsorption and air scattering. The transmission signal quantifies the amount of beam that passes through the sample, allowing the comparison between different samples. It has been detected by a diode mounted in the beamstop, as shown in *Figure 12*. Air background has been quantified before each measurement measuring the scattering intensity $I_{air}(q)$ and the transmission signal J_{air} without the sample. Then a transmission factor has been calculated for each sample by the ratio

$$T_{s+air} = \frac{J_{s+air}}{J_{air}} \qquad (12)$$

where J_{s+air} is the transmission signal of the sample in air environment. The scattering intensity relative to the transmission factor of the sample can be normalized with respect to air

$$\bar{I}_{s+air}(q) = \frac{I_{s+air}(q)}{T_{s+air}} \qquad (13)$$

where $I_{s+air}(q)$ is the scattering intensity of the sample in air environment. Then it is possible to subtract the background caused by air from the scattering intensity of the sample

$$I_s(q) = \bar{I}_{s+air}(q) - I_{air}(q) \qquad (14)$$

The normalized and corrected scattering intensity curves have then been fitted with an analytical model that describes the scattering of the electrocatalyst nanoparticle system within the MEA.

3.4.2 Fitting model

The model used to fit the experimental data represents analytically the x-ray scattering of a polydispersed system of spherical particles. Electrocatalyst nanoparticles are considered as adhesive hard-spheres: they are impenetrable and an attractive potential is present between one and the other. This model, described by Pontoni et al. [81], considers a deep and attractive potential between the particles and a log-normal volume distribution of particle sizes. The volume size distribution has been employed to improve the stability of the fitting. Moreover, a generalized Porod law [82] has been used to take into account the contribution of the carbon of the GDL and the electrocatalyst support. *Figure 13* shows the parameters of the model and the inter-particles potential described by hard-sphere repulsion with an attractive square-well. R_{hs} is the hard-sphere radius, $U(r)$ is the inter-particle potential, ε is the depth of the attractive square-well and α-1 is the range of the potential in units of r. The interaction potential $U(r)$ is infinitely repulsive for $r \leq 2R_{hs}$ and the particles are thus impenetrable. When $r > 2R_{hs}$ the potential is attractive with a constant value of $-\varepsilon$ until $r = 2\alpha R_{hs}$, where it becomes zero.

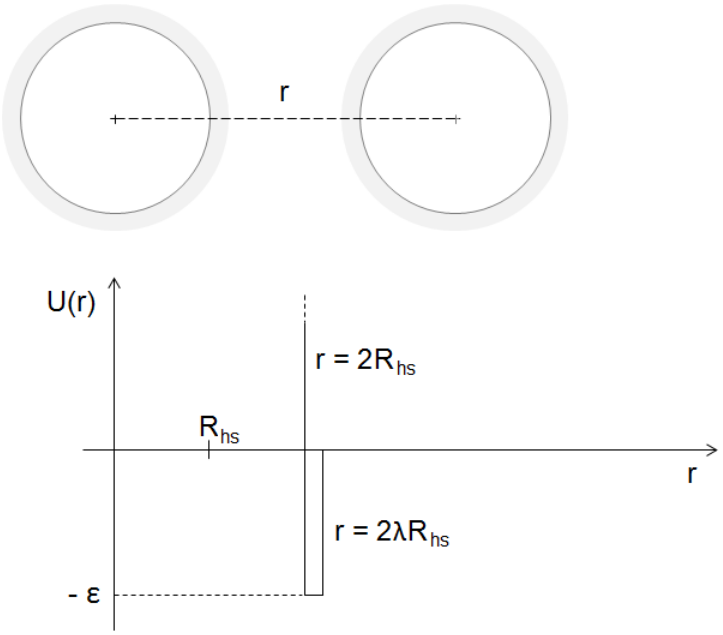

***Figure 13**. Schematic of the inter-particle potential assumed in the model employed to describe the Pt nanoparticles interactions. R_{hs} is the hard-sphere radius, U(r) is the inter-particle potential and r is the inter-particle distance [81].*

If the particles have a narrow size distribution, the formulation of the scattering intensity can be approximated as the product between the particle form factor *P(q)* and the structure factor *S(q)*, as described in *Equation (4)* of *Paragraph 2.5.3.1*. The structure factor *S(q)* has been assumed to be the same for all the particles, taking into account the same distribution for all the size-ranges of the particles. The total scattered intensity from an interacting distribution of spherical particles is proportional to the form factor averaged on all the particles $\tilde{P}(q)$, which is dependent on the size and shape of each single particle, and the structure factor *S(q)*, which is a measure of the inter-particle interference

$$I(q) \propto \tilde{P}(q) \cdot S(q) \qquad (15)$$

where

$$\tilde{P}(q) = \int_{r_{min}}^{r_{max}} f_R(r) \cdot V_P(r)^2 \cdot P(q)\, dr \qquad (16)$$

$f_R(r)$ is the distribution function of the particles size and V_P the volume of the single particle. For uniform spherical particles, $P(q)$ may be obtained with

$$P(qr) = A(qr)^2 = \left\{\frac{3[\sin(qr) - qr \cdot \cos(qr)]}{(qr)^3}\right\}^2 \qquad (17)$$

where $A(qr)$ is the scattering amplitude of a sphere of radius r. The size distribution of this type $f_R(r)$ has been described by the Schulz distribution function

$$f_R(r) = \left(\frac{Z+1}{R}\right)^{Z+1} \cdot r^Z \cdot \left[\frac{exp\left(\frac{-(Z+1)\cdot r}{R}\right)}{\Gamma(Z+1)}\right] \qquad (18)$$

where R is the particles mean radius, $\Gamma(Z)$ the gamma function and Z (Z > -1) is the width parameter related to the root mean square deviation of the radius

$$\sigma_R = \frac{R}{\sqrt{Z+1}} \qquad (19)$$

An analytical solution can then be found for the total scattered intensity [81].

The structure factor *S(q)* can be obtained by solving the Ornstein-Zernicke integral equation [81] using an appropriate interaction potential *U(r)*. The calculated structure factor can then be compared with the experimental data and information on the microscopic interactions in the system can be obtained. The particle interaction potential *U(r)* can be approximated by a square-well for colloidal systems with short ranged attraction as seen in *Figure 13*

$$U(r) = \begin{cases} \infty & r \leq 2R_{hs} \\ -\varepsilon & 2R_{hs} \leq r \leq 2\alpha R_{hs} \\ 0 & r \geq 2\alpha R_{hs} \end{cases} \qquad (20)$$

In addition to the scattering of the particles, two terms have been added: a generalized Porod scattering that accounts for large particles in the sample (like Pt aggregates, carbon fibers and polymers) and a constant that accounts for additional diffuse scattering [82]. The whole expression of the intensity scattering used to determine the structural parameters of the sample is

$$I(q) = I_0 \cdot P(q) \cdot S(q) + \frac{c_p}{q^p} + c \qquad (21)$$

where I_0 is the fitting constant for the scattering intensity of the particles, c_p is the Porod constant, p the Porod exponent and c a constant due to the diffuse scattering.

The most significant parameters imposed into the model are: the mean radius of the particles R, the root mean square deviation of the radius σ_R, the volume fraction of the particles surrounding every single particle V_f, the width α and the depth ε of the square-well of the inter-particle potential. Their numerical value has been determined as result of the fitting. Anyway, only the mean radius of the particles R and the root mean square deviation of the radius σ_R

have been considered in the present study of the MEA catalyst nanostructure.

3.4.3 Sample preparation

An experimental method to characterize the electrocatalyst nanostructure with SAXS has been specifically developed for H_3PO_4/PBI high temperature PEMFCs. For this purpose, a preliminary experiment has been carried out [83]. Some samples have been cut from a Celtec®-P 1000 MEA and the GDL has been separated from the electrolytic membrane. It was difficult to separate the catalyst layer from the electrolytic membrane because they are strongly stuck together. There was the risk that this operation would modify the structure of the electrocatalyst and thus it has been avoided. To overcome this issue, it was assumed that the sub-gasket polymer surrounding the active area of the MEA has the same scattering contribution of the polymeric electrolyte. The scattering contribution of the catalyst layer has then been assessed looking at the differences between the scattering intensity curve of the electrolyte and the curve of the electrolyte stuck with the catalyst layer. The separated layers and the entire MEA have been investigated by SAXS in transmission and the scattering intensity curves compared, as shown in *Figure 14*. The scattering intensity of the polymer (1) is two orders of magnitude lower than the others, giving a negligible contribution to the scattering of the entire MEA. The samples containing the electrocatalyst (4 and 5) showed a knee for values of the scattering vector magnitude q around 0.8. A knee in the scattering intensity curve is a signal of the presence of agglomeration of colloids with similar sizes. The curves of the polymer (1) and the GDL (3) did not showed this feature, as expected, since they do not contain electrocatalyst. The information relative to the electrocatalyst is thus considered distinguishable and not altered by the scattering of the other materials in that range of the scattering vector. Therefore it has been concluded that the

scattering intensity curve of the entire MEA can be analysed by SAXS in transmission, avoiding specific manipulations of the samples.

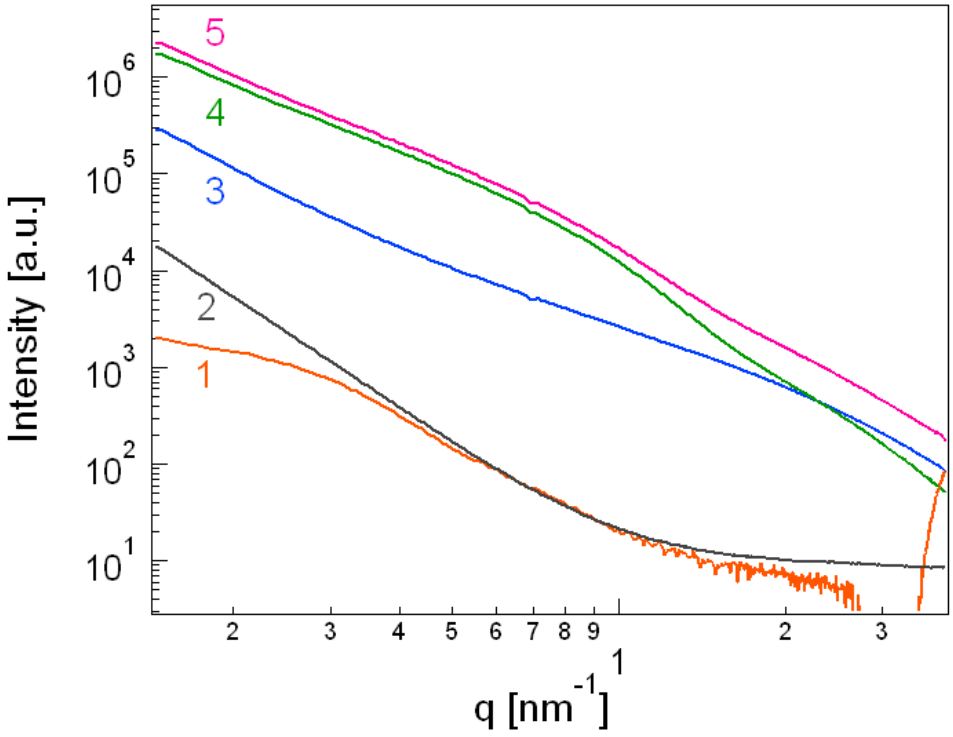

***Figure 14**. Scattering intensity curves of different layers of a Celtec®-P 1000 MEA. (1) is the polymer, (2) the carbon support in the catalyst layer (Vulcan XC-72), (3) the GDL,(4) the MEA without the GDLs, (5) the entire MEA.*

From the difference between the scattering intensity curves of the MEA without the GDL (4) and the polymer (1) it was thus possible to obtain the information of the catalyst layer, but not of the catalyst alone. The catalyst layer is composed by the catalyst, Pt and Pt-alloy nanoparticles of 3-4 nm [60], and the support, carbon particles of about 30 nm [84]. Besides the different size-scale of the particles of catalyst and support, even the electron density is significantly different between Pt and Vulcan XC-72. However, the porosity of carbon in Vulcan XC-72 particles could be comparable with the Pt

particle size. As discussed in *Paragraph 2.5.3.1*, SAXS is sensible to the differences in electron density. The difference of electron density between electrocatalyst nanoparticles and the background could be comparable with the difference in electron density between pores in Vulcan XC-72 and the surrounding carbon. For this reason it has been necessary to prove that the information of particle aggregation observed in the scattering curves is caused by electrocatalyst particles and not by porosity in the carbon support. A glass capillary has been filled by Vulcan XC-72 and analysed by SAXS. The resulting scattering intensity curve has then been compared with the curve of the MEA without GDL and the polymer, as shown in *Figure 14*. The knee relating to nanoparticle aggregation for values of q around 0.8 is visible only in curve 1. Both the curve of the polymer and the one of Vulcan XC-72 have a different shape in that range of scattering vector. Therefore it has been assumed that the observed nanoparticles are the electrocatalyst and they are also distinguishable in the scattering curve of the entire MEA (*Figure 14*).

3.4.4 Mapping procedure

In order to investigate the electrocatalyst structure on large areas of the MEA active area, a specific procedure has been developed using SAXS by transmission. The same methodology described in *Paragraph 3.4.1* and the experimental procedure to characterize HT-PEMFC MEAs presented in *Paragraph 3.4.3* have been repeated on a multitude of spots on the MEA surface. This procedure allowed the mapping of a wide area of the MEA by means of many single exposition points. The purpose of this operation was the investigation of possible changes in the electrocatalyst structure in different areas of the MEA surface. Moreover, as it will be shown in *Paragraph 3.6.5*, SAXS mapping could also be very useful to observe a two-dimensional evolution of electrocatalyst structural properties due to operation.

A HT-PEMFC MEA has been used to test the effectiveness of this method. 3,200 single expositions have been performed on a 40×40 mm area of the MEA. The schematic of the SAXS multiple expositions on the MEA is shown in *Figure 15*, where each single exposition is indicated by a red dot.

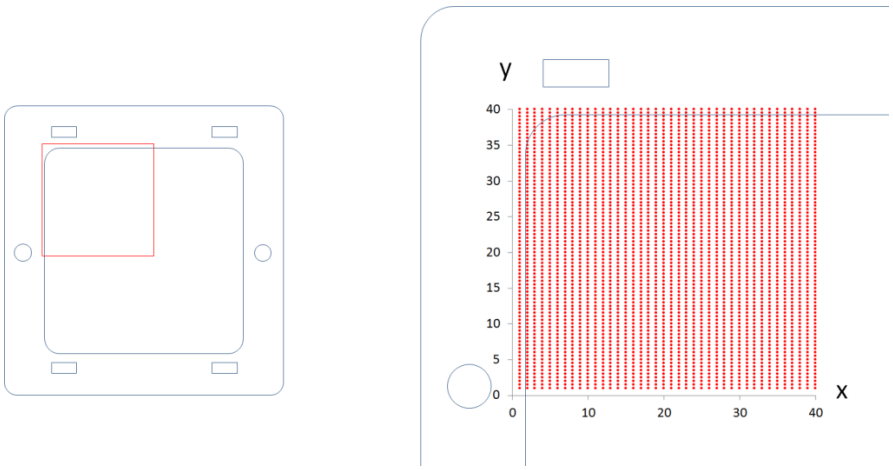

***Figure 15**. Schematic of the multiple expositions that have been performed during the SAXS mapping of the MEA. 3,200 single expositions have been performed on a 40×40 mm area of the MEA.*

Referring on *Figure 15*, the expositions have been performed every mm on the x-axis and every 0.5 mm on the y-axis. The size of the x-ray beam was 800×1,800 μm and the exposition time 3 s. From the scattering collected in each position, the intensity scattering curves have been calculated, as described in *Paragraph 3.4.1*. The correlation length is a scattering parameter proportional to the mean radius of the particles, as shown in *Equation (11)* of *Paragraph 2.5.3.1*, and it can be determined directly from the scattering data by means of *Equation (10)*, without the need of a fitting procedure. The correlation length has been calculated for each scattering intensity curve and then plotted according to the position of each exposition on the MEA surface, as shown in *Figure 16*.

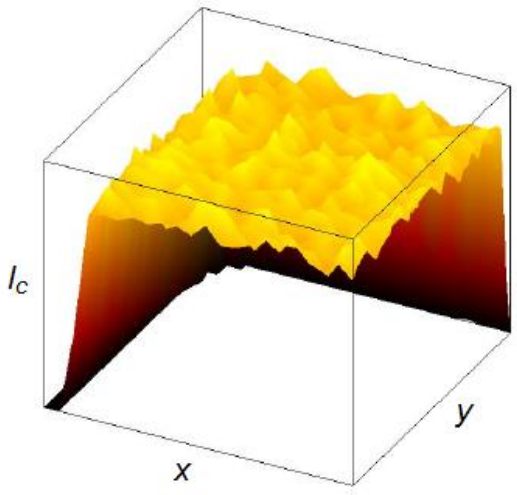

***Figure 16**. Plot of the correlation length calculated from the scattering data collected from the MEA according to the schematic shown in Figure 15.*

Additional structural information on the electrocatalyst could also be obtained for all the scattering intensity curves after the fitting. In order to fit 3,200 scattering intensity curves, an automatic procedure is necessary. Moreover, a stable and reliable fitting procedure has to be developed for a continuous and autonomous elaboration of the data. In order to fit automatically all the experimental curves, two procedures are necessary: a procedure of multiple fit to determine a reliable fit for a single curve and a procedure to repeat the multiple-fit procedure for all the curves.

The multiple-fit procedure consists in the repetition of the fitting procedure described in *Paragraph 3.4.1* with different starting values of the fitting parameters. The choice of the starting values of the fitting parameters should been done covering all the variability range of each parameter. For a first attempt of this method, 21 configurations of the 10 fitting parameters have been implemented. After the fitting of the scattering curve in the 21 configurations, a chi-square analysis has been employed to evaluate the effectiveness of the fit. The fitting curves with a high value of the chi-square have been excluded, while the fitting results of the others have been

averaged. These averaged values have then been considered the results of the multiple-fitting procedure. This method has been improved employing a genetic algorithm. The algorithm was used to optimize the combination of the fitting starting points in order to get the minimum value of the chi-square.

The second step for the data analysis was the repetition of this fitting procedure to all the 3,200 scattering intensity curves. The development of this procedure is still in completion phase. The main problem that has been faced during the elaboration of this procedure was the reduction of the calculation time. Two strategies have been considered: the improvement of the computing power of the machine used for the calculation and the use of a lower resolution for the curves to fit. The second strategy consists in the reduction of the experimental points that define the scattering curve in order to speed up the fitting process.

3.5 Design of a test bench for long-term testing

A fully autonomous test bench has been developed for single HT-PEMFC long-term durability testing. The following paragraphs describe purposes, hardware, software and operating strategies that have been implemented in the test bench.

3.5.1 Components and assembly

The test bench has been assembled at the Department of Engineering and Architecture of the University of Trieste. A picture of the test bench is shown in *Figure 17*.

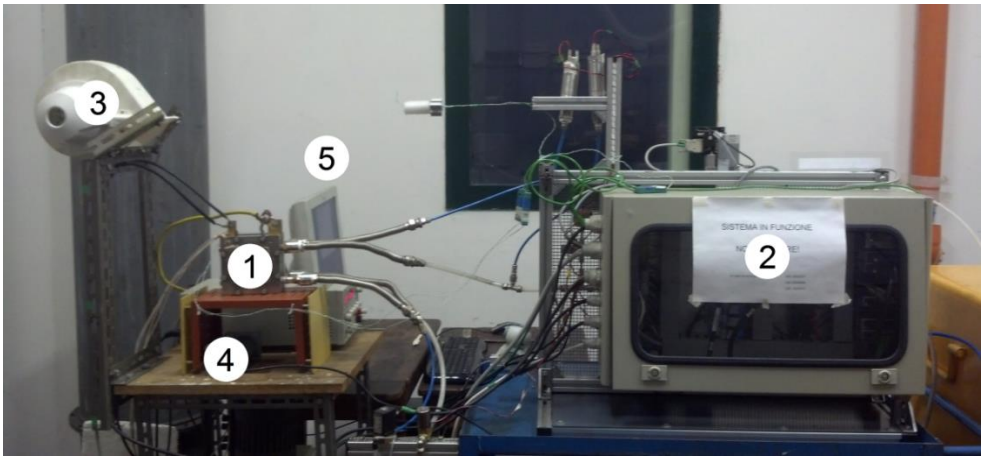

***Figure 17**. Picture of the test bench developed for the long term durability tests. (1) is the fuel cell, (2) the control system, (3) the main fan, (4) the secondary fan, (5) the PC for the control.*

The system is based on two separate lines for the supply of the reactants to the fuel cell and a third line used to introduce inert gas to purge the fuel cell. The schematic of the test bench is shown in *Figure 18*. One line feeds the anode of the fuel cell with the fuel and the other feeds the cathode with the oxidant. The fuel employed is research grade hydrogen stored in 200 bar cylinders, while the oxidant is air at ambient conditions supplied by an oil-free compressor. The gas-line used to supply inert gas to purge both electrodes is connected to the air conduit between the air inlet valve and the air flow meter, as shown in the schematic of *Figure 18*. Air circuit is then connected to the hydrogen line between the input valve and the inlet in order to allow inert gas to reach anode. During the purge operation of electrodes, air compressor is switched off, hydrogen inlet valve is closed and the valves on the line that links air and hydrogen line get open. The line that connects the air line with the hydrogen line is a critical point of the gas circuit system, since it physically could put in contact fuel with oxidant. Two solenoid valves have been placed on this linking line because of security reasons, in order to avoid the link between air and hydrogen during an unexpected failure of a valve. The inert gas that has been employed to purge the electrodes is nitrogen. It has been stored in a

200 bar cylinder, as did for hydrogen. Other inert gases could also be used to purge the fuel cell. In order to reduce the air pressure supplied by the pump, a derivation has been inserted after the pump to discharge in ambient the pressure in excess. A manual valve has been used to regulate the pressure between the two branches. The pressure reduction in the air line helped to avoid water condensation in the pipes.

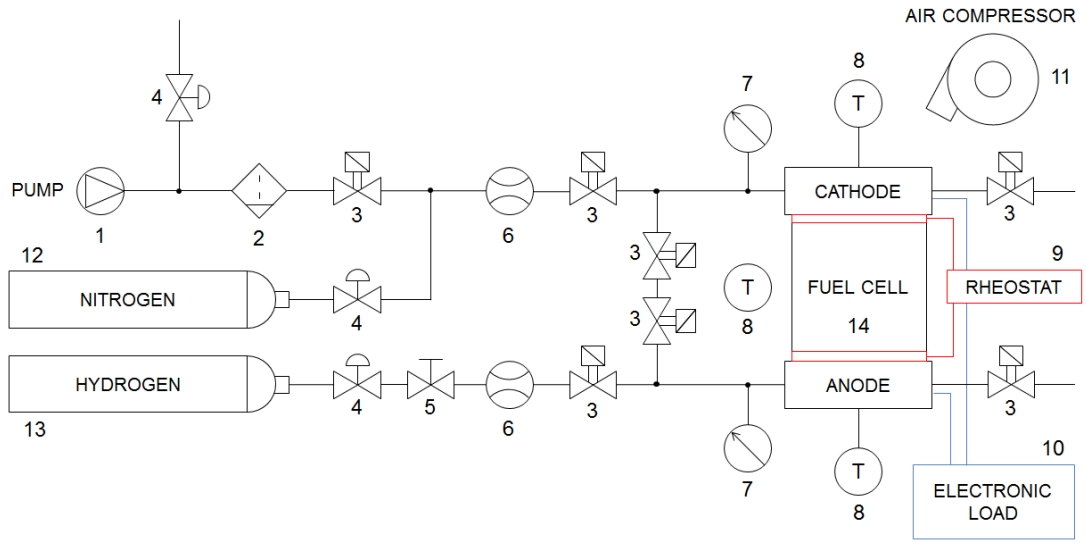

***Figure 18**. Schematic of the test bench used for the single HT-PEMFC long-term durability tests. (1) air compressor, (2) air filter, (3) solenoid valve, (4) pressure regulator,(5) manual valve, (6) mass flow controller, (7) pressure gauge, (8) thermocouple, (9) rheostat, (10) electronic load, (11) fan, (12) nitrogen cylinder, (13) hydrogen cylinder, (14) fuel cell.*

In order to control the gases supply, the test bench has been equipped with seven electromagnetic valves, two manual valves and two manual cylinder regulators. Three electromagnetic valves have been installed on the air line: one is placed before the connection with the inert gas line to stop air supply during purge operation; a second one is placed before the connection with hydrogen line; a third one is placed on the outlet of the fuel cell cathode. Two electromagnetic valves have been installed on the hydrogen line: one is placed between the manual regulator of the hydrogen

cylinder and the connection with the air line; the second one is placed at the outlet of the fuel cell anode. Two electromagnetic valves have been placed in the line that connects air line with hydrogen line, as discussed before. A manual valve has been placed after the connection of the hydrogen cylinder with the hydrogen line to allow an emergency stop of the hydrogen supply. Another manual valve has been placed in the derivation after the pump to regulate air pressure. Finally, two manual cylinder regulators have been connected between the hydrogen and nitrogen cylinders and the respective gas-lines to reduce the inlet gas pressure to a more manageable working pressure.

Two pressure transmitters have been used to measure the reactants inlet pressures. A *Sierra SmartTrack M100* and a *Bronkhorst El-Flow F201* flow-meter were used to measure air and hydrogen flow rates, respectively. Fuel cell operating temperature is regulated by a heating system based on two electric resistances placed on the fuel cell endplates and controlled by a rheostat. During shutdowns an external fan has been used to accelerate the cooling down process. K-type thermocouples have been inserted in cathode and anode endplates to measure cell temperature. A third thermocouple is used to measure ambient temperature nearby the fuel cell. Load has been controlled in galvanostatic mode by a *Thurlby Thandar Instruments TTi LD 300* electronic load. A specifically developed measurement and control system based on *National Instruments Compact Rio* hardware is used to control the whole fuel cell system and to acquire the experimental data.

3.5.2 Software development

A dedicated software has been developed in *LabVIEW*® environment to control test bench operation and acquire experimental data. All electromagnetic valves, heating system, air pump and fans are controlled by the software. Gas flow rates, gas pressures and

temperatures are measured. The software allows system control and real time visualization by means of a GUI. A screenshot of the user interface is shown in *Figure 19*.

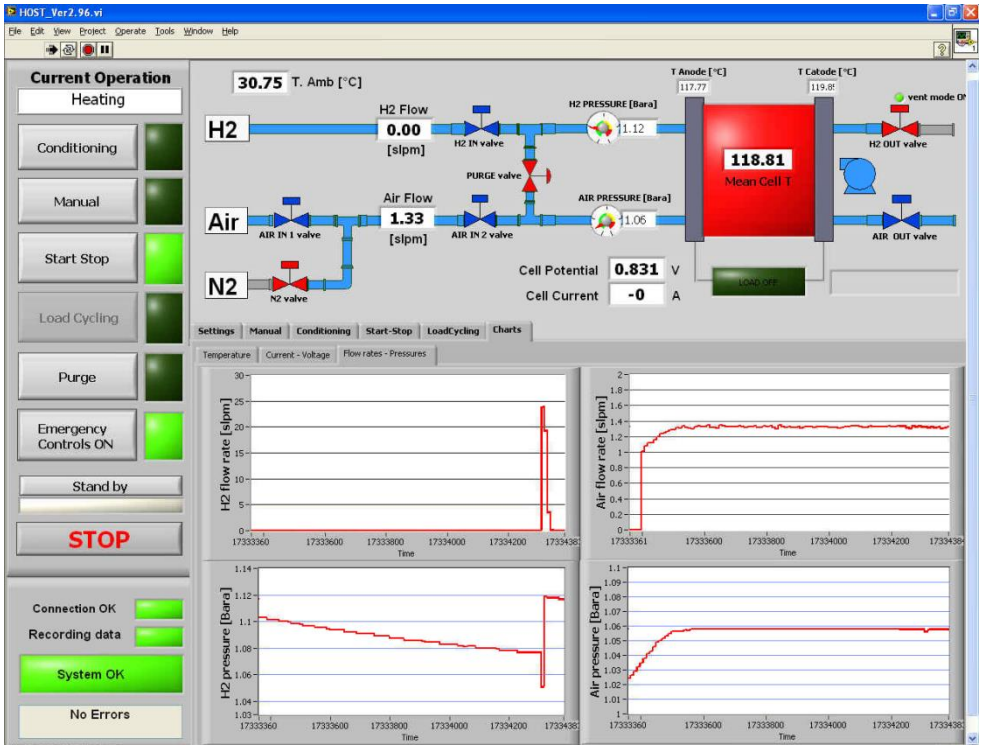

***Figure 19**. User interface of the software developed in LabVIEW® environment to control the test bench and acquire experimental data.*

A schematic of the test bench is present in the main window to offer an overview of the system status to the user. Below the schematic of the test bench, a series of windows can be activated to set several operating and diagnostic parameters. The main operative parameters are plotted in real time in a series of graphs in some dedicated slides; one of them is shown in *Figure 19*. Automatic operation modes can be started by appropriate buttons. The control system is designed to allow six operation modes of the test bench. These operative modes are described in *Table 4*.

***Table 4**. Operative modes of the test bench.*

Stand-by	All the flows, heating system, fans and electric load are off.
Conditioning	Current and temperature are set constant; this mode has been used to activate the MEAs before the durability tests.
Manual	All the operating parameters can be manually controlled by the user.
Start/stop	This mode follows the start/stop procedure described in *Paragraph 3.7.1*.
Load Cycling	The system keeps constant fuel cell temperature, while the electric load follows any specific profile.
Purge	A specific procedure is activated to purge with inert gas fuel cell electrodes.

In all the automatic operative modes, fuel cell temperature can be set. Other specific parameters can be set for each operative mode. In the "*Start-stop*" operative mode, temperature range, stand-by time and regime time between start-ups and shutdowns can be set by the user. In the "*Load Cycling*" operative mode, specific load cycle profiles can be chosen by the user. For triangular cycles a specific tool has been included to help the implementation, for more sophisticated profiles a file with the coordinates that describe the profile can be uploaded on the program. In the "*Purge*" operative mode, purging time and flow rate can be set. All these parameters are initially set to default values.

An emergency system has been implemented for an automatic management of unexpected events. It can be activated by an appropriate button. All the information acquired from the control system during operation is monitored by the emergency system and, according to the current operation mode, specific emergency procedures are activated in case of unexpected conditions. For all the operative parameters, specific numerical ranges have been

imposed. When the values of those parameters exceed the imposed range for a sufficiently long time, a safety procedure is activated. The safety procedure consists in the shut-down of the electric load, heating system and fans. Then "*Purge*" mode is activated in order to remove traces of reactant gases from the system lines and fuel cell electrodes. Moreover, the emergency procedure activates an alerting sound on the test bench and informs the users by means of emails and text messages on mobile phones.

All the operative parameters are normally recorded with frequency of 1Hz. A frequency of 10 Hz can be specifically requested. The software can be operated by remote by means of a *TeamViewer* connection. A webcam has been installed and the video is constantly uploaded online on a specific web address to allow the user to observe the test bench from remote.

3.6 Load cycling stress test

In high temperature PEM fuel cells most of the durability tests are performed to investigate the cell degradation during the operation modes that they should perform in real applications, such as constant load and start/stop. In low temperature PEMFC, dynamic load operation is widely investigated because of its importance for automotive applications. Carrying out ageing tests based on load cycling on high temperature PEM fuel cells is not intended to study their behaviour in real applications, but it could be of great interest in order to isolate the effects of electrocatalyst degradation from other mechanisms that can be favoured during other operation modes. Load cycling indeed has been proved to be a significant stressor for catalyst degradation [1,40] and it is possible to perform this operation keeping constant other parameters such as temperature and the presence of reactants flow. In this experiment, two HT-PEMFC MEAs have been subjected to 100,000 load cycles

with the purpose to accelerate the electrocatalyst degradation and limit other ageing mechanisms. The cycle profile was different in the two tests in order to investigate the effect of voltage range on degradation.

3.6.1 Methodology

All the tested MEAs have been stored in inert atmosphere before and after operation to avoid loss of phosphoric acid. Due to the hygroscopic property of H_3PO_4/PBI MEAs, they absorb water from humid environments that dilute the internal phosphoric acid content and transport it out of the polymeric membrane. The MEAs experienced humid conditions only for short periods during the assembling and disassembling of the fuel cell. Moreover, shutdowns have been performed following specific procedures based on N_2 purging in order to minimize the effects of the presence of reactants and water at low temperature. Degradation due to H_3PO_4 loss when the cell was not in operation has not thus considered. The operative temperature range recommended by the MEAs producer is between 120°C and 180°C. In all the tests the operative temperature has been set to 160°C with oscillations in the range of 3°C. Single fuel cells have been fed with pure hydrogen and air, and operated in galvanostatic mode. Before each durability test the MEAs have been activated following a break-in procedure (constant operation at 160°C and 222 $mAcm^{-2}$ for 100 h) similar to the one suggested by the producer [85]. An over-stoichiometric air flow (1.4 slpm) has been kept constant at the cathode, while the anode has been operated in dead-end mode, with a 200 mbar H_2 overpressure and a vent of 1 s every 3 min.

Fuel cell performance has been monitored during the durability tests through the measurement of cell voltage and polarization curves. The MEAs have then been analysed *ex situ* with transmission electron microscopy (TEM) and small angle x-ray scattering (SAXS)

in order to investigate the evolution of the electrocatalyst structure. A pristine MEA has been used as reference sample in order to quantify the changes occurred during the ageing tests. This process has been necessary to make a comparison between the initial and final state of an MEA through destructive *ex situ* methods such as TEM and SAXS. SAXS is not a destructive method itself, but in order to perform the experiment it has been necessary to keep the MEA in air for long periods, causing water absorption in the electrolytic membrane and consequently loss of phosphoric acid. The measurement has thus been avoided before the tests. All the MEAs used in the experiments were fresh materials and have been assumed to possess the same properties before the tests. This assumption was important not only to quantify the changes before and after the tests, but also to compare the effects on performance and degradation of the two cycling profiles.

Triangular load cycling is a common testing procedure for the aging of PEM fuel cells [7,86–88]. According to the current knowledge of the author there are no specific testing procedures available for electrocatalysts in high temperature PEM fuel cells. The load cycling protocols used in this research have been derived from the accelerated stress test protocol developed in 2009 for electrocatalysts in low temperature PEM fuel cells by U. S. DOE [86,87]. The detailed description of this testing protocol is reported in *Appendix A2*. *Table 5* compares the features of the U. S. DOE procedure and the procedures employed in this experiment. In the testing procedure proposed by U. S. DOE the voltage is cycled, but the fuel cell is not in operation, since N_2 is supplied at the cathode. The samples tested in this experiment have been operated in galvanostatic mode. The current density range of the cycles has been determined in order to obtain at the beginning of life of the MEAs a voltage range that is similar to the one suggested by U. S. DOE. In this operation it has also been taken into account the different performance between low and high temperature PEM fuel cells.

Finally, it has been preferred to operate the fuel cell in order to study the fuel cell behaviour during real operative conditions.

***Table 5**. Accelerated degradation test protocols for electrocatalysts: procedure proposed by U. S. DOE* [86,87] *and the two procedures followed in this work.*

	U. S. DOE	**MEA_a**	**MEA_b**
Fuel cell	LT-PEM	HT-PEM	HT-PEM
Configuration	Single cell	Single cell	Single cell
MEA active area	25-50 cm^2	45.16 cm^2	45.16 cm^2
Cycle profile	triangle	triangle	trapezium
Range	0.6-1.0 V	10-500 $mAcm^{-2}$	0-500 $mAcm^{-2}$
Sweep rate	50 mVs^{-1}	61.25 $mAcm^{-2}s^{-1}$	71.43 $mAcm^{-2}s^{-1}$
Number	30,000	100,000	100,000
Cycle period	16 s	16 s	16 s
Temperature	80°C	160°C	160°C
Relative humidity	100% RH a/c	non-humidified	non-humidified
Reactants	H_2/N_2	H_2/air	H_2/air
Pressure	atmospheric	atmospheric	atmospheric

The load profile used on the sample MEA_a consisted in a triangle sweep cycle of 16 s between 10 and 500 $mAcm^{-2}$. The one used on MEA_b consisted in a trapezoidal sweep cycle of 16 s between 0 and 500 $mAcm^{-2}$. The cycle profile in MEA_b is a trapezoid because the minimum load (OCV) is kept constant for 2 s. The purpose was to observe the effects of OC cyclic operation on performance and catalyst evolution during long-term operation. Since the cell voltage needs some seconds to stabilize after a change in current density, the latter has been kept constant for 2 s to approach the OC condition in each cycle. The two load profiles are shown in *Figure 20*.

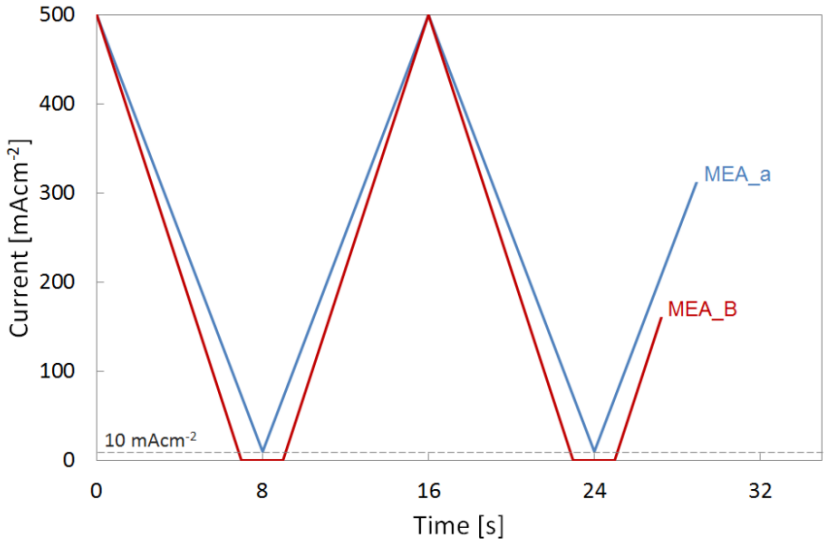

***Figure 20**. Current density profile used for the load cycling test on MEA_a and MEA_b.*

The two load profiles are similar: they have the same maximum current (500 $mAcm^{-2}$), the same period (16 s), a similar shape, similar minimum current (10 and 0 $mAcm^{-2}$) and similar sweep rates (61.25 and 71.43 $mAcm^{-2}s^{-1}$). The sweep rate and the cycle profile are slightly different because of the permanence of 2 s at 0 $mAcm^{-2}$ in MEA_b. The difference in the minimum current density of the two profiles (10 $mAcm^{-2}$) is small if compared to the entire sweep range, but it is significant because OC condition strongly accelerates degradation, as discussed in *Paragraph 2.3.3*. The purpose of these testing procedures is thus to quantify the effects of periodic OCV time during dynamic operation on performance and state of the electrocatalyst comparing the results of the two tests. MEA_a and MEA_b have been thus cycled with slightly different load profiles, but both total number of cycles, period of the cycle and fuel cell operative conditions, such as temperature, pressure and reactants, were identical. The total number of load cycles performed in each test was 100,000. Considering both the activation time and load cycling, each MEA reached almost 450 h of continuous

operation without significant interruptions. The start-up at the beginning of the break-in procedure and the shutdown at the end of the test followed specific automatic procedures that have been implemented in the test bench in order to avoid water condensation in the cell. During the start-up the fuel cell has been heated up from ambient temperature to 120°C, a minimum current density of 100 $mAcm^{-2}$ has been set, and then it has heated up to 160°C and the nominal current density of 222 $mAcm^{-2}$ has been applied in order to start the beak-in procedure. The shutdown procedure consisted in disconnecting the load, purging anode and cathode with N_2, cooling down to 120°C, stop the N_2 purge, cooling down to 80°C with the outlets open, closing the outlets and cooling down to ambient temperature. The parameters that have been measured and saved during the whole test, including the activation time, are: anode temperature, cathode temperature, ambient temperature, anode inlet pressure, cathode inlet pressure, anode flow rate, cathode flow rate, current density and cell voltage. Moreover, polarization curves have been recorded after the activation time and every 10,000 cycles until the end of the test. The procedure followed to obtain the polarization curves is the FCTESTNET variable current sweep method described and discussed in *Paragraph 3.2*.

3.6.2 Performance analysis

The performance of the two cycled MEAs has been assessed by means of the polarization curves that have been periodically measured during the tests. During the activation period of 100 h in steady-state operation at 222 $mAcm^{-2}$ the trend of the cell voltage was very similar in the two MEAs. This result allows supposing equivalent initial performance in the two samples. *Figure 21* shows the first 50 h of break-in time of MEA_a and MEA_b.

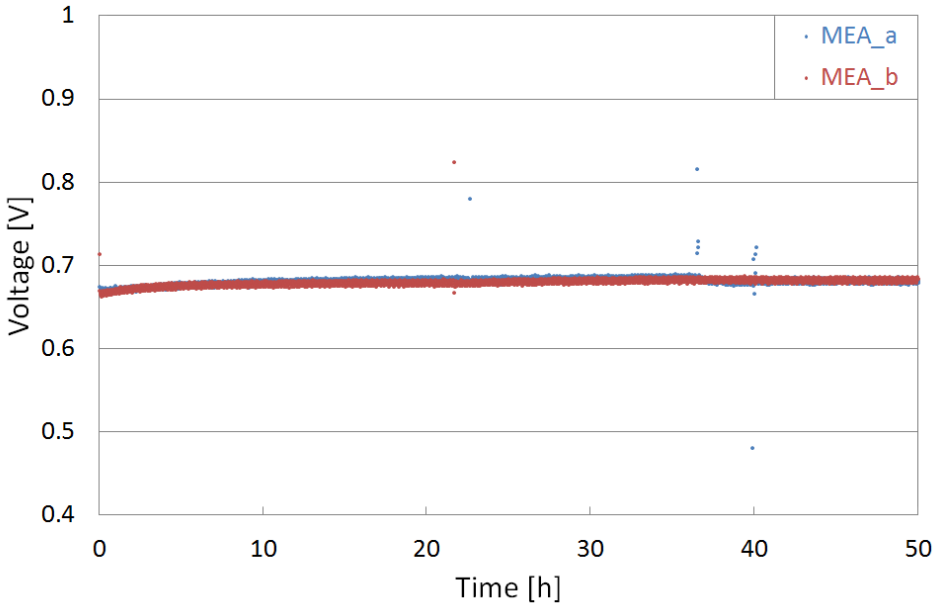

Figure 21. *First 50 h of 100 h break-in time at 222 mAcm^{-2} of MEA_a and MEA_b.*

The voltage of MEA_a presents a slight step at about 37 h of operation: the cause could be a small reduction of the H_2 inlet pressure. The initial cell voltage at 222 mAcm^{-2} was 0.66 V at the beginning of the tests, it increased for the first 30 h and then it kept constant at 0.68 V for the 60 h left. The voltage increment during the activation time was thus about 20 mV in both the MEAs.

During load cycling the averaged voltage decay rate at 200 mAcm^{-2} was about 152 nV/cycle for MEA_a and 203 nV/cycle for MEA_b or 34 µVh^{-1} for MEA_a and 45 µVh^{-1} for MEA_b, considering 450 h of operation. The voltage decay rate obtained by Galbiati et al. [61] in a 540 h steady-state durability test on a similar MEA was 6 µVh^{-1} at 200 mAcm^{-2}. The load cycling operation significantly enhanced performance degradation. Furthermore, comparing the two dynamic tests, the presence of OC operation in the cycle (MEA_b) had a noticeable effect on voltage decay. *Figure 22* and *Figure 23* show the polarization curves of MEA_a and MEA_b, respectively, just after the activation time and after the durability test.

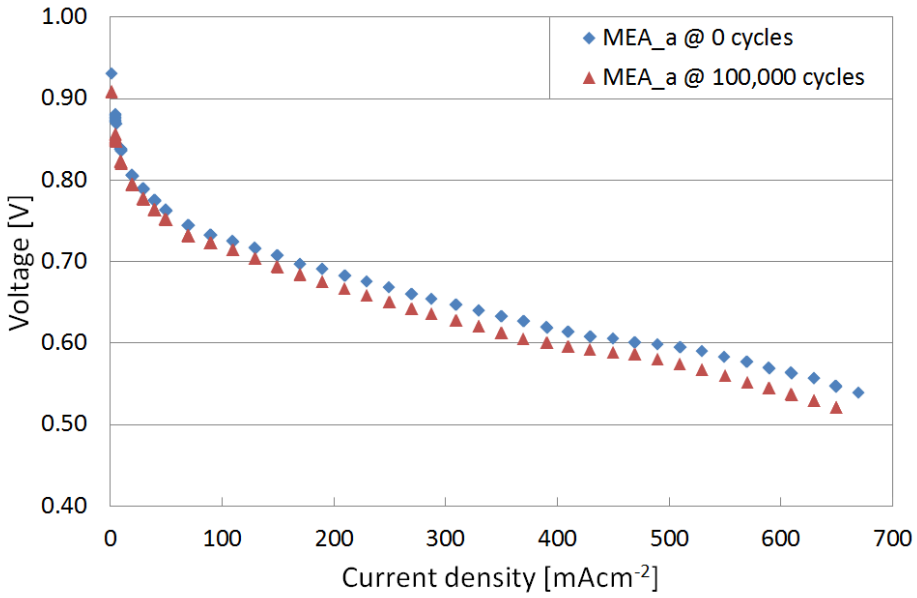

Figure 22. *Polarization curves of MEA_a after 0 and 100,000 load cycles. The curve at 0 cycles has been obtained just after the activation period of 100 h at steady-state operation.*

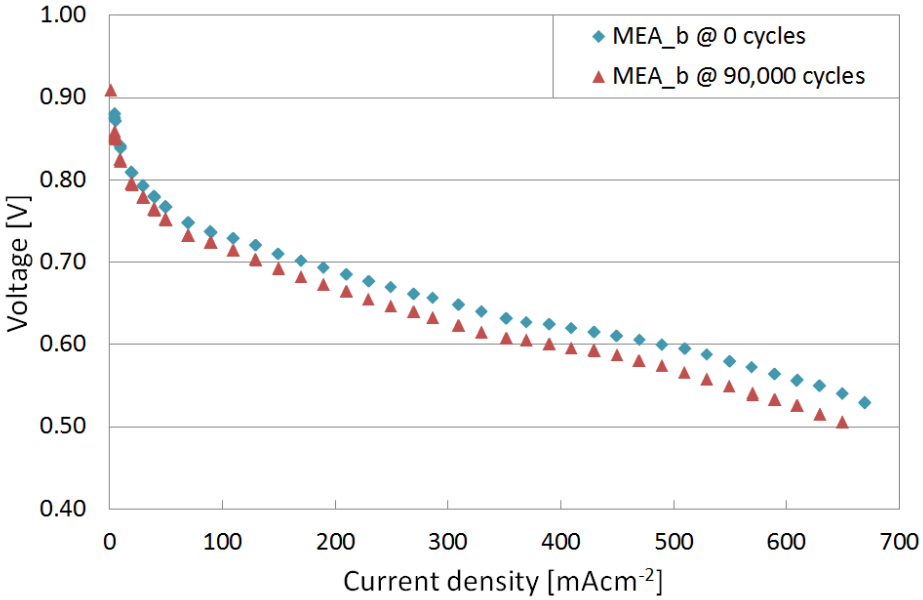

Figure 23. *Polarization curves of MEA_b after 0 and 90,000 load cycles. The curve at 0 cycles has been obtained just after the activation period of 100 h at steady-state operation.*

The second curve reported in *Figure 23* for MEA_b is the polarization curve after 90,000 cycles because the one at the end of the test (100,000 cycles) was difficult to compare with the one at 0 cycles, due to the oscillations caused by temperature described in *Paragraph 3.2*. The difference between the polarization curves after 90,000 and 100,000 cycles, however, is negligible. The performance decay of both MEAs during the accelerated degradation test is lower than 3% at 200 $mAcm^{-2}$. At higher current densities (600 $mAcm^{-2}$) the performance loss is more than 4% in MEA_a and more than 5% in MEA_b. The larger performance degradation at higher current densities in MEA_b can be attributed to the voltage cycling up to OCV, since all the other operative conditions in the two tests were similar, as previously discussed. A possible explanation could be an increase of the carbon support corrosion in the catalyst layer due to higher cycling potentials. The modification of the pore structure of the catalyst layer may have increased the mass transport losses and decreased the cell performance at high current densities. An intermediate value of the cell voltage is shown in *Figure 24* and *Figure 25*, where it is reported at 50, 200 and 600 $mAcm^{-2}$ during the load cycling test of MEA_a and MEA_b, respectively.

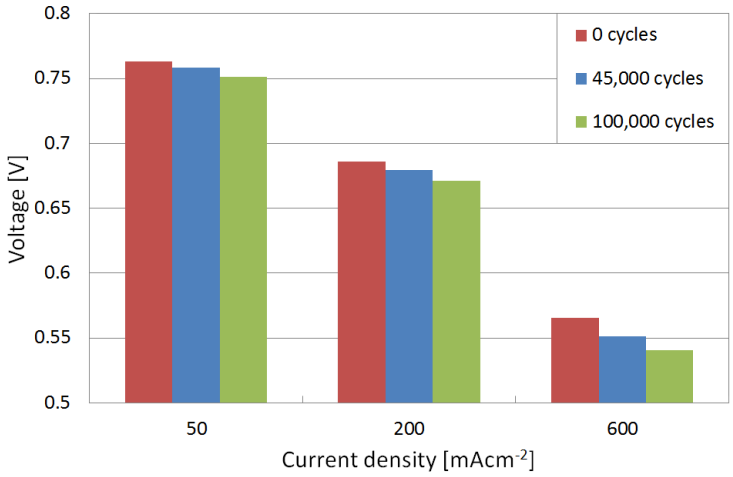

Figure 24. *Voltage recorded at 50, 200 and 600 $mAcm^{-2}$ during the load cycling test of MEA_a.*

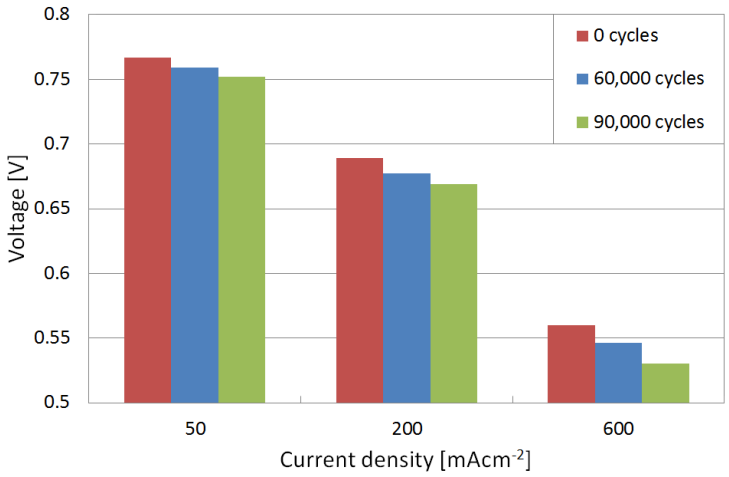

Figure 25. *Voltage recorded at 50, 200 and 600 mAcm^{-2} during the load cycling test of MEA_b.*

Both in MEA_a and MEA_b the cell voltage decay is almost linear for all the current densities considered in *Figure 24* and *Figure 25*. This suggests uniform performance decay during both the tests.

These results have been compared with the targets suggested in the U. S. DOE protocol revised in 2009 reported in *Table 13* of *Appendix A2*. This protocol refers to low temperature PEM fuel cells and the test procedure is substantially different than the one employed in these tests. However, the comparison could be interesting in order to assess the performance degradation. *Table 6* reports the U. S. DOE performance targets for the accelerated degradation test [86,87] described in *Table 5* for the electrocatalyst in single PEMFCs and the results obtained from the samples MEA_a and MEA_b after the long-term durability test.

***Table 6**. U. S. DOE targets for the accelerated degradation test for PEMFCs* [86,87] *described in Table 5 (Paragraph 3.6.1) compared with the voltage loss in MEA_a and MEA_b after the long-term durability tests.*

	U. S. DOE	**MEA_a**	**MEA_b**
Fuel cell	LT-PEM	HT-PEM	HT-PEM
Configuration	Single cell	Single cell	Single cell
Reactants (a/c)	H_2/ N_2	H_2/ air	H_2/ air
Number of cycles	30,000	100,000	100,000
Temperature	80°C	160°C	160°C
Voltage loss	<30 mV	24.8 mV	29.6 mV
	@ 800 $mAcm^{-2}$	@ 600 $mAcm^{-2}$	@ 600 $mAcm^{-2}$

Both the MEAs operated in this research showed voltage decay lower than 30 mV at 600 $mAcm^{-2}$ after the 100,000 load cycles test. The comparison of these results with the U. S. DOE protocol, however, has to be done considering that fuel cell technology and operating conditions are different, even if some parameters like the cycle profile are similar.

3.6.3 SAXS characterization

The two cycled samples (MEA_a and MEA_b) and a pristine one (MEA_ref) have been analysed with SAXS in transmission. The experimental methodology and the fitting model are the same described in *Paragraph 3.4*. The Schultz distribution described in *Equation (18)* has been substituted with a log-normal distribution since it has been noted that it improves the fitting quality. Three different points have been analysed on each MEA with the purpose to determine eventual macroscopic changes of the electrocatalyst properties in different areas of the MEA. The position of each point was the same in all the samples. *Figure 26* shows the position of these points on the MEA surface.

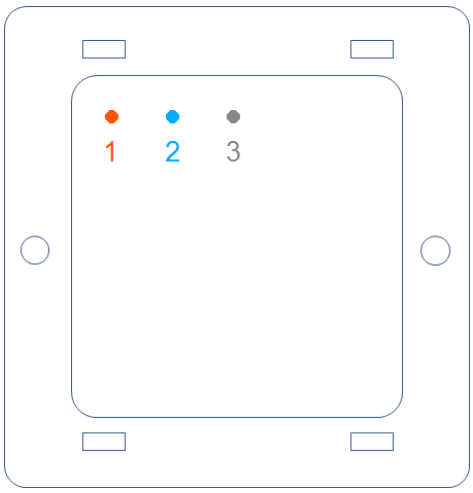

Figure 26. *Position of the beam expositions that have been performed on each sample during the SAXS characterization.*

The nine scattering intensity curves (three for each sample) are shown in *Figure 27*.

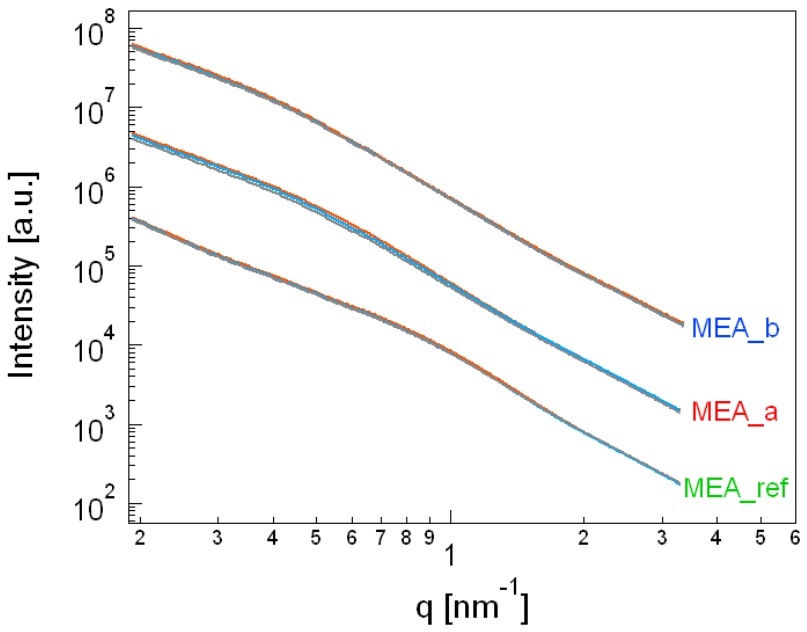

Figure 27*. Scattering intensity curves of MEA_ref, MEA_a and MEA_b. The intensities of the three sets of curves (one for each MEA) have been scaled by a factor of 10 to each other in order to resolve better the differences.*

The curves of each sample are very similar to each other: this feature suggests absence of macroscopic differences in the nanostructure of the electrocatalyst in different areas of the same MEA active area. Comparing the curves of the different samples, a different shape is visible. In particular, the knee indicating the nanoparticles agglomeration is shifting towards lower values of q moving from MEA_ref to MEA_b. This feature indicates an increase of the mean particle size due to the Bragg's law. The main parameters determined with the fitting of those curves are the mean radius of the nanoparticles and their standard deviation: they are reported in *Table 7* for each sample. The results obtained in the three different positions of the same sample are very similar, while they differ between different samples. The mean radius averaged on the three analysed points of the reference sample MEA_ref is 2.61 nm, the one of MEA_a is 4.54 nm and the one of MEA_b is 5.28 nm. Referring to the sample MEA_ref, electrocatalyst nanoparticles are thus the 74% larger in MEA_a and the 102% larger in MEA_b. The fitting error in the mean radii calculated for the three single measurements for each set is lower than 0.2 nm.

***Table 7**. Mean radius and standard deviation resulted from the fitting of the three points analysed for each sample (MEA_ref, MEA_a and MEA_b). For each sample, both mean radius and standard deviation are averaged on the three analysed points.*

Sample	**Position**	**Mean radius (R)** [nm]	**Standard deviation (σ_R)** [nm]
MEA_ref	1	2.596	0.822
	2	2.638	0.782
	3	2.609	0.774
	average	**2.614**	**0.793**
MEA_a	1	4.385	1.783
	2	4.651	2.077

	3	4.582	2.038
	average	**4.539**	**1.966**
MEA_b	1	5.379	3.002
	2	5.248	2.928
	3	5.224	2.949
	average	**5.284**	**2.960**

The size distribution curves showed in *Figure 28* have been calculated with the mean radius and the standard deviation obtained from each fit.

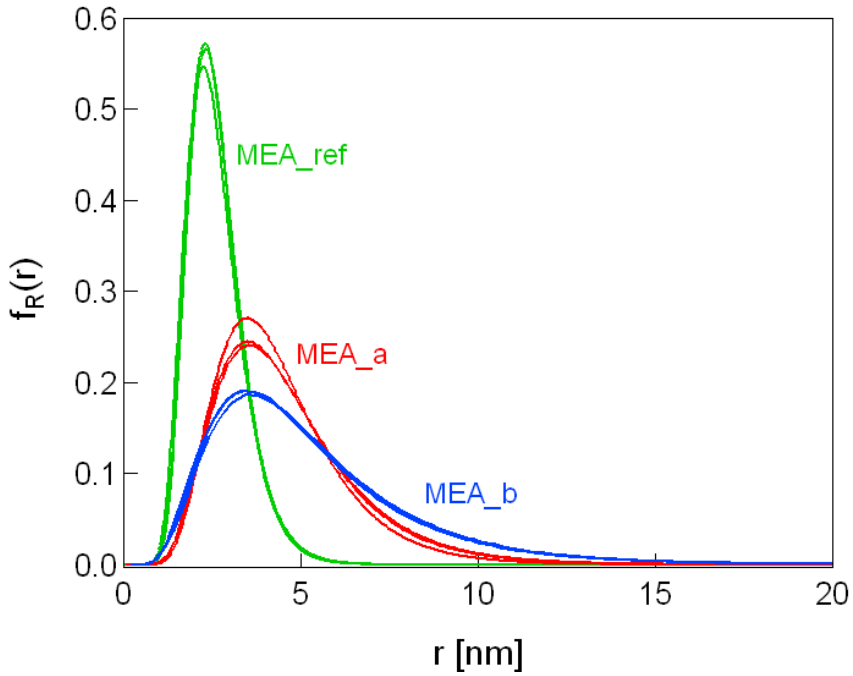

***Figure 28**. Volume size distributions of each of the three points in MEA_ref, MEA_a, and MEA_b. The distributions have been calculated from the mean radii and standard deviations reported in Table 7.*

The size distribution curves calculated for each MEA in different points are very similar, while a substantial difference is visible between the curves of different samples. The width of the size

distribution curves of MEA_ref is significantly smaller than the one in the other two sets of curves. This change indicates a large increase of the particle size polydispersity in the cycled samples. The reason of this phenomenon could be a growth of the particles by coalescence. Since the results are an average of the features of cathode and anode, the polydispersity could also be enhanced by different growth dynamics in the two electrodes. Indeed, both electrocatalyst composition and electrochemical environment are different in cathode and anode [29,39,89]. A separate analysis of anode and cathode electrodes could clarify this supposition. Grazing incidence SAXS could be used for this purpose. Comparing the curves of the cycled samples MEA_a and MEA_b, it is possible to note that the width of the size distribution is larger in MEA_b, while the position of the maximum of the two curves on the axis of the mean radius is similar. The extension of the current cycle profile down to OCV condition, as expected, seems to have a significant influence on the evolution of the electrocatalyst during operation in the durability tests. Both polydispersity and mean size of the electrocatalyst particles seems to be affected by this operative condition.

3.6.4 TEM characterization

Transmission electron microscopy (TEM) has been employed as a complementary technique to SAXS to investigate the electrocatalyst nanoparticles. It was necessary to prove some assumptions introduced in the analytical scattering model such as the nanoparticle shape and polydispersity. Moreover the particle sizes measured on the TEM images have been compared with the SAXS results in order to prove the validity of the experimental procedure.

3.6.4.1 Methodology

Samples of about 5×20 mm have been cut off from the MEAs and the GDL has been removed by peeling. The catalyst layer that was still stuck to the electrolytic membrane has been scratched off and the resulting powder has been stored in plastic vials before the TEM analysis. The samples of the catalyst layers of the three MEAs have been analysed at the Chemical Engineering department of the Delft University of Technology, The Netherlands. A *Philips CM300UT-FEG* electron transmission microscope has been used with a point resolution of 0.17 nm and an information limit of 0.1 nm. The microscope has been operated at 200 kV and the images were acquired with a *TVIPS CCD* camera. The samples were prepared by immersing a *Quantifoil R* copper micro-grid in a dispersion of powder consisting of catalyst prepared in ethanol. The obtained TEM images have been analysed with the software *ImageJ* [90] in order to determine the mean particle size and the standard deviation. Since the contrast of the images was too low for an automatic analysis, the determination of the particles size has been done manually. The images have been first normalized in nm. Then, each single particle has been drawn by hand on the TEM images and the particle shapes have been separated from the background. The steps of this procedure are shown in *Figure 29*.

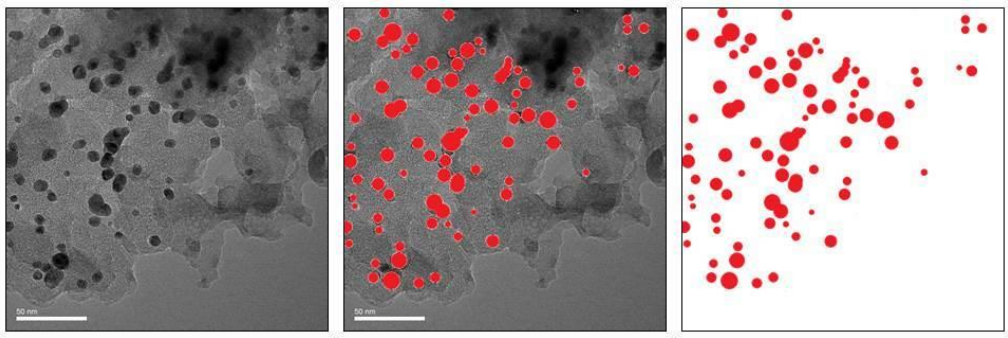

***Figure 29**. Procedure for the identification of the electrocatalyst nanoparticles in the TEM images. The first image is the raw TEM image; the second one shows the draw of the particles on the original TEM image; the third one shows the drawn particles alone after the removal of the background. The calculations have been done on the third image.*

Then the area of each single particle has been calculated by an automatic procedure of the software and the size has been calculated from those values assuming spherical particles. For each image, the sizes have been averaged and the standard deviation has been calculated.

3.6.4.2 Results and discussion

Several TEM images have been obtained for both cathode and anode side of each sample. A representative image of cathode and anode of each sample is shown in *Figure 30*. The shape of the catalyst nanoparticles is almost spherical in most of the particles visible in the 2D images. The assumption done in the SAXS model is thus verified. Moreover, it is visible a growth of the particles from the reference state in MEA_ref to the operated samples MEA_a and MEA_b. In the pristine sample MEA_ref is also evident a good monodispersity of the particle size, especially in the image obtained from the anode side. The statistical results obtained from the images of all the samples are reported in *Table 8*. The size of the fresh sample is similar to the values reported in literature [60] and the high monodispersity is confirmed by a low standard deviation. According to the TEM results, the averaged particle size increased by 28% and 47% in the operated samples MEA_a and MEA_b, respectively. The standard deviation increased the 51% in MEA_a and the 96% in MEA_b.

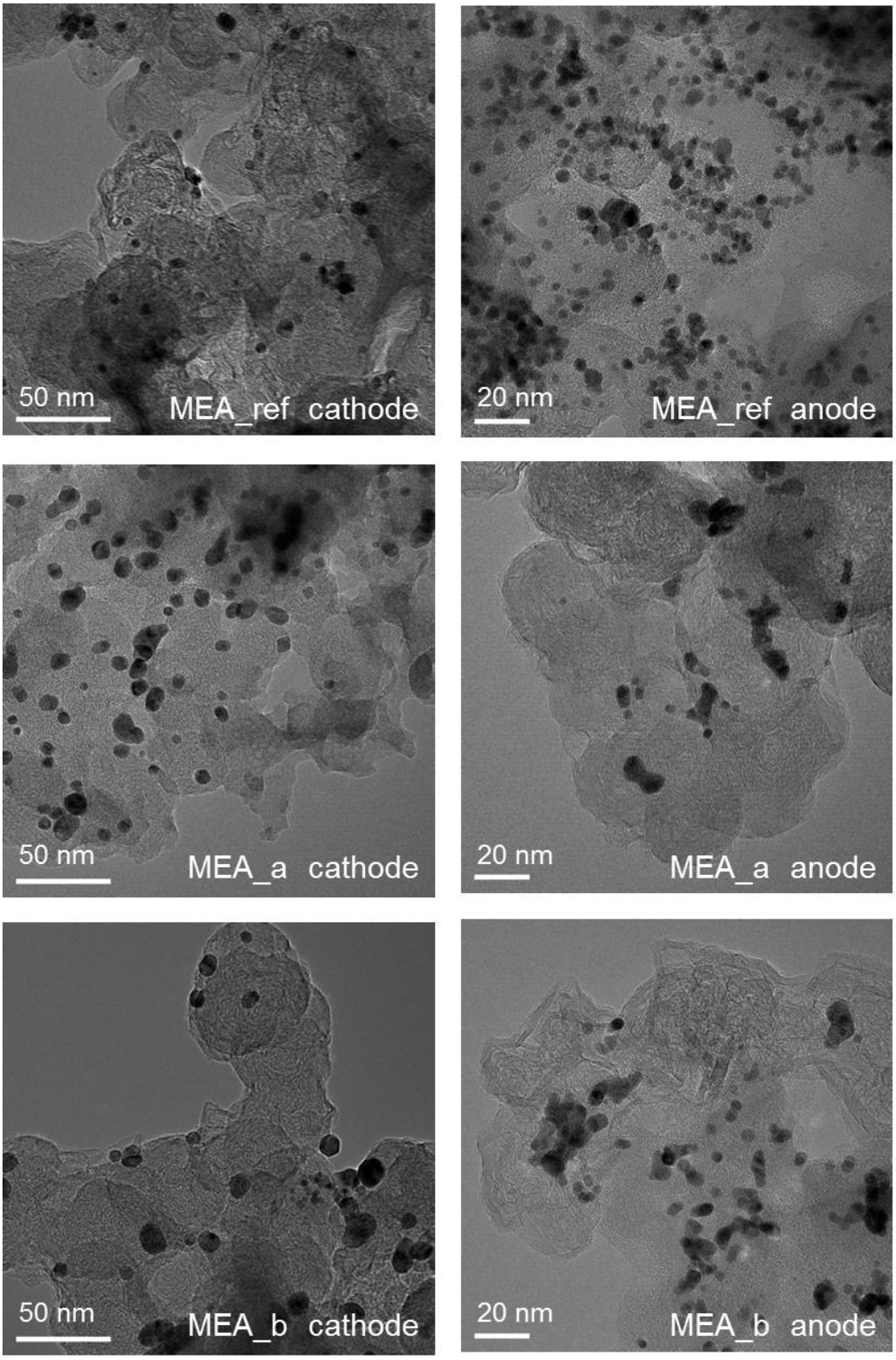

Figure 30. *TEM images of the electrocatalyst nanoparticles sampled from the anode and cathode side of MEA_ref, MEA_a and MEA_b.*

***Table 8**. Mean radius and standard deviation of the electrocatalyst nanoparticles averaged for all the TEM images obtained for the samples MEA_ref, MEA_a and MEA_b.*

	MEA_ref	**MEA_a**	**MEA_b**
Mean radius cathode	2.85	3.91	4.18
Standard deviation cathode	0.81	1.31	1.77
Mean radius anode	2.26	2.62	2.92
Standard deviation anode	0.81	0.66	1.37
Mean radius averaged	**2.55**	**3.26**	**3.75**
Standard deviation averaged	**0.86**	**1.29**	**1.68**

Comparing the results obtained with TEM analysis with the ones obtained with SAXS analysis, the particle mean radii obtained by TEM analysis are about the 30% lower than the SAXS values. The gap between TEM and SAXS results can be caused by several factors and a deeper analysis should be carried out to clarify this incongruence. Some hypothesis, however, have been considered. It is important to remember first that the population size of the electrocatalyst nanoparticles analysed with the two techniques is very different. The area covered by the SAXS beam in a single exposition is 10^6 times larger than the area of a TEM image. Moreover, the scattering information detected in SAXS represents the three-dimensional space invested by the beam, while the TEM result is a two-dimensional image. An additional issue related to the TEM methodology is that the identification of the single nanoparticles in 2D images could be difficult when those overlap one with one another. Since the number of detected nanoparticles in TEM is several magnitude orders lower than SAXS, it could be possible that the samples analysed with TEM are not very representative as the ones analysed with SAXS. Moreover, as

discussed in *Paragraph 2.5.3*, the scattering emitted from polydisperse systems is more sensitive to large objects than small ones because the scattering intensity is directly proportional to the volume square of the objects. A third hypothesis that could justify the gap in SAXS and TEM results is related with the experimental methodology used in TEM to prepare the samples before the microscopic analysis. The TEM sampling procedure described in *Paragraph 3.6.4.1*, indeed, is highly destructive, since it includes the cutting and scratching of the sample. This operation could alter the original structure of the electrocatalyst and lead to different results. Moreover, the separation of the catalyst layer from the electrolytic membrane by scratching could not remove all the electrocatalyst. This event could occur if the electrocatalyst is accumulated in the interface between catalyst layer and electrolytic membrane or even into the electrolytic membrane itself. The formation of a Pt band on the electrolytic membrane has been observed by different authors [1,2,66]. The presence of bigger particles into the electrolytic membrane or close to the interface could justify the smaller mean radii obtained by TEM analysis. Additional experiments could clarify those suppositions. A detailed analysis of the MEA cross section could be useful to detect the presence of a Pt band nearby to the electrolytic membrane. SAXS or XPS could be used for this purpose.

3.6.5 Mapping of electrocatalyst evolution

SAXS has also been used to obtain structural information on the electrocatalyst on a large area of the MEAs. A 40×40 mm area has been mapped by means of a multiple exposition procedure on each sample, as described in *Paragraph 3.4.4*. The expositions have been performed with a frequency of 1 mm on the x-axis and 0.5 mm on the y-axis (referring to *Figure 15*) for a total of 3,200 single expositions for each sample. The purpose of this measurement was the investigation of the spatial distribution of electrocatalyst structural properties and its evolution after the stress tests. From all

the scattering intensity curves of the three analysed MEAs, the correlation length has been calculated and plotted in *Figure 31*. Since the correlation length is a scattering parameter that is proportional to the size of the nanoparticles, the 3D graphs of *Figure 31* could be used to investigate the spatial distribution of the electrocatalyst growth on a large area of the MEA surface.

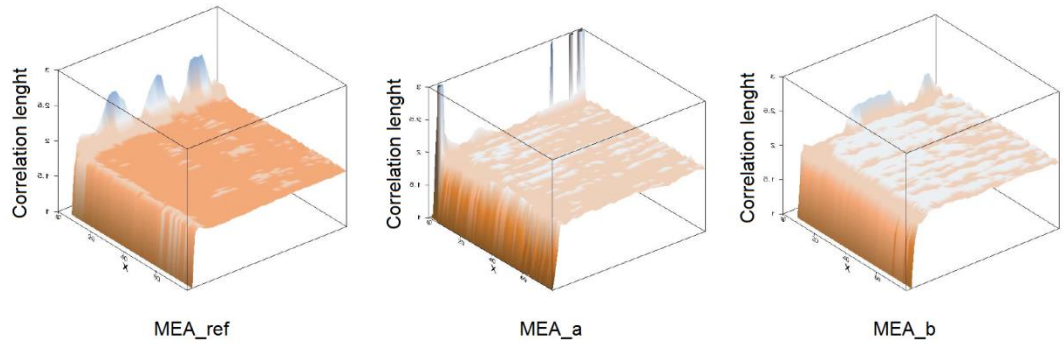

***Figure 31**. Correlation length calculated from the 3,200 scattering intensity curves that have been obtained on a 40×40 mm of MEA_ref, MEA_a and MEA_b, in reference to Figure 15.*

As described in *Figure 15*, the plots of *Figure 31* cover a corner of the MEAs active areas. The borders of the corner include part of the polymer outside the MEA active area. This is visible in *Figure 31* where the correlation length decreases to zero, since no electrocatalyst nanoparticles are present outside of the MEA active area. The area that has been considered for the analysis is only the active area of the MEA. The plot of the spatial resolved correlation length is very uniform in the active area of MEA_ref, while significant variations are visible in the aged samples, particularly in MEA_b. The mean values of the correlation length are in agreement with the particle size distribution calculated from the fitting parameters shown before. The local variations on the cycled samples show a preferential path on the y-axis direction. It has been observed that the parallel paths are spaced about 2 mm one each other. The

pattern is very similar to the one of the flow-field channels on the plates that encloses the MEAs in the fuel cell. Moreover, the direction of the paths on the plots of the correlation length corresponds with the direction of the channels during the operation of the MEAs. It could be possible, thus, that the flow-field geometry of the channels causes a different evolution of the electrocatalyst in the MEA. Further experiments are necessary in order to prove this supposition. Additional SAXS mapping measurements could be useful to deepen this phenomenon. In particular, a scan could be performed with higher x-axis sampling frequency in order to get a more detailed definition of these paths. The fitting of all the scattering intensity curves by means of a multiple-fitting procedure, as described in *Paragraph 3.4.4*, could give additional information. Moreover, the employment of additional diagnostic techniques could help to define the causes of this orientation. XPS, for example, could be used to verify the uniform distribution of the electrocatalyst on the active area of the MEA.

3.7 Start/stop cycling test

Degradation due to start/stop operation is one of the main issues in HT-PEM fuel cells because it implies different transient mechanisms that can affect the proper performance of the single components. Differently than in low temperature PEMFCs, start/stop cycling in HT-PEMFCs leads also to a significant temperature cycling (about 140°C range) that can favour several degradation processes such as the delamination of the different layers of the MEA and the leaching of the phosphoric acid present in the electrolytic membrane due to water condensation. Moreover, the reverse-current mechanism (see *Paragraph 2.3.4*) takes place during start-ups and intensifies the carbon corrosion. A start/stop long-term durability test has been

carried out with the purpose to study the performance behaviour during this operation mode.

3.7.1 Methodology

The temperature range of the start/stop cycle was imposed between 40°C (in standby condition) and 160°C (in regime operation). The start/stop cycle consisted in heating up the fuel cell to 160°C, keeping regime operation for 5 min, cooling down to 40°C and keeping standby condition for 5 min. A start-up and a shutdown procedure have been developed in order to minimize the degradation due to water condensation and reverse-current with the purpose to focus the attention on other aspects such as temperature and load cycling. Those procedures have been defined by a series of operational phases controlled by the value of cell temperature. At the beginning of the start-up process the fuel cell was at ambient temperature and both inlets and outlets were closed. The cell has been heated up to 80°C and then outlets have been opened in order to allow the expansion of the gases present within the cell. When the cell reached 115°C the reactants (H_2 and air) have been flowed in, leaving the fuel cell in OC condition for a short time before drawing a current of 222 $mAcm^{-2}$ (10 A) when the temperature was higher than 120°C. The regime operating condition was achieved when the cell temperature reached 160°C. This condition (160°C and 222 $mAcm^{-2}$) has been kept for 5 min before starting the shutdown procedure. In order to accelerate the cooling down process, the heating elements have been deactivated and the external fan switched on. The load has been set to 11 $mAcm^{-2}$ (0.5 A) until the cell temperature was lower than 120°C, then it has been deactivated and the reactants flows have been substituted with N_2. The N_2 purge was terminated at 100°C and at 80°C the outputs of the fuel cell have been closed. When the cell temperature decreased to 40°C the fan was switched off and the fuel cell was kept in stand-by condition for 5 min before starting the successive cycle.

Reactants flow rates have been set constant during all the phases of the procedure in which they were used. Air flow was 1.4 slpm, while hydrogen has been flowed in dead-end mode, with a 200 mbar overpressure and a vent of 1 s every 3 min. Nitrogen flow rate during purging was set constant at 2 slpm. All the steps of this procedure have been activated according to the fuel cell operative temperature. In *Figure 32* all the steps of this procedure are indicated on the temperature plot of a generic start/stop cycle.

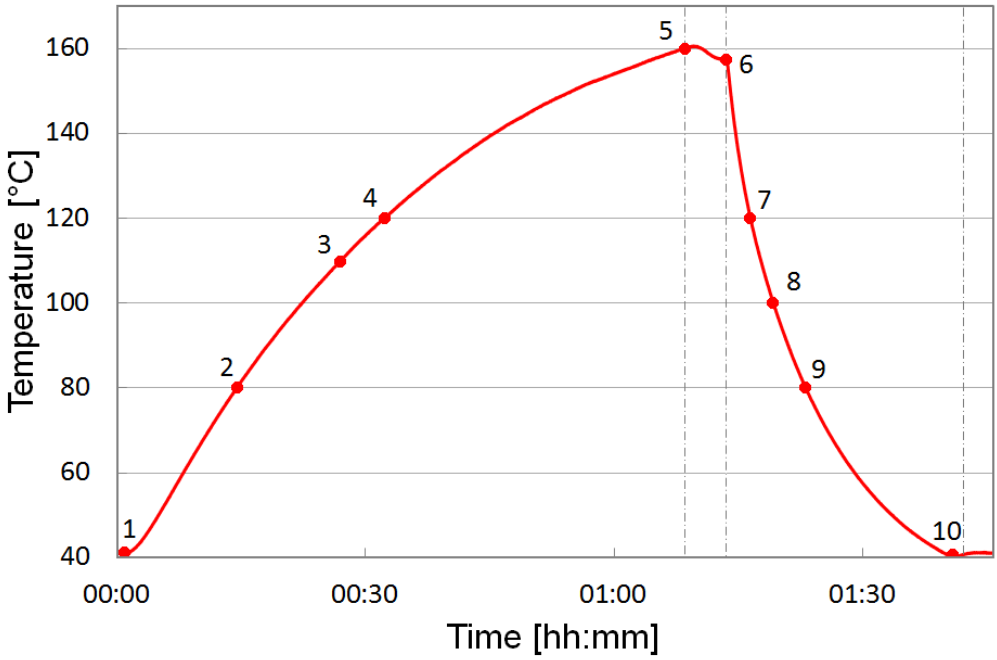

***Figure 32**. Plot of temperature versus time of a generic start/stop cycle performed in the durability test. The steps of the start-up and shutdown procedures followed during the test are indicated on the curve: start heating (1), output valves opening (2), reactants introduction (3), switching on load (4), regime operation with constant temperature (5), load to minimum and fan on (6), N_2 purge (7), stop N_2 purge (8), output valves closing (9), fan off and standby mode (10).*

A complete start/stop cycle lasted about 1 h and 45 min. The durability test consisted in 100 h of activation time (160°C and 222 $mAcm^{-2}$) and 1,000 start/stop cycles, for a total of more than 1,800 h

of testing time. A polarization curve has been recorded just after the activation time and then every 50 cycles during the entire test.

3.7.2 Performance analysis

Fuel cell performance has been monitored during the test with the measurement of cell voltage and polarization curves. In the first 450 cycles, the averaged voltage decay rate at 222 $mAcm^{-2}$ was just about 18 μV/cycle. After about 450 cycles, cell performance started to decrease more significantly, up to 550 cycles, where it strongly declined. From 660 to 850 cycles cell performance was more stable and then it fell again. Considering the entire stress test (1,000 start/stop cycles), the averaged voltage decay rate at 222 $mAcm^{-2}$ was about 85 μV/cycle.

Comparing the evolution of cell voltage during the test with the H_2 mass flow, it is possible to observe an inverse symmetry between the trends. In the points in which cell voltage fell down (550 and 850 cycles) there is a fast increase of the H_2 mass flow. This relation is shown in *Figure 33*, where cell voltage and H_2 mass flow are plotted in the same graph. It is supposed that a significant H_2 crossover between anode and cathode started after 450 cycles. The cause could be a micro-hole in the electrolytic membrane that widen during operation due to the formation of a hot spot. *Figure 34* shows five of the polarization curves that have been recorded during the durability test. Up to 450 cycles, the curves are very similar in all the current range, except for the OCV value, that is significantly lower after 450 start/stop cycles. The curves recorded after 450 cycles are shifted to lower cell voltages for all current densities, until the end of the test. This behavior is compatible with the supposition of a significant hydrogen crossover after 450 cycles. At the beginning of the test, OCV was higher than 0.9 V, it decreased to 0.84 V after 450 cycles, then to 0.75 V at 600 cycles, and lower than 0.70 V after 750 cycles. The procedures employed to start-up and shutdown the fuel

cell seem to have a central importance in fuel cell durability. During the startup, between 115°C and 120°C the fuel cell was subjected to OC condition for a period of about 2 min. The purpose of this gap between the opening of reactants and the setting of a load was intended to allow the reactants to diffuse into the electrodes. Consequently, OCV value was not instantaneously reached, but cell voltage was anyway very high during this period. This step in the startup procedure may have contributed significantly in the long-term degradation.

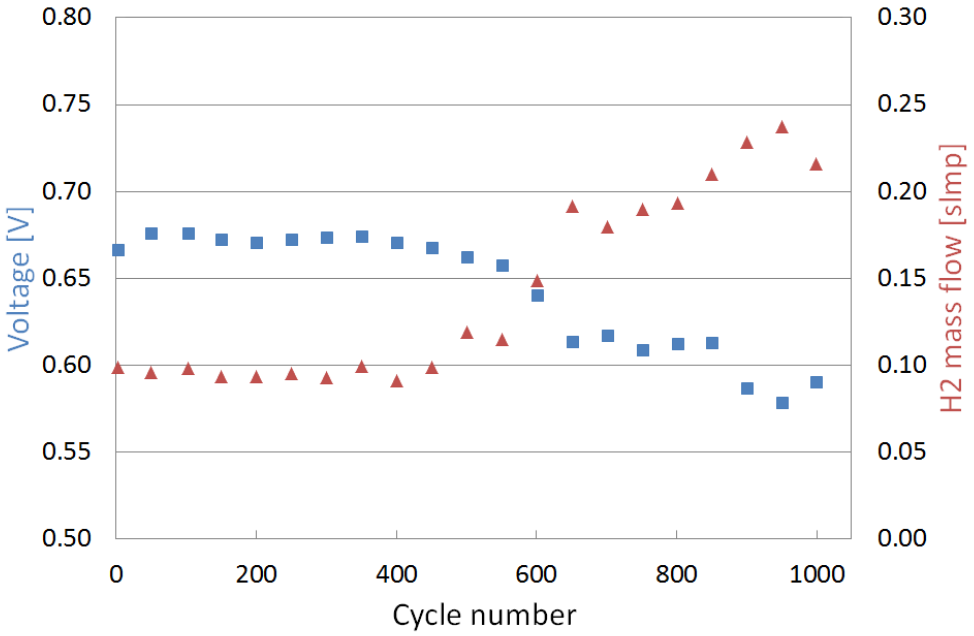

***Figure 33**. Cell voltage and H_2 mass flow evolution at 222 $mAcm^{-2}$ during the 1,000 start/stop cycles durability test.*

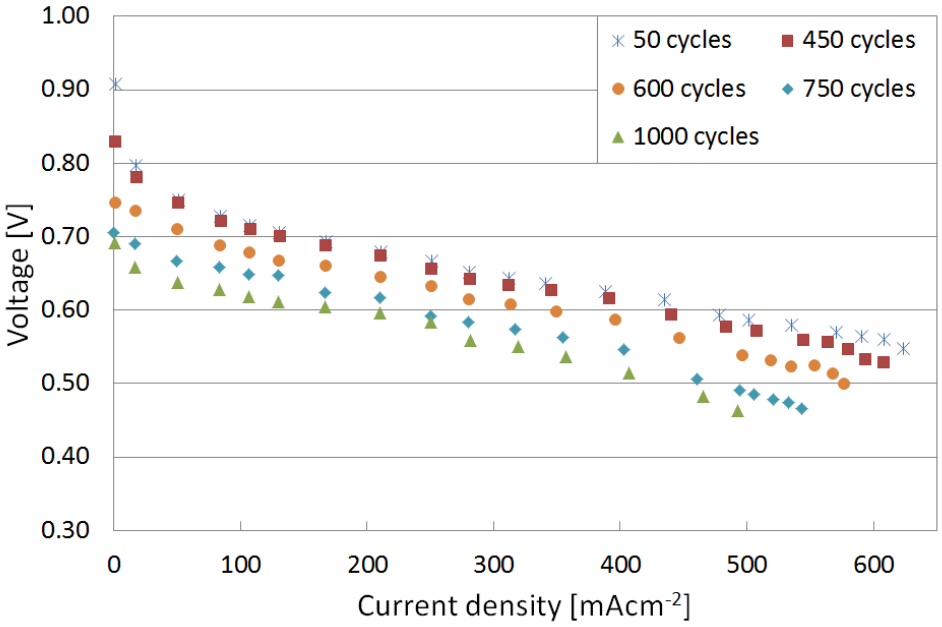

***Figure 34**. Some of the polarization curves that have been recorded during the 1,000 start/stop cycles test.*

Schmidt and Baurmeister [39] carried out, on the same type of MEA, a durability test consisting of 240 start/stop cycles. The authors measured a cell voltage decay rate of 200 μV/cycle or 11 μVh^{-1} at 200 $mAcm^{-2}$ during the entire test. The start/stop cycling procedure proposed by Schmidt and Baurmeister included 12 h of regime operation followed by 12 h of shutdown. Moreover, no purge with inert gas has been done during shutdown. Comparing the performance loss in the 240 start/stop cycles of this test, with the first 450 start/stop cycles of the test presented in this study, the voltage decay is much higher in the former. It is important, however, to consider that the start/stop cycle covers 24 h in the test carried out by Schmidt and Baurmeister, while the cycle presented in this research covers less than 2 h. On the other hand, as shown also in the same paper, voltage decay during steady-state operation is not the main cause of degradation. The tests could thus be compared even if the cycle duration is different. The substantial difference in performance loss during the tests could be attributed to the

different procedure followed to shut-down the fuel cell to ambient temperature. Purging the fuel cell anode and cathode with N_2 seems thus to increase significantly fuel cell durability. A further experiment based on the same start/stop cycling test, but without N_2 purging could be very useful to quantify the real effect of purging at shutdowns.

4

Conclusions

The comparison between the current status of PEMFC technology and the targets imposed by the main international organizations (as described in *Appendix A1*) evidences that current durability and cost are not satisfactory. As discussed in *Paragraph 1.1*, electrocatalyst degradation seems to be the main responsible of performance loss during long-term fuel cell operation, as well as the largest part of the total cost of a fuel cell system. A better understanding of electrocatalyst degradation mechanisms and their effect on fuel cell performance could be very useful for the development of novel materials and mitigation strategies to increase durability and limit the overall cost. The research presented in this dissertation had the purpose to investigate the evolution of fuel cell performance and electrocatalyst structural properties during long-term operation in single high-temperature PEM fuel cells (HT-PEMFCs).

4.1.1 Diagnostics methodology

Two different methods to record polarization curves proposed by EU JRC (FCTESTNET [51]) have been compared and discussed. The procedure based on a variable current with different rates have

been preferred to the traditional procedure based on fixed current points because of the need to reduce the contribution of the measure itself on fuel cell degradation during the durability tests. Effectiveness of specific diagnostic techniques for the characterization of electrocatalyst structure in HT-PEMFCs has been studied and tested. Cyclic voltammetry (CV) has been investigated by means of a sensibility analysis in order to understand its reliability to assess electrocatalyst degradation in high temperature PEM fuel cells. CV utilization in H_3PO_4/PBI HT-PEMFCs is quite complex as results are strongly influenced by MEA humidification state. It has been observed, as discussed in *Paragraph 3.3.4*, that the conditions in which the fuel cell has been subjected before the CV measurement have a significant effect on the cyclic voltammogram. Small angle x-ray scattering (SAXS) has been studied as a complementary diagnostic technique to CV for the characterization of electrocatalyst structural properties. Indeed, from a cyclic voltammogram it is possible to calculate the ECSA value, while from SAXS analysis structural properties of the nanoparticles are observed. An experimental procedure has been developed to characterize the electrocatalyst properties directly from the MEA, without specific sample preparation. The results allowed the determination of size and distribution of the electrocatalyst nanoparticles. Moreover, a specific experimental method based on SAXS has been developed to investigate the electrocatalyst properties on a large area of the MEA. SAXS seems to be an effective diagnostic technique for this purpose. Nanoparticle size and distribution can also be obtained from TEM analysis, but SAXS method owns significant advantages. First of all the MEAs can be analysed with SAXS without specific sample preparation, while TEM requires a destructive sampling procedure that could strongly influence the results. Another fundamental difference is the population size of electrocatalyst nanoparticles that is analysed in a single measurement. The area covered in a single SAXS exposure is 10^6 times larger than the area of a TEM image. Moreover, SAXS

analysis covers the three-dimensional space illuminated by the beam, while TEM analysis is limited to two dimensions. Consequently, the number of detected nanoparticles is several magnitude orders higher in SAXS. The identification of the single nanoparticles in the two-dimensional TEM images could also be difficult when those overlap one with one another. SAXS analysis moreover offers additional information on the structural status of electrocatalyst nanoparticles: state of aggregation can also be obtained from the data fitting. On the other hand, TEM is able to offer direct information on the single particles that in this research has been useful for the SAXS analysis. These techniques, thus, have to be considered complementary and the combination of their results can lead to a deep analysis of electrocatalyst structure in PEMFCs.

4.1.2 Durability tests

Performance degradation and electrocatalyst structural evolution have been studied during long-term fuel cell operation. Accelerate stress test procedures have been used to reduce the testing time. Few testing protocols have been developed by international organizations to assess electrocatalyst long-term degradation in low temperature PEM fuel cells, as discussed in *Appendix A2*. Currently, to the knowledge of the author, there are no standard protocols to accelerate electrocatalyst degradation in high temperature PEM fuel cells. Specific procedures have been developed in this research for this purpose, trying to limit the degradation of other components of the MEA. A test bench for long-term durability tests has been designed and assembled. Specific software has been developed in *LabVIEW®* environment to control the test bench and to acquire the experimental data. Testing procedures and emergency strategies have been implemented in the software in order to allow the autonomous operation of the test bench. Two MEAs have been

subjected to different load cycling profiles and a third one followed a start/stop procedure. The results demonstrated the effectiveness of these procedures to accelerate degradation. At 200 $mAcm^{-2}$, the load cycling tests caused voltage decay rates higher than 30 μVh^{-1}, while in the start/stop procedure the voltage decay was 18 μV/cycle during the first 450 cycles of the test. After 450 start/stop cycles, cell voltage decreased very quickly due to an unexpected failure of the MEA, probably due to the formation of micro-holes in the electrolytic membrane that increased hydrogen crossover. This hypothesis agrees with the significant decrease of OCV value after 450 cycles. The samples subjected to load cycling, on the contrary, did not show significant decreases in OCV value during the test and the voltage decay seems to be constant during the tests. This means that start-ups and shutdowns could have a significant influence on the kinetic-related activation losses. The degradation induced by start/stop cycling, however, seems to have been limited in the test thanks to the specific start-ups and shutdowns procedures described in *Paragraph 3.7.1*. The comparison between the results of the two load cycling stress tests has been effective to quantify the effect of current range in the profile of the cycle. The voltage decay rate (μVh^{-1}) at 200 $mAcm^{-2}$ in the test in which current has been cycled between 0 and 500 $mAcm^{-2}$ was 34% higher than in the test in which current has been cycled between 10 and 500 $mAcm^{-2}$. Frequent OC condition, even for limited times, seems thus to have an influence on performance degradation. Similar results have been obtained in terms of electrocatalyst evolution: the mean radius measured by SAXS increased by 74% in the sample cycled between 10 and 500 $mAcm^{-2}$, while it increased by 102% in the other. The polydispersity of the cycled samples increased as well. From the shape of the size distributions (see *Figure 28*), according to the method proposed by Ascarelli et al. [13] and described in *Paragraph 2.2.1*, the predominant particle growth mechanism seems to be coalescence, since the size distribution is log-normal, with a maximum shifted towards the small-particles side and a tail on the

large-particles side. The particle mean radii obtained by TEM analysis are about the 30% lower than the SAXS values. This gap could be caused by the different population size analysed by the two techniques or by the highly destructive sampling method used in TEM analysis, as previously discussed. An additional hypothesis could be the formation of a Pt band on the interface between catalyst layer and electrolytic membrane, as observed by other authors [1,2,66]: in this case, the removal procedure of the catalyst layer used to obtain the samples for the TEM analysis (see *Paragraph 3.6.4*) could had be not successful to collect all the catalyst nanoparticles, and in particular the bigger ones, from the MEA. The mapping procedure that had been developed in order to investigate electrocatalyst evolution on large areas of the MEA seems to have been effective. The plot of the correlation length of the cycled MEAs (*Figure 31*) showed preferential directions of the nanoparticles growth in correspondence of the channels on the flow-field plates.

4.1.3 Future developments

The statistics of the experimental results could be improved in the future in order to validate the SAXS methodology proposed in this research. More samples should be analysed and more measurements should be repeated on the same sample. This approach is particularly necessary in the comparison between SAXS and TEM results, where the sampled population of nanoparticles is much lower. More information may be obtained from the fitting of the data collected during the SAXS experiment on large areas of the MEAs. For this purpose a specific procedure of multiple fitting is currently in development phase. The validation and improvement of the presented SAXS methodology could be supported in a future research by the employment of additional diagnostic techniques, such as wide angle x-ray scattering (WAXS), as done by Stevens et al. [70] on samples of carbon-supported Pt electrocatalysts, grazing

incidence SAXS (GISAXS) and x-ray photoelectron spectroscopy (XPS). From GISAXS analysis it could be possible to differentiate the electrocatalyst information between anode and cathode of the MEA. This operation could be useful to determine the contribution of each electrode to the averaged result obtained by SAXS in transmission. Moreover, a separate investigation of the two electrodes is also important because electrocatalyst evolution is different in anode and cathode, as discussed in *Paragraph 2.2.1*. XPS could be used as a complementary technique to SAXS for the mapping of the electrocatalyst evolution on large areas of the MEAs. Moreover, also the cross-section of the MEA could be similarly investigated by the combination of SAXS and XPS, in order to verify the hypothesis of the formation of a Pt band in the interface between catalyst layer and polymeric membrane. Another future development of the SAXS methodology proposed in this research for the characterization of HT-PEMFC MEAs could be an *in situ* experiment in which SAXS is performed during fuel cell operation. It could be possible in this way to monitor in real time the evolution of electrocatalyst structural properties.

Further investigations are also necessary to better understand the effects of load cycling and start/stop cycling on electrocatalyst and carbon support. Additional load cycle profiles could be used in a future research to deepen the effects of load cycling on fuel cell degradation. An analysis of the amount of CO in the products at the outlet of the fuel cell could quantify the effects on carbon corrosion of the shutdown procedure based on N_2 purging used during the start/stop test. Moreover, additional tests with different start-up and shutdown procedures could help to identify other advantageous strategies from the comparison of the results. The development of separate cycling procedures for start-ups and shutdowns, as proposed by Dillet et al. [38], could also be an effective method for this purpose.

Finally, the procedure used to record the polarization curves during the durability tests could be improved in future experiments with the purpose to obtain more reliable results. One way could be the use of the fixed current method in order to avoid the drawbacks caused by the variable current method. In this case, the measurement time will be longer and the permanence at high voltages could affect the fuel cell degradation rate. A second way could be the limitation of the issues related to the variable current method. The voltage oscillations in the high-currents region could be reduced by improving the temperature control system and minimize the temperature excursion. The current sweep rate could be kept constant during the measurement or at least the variations should be progressive in order to avoid steps in the resulting polarization curve.

Appendix

A1

Durability targets for PEM fuel cells

The governments of countries like United States, Japan and Europe promote the development of PEMFCs through the founding of specific R&D programs. The U. S. Department of Energy (U. S. DOE), Japan ministry of Economy, Trade and Industry (METI), and the European Commission are supporting the research and development of PEM fuel cells for stationary and transportation applications. One of the purposes of these programs is to establish specific technical targets for the commercialization of fuel cells. Common targets can be very helpful in addressing research and industrial development towards the real challenges that limit the

widespread commercialization of these devices. Moreover, they can be used by fuel cells developers as a guideline to quantify the maturity of this technology and compare it with other alternatives.

A1.1 U. S. DOE program

The Fuel Cell Technologies Program Multi-Year Research, Development, and Demonstration Plan (MYRD&D Plan) describes the goals, objectives, technical targets, tasks and schedules for all activities within the Fuel Cell Technologies Program (FCT Program) which is part of U. S. Department of Energy's Office of Energy Efficiency and Renewable Energy (EERE) [3]. The Technology Validation sub-program defines some technical targets that are based on a combination of technical needs identified by the RR&D sub-programs (fuel cells, storage, production, etc.) and the market needs identified by current validation projects and industrial partners. The purpose of the sub-program is to advance fuel cell technologies for transportation, portable and stationary applications and make them competitive in terms of cost, durability and performance. The DOE Technology Validation sub-programs technical targets for fuel cell durability and electrical efficiency are reported in *Table 9* and *Table 10*, respectively [3].

***Table 9**. Fuel cell durability targets by U. S. DOE (2015 and 2020) for different applications [3].*

Application	2011 (status)	2015	2020
Light duty passenger durability (h)	2,521	3,600	5,000
Residential power durability (h)	12,000	25,000	50,000
Commercial power durability (h)	40,000 - 80,000	45,000	65,000
APU durability (h)	3,000	10,000	15,000

***Table 10**. Fuel cell electrical efficiency targets by U. S. DOE (2015 and 2020) for different applications [3].*

Application	2011 (status)	2015	2020
Light duty passenger vehicles - FC systems efficiency @ 25% power	59 %	60 %	60 %
1 – 10 kW residential power system efficiency	34 – 40 %	40 %	42 %
100 kW – 3 MW commercial power system efficiency	42 – 47 %	43 %	48 %
APU system efficiency	25 %	33 %	38 %

Automotive fuel cell systems need to meet the same durability and reliability of current ICE automotive engines. For this reason fuel cell systems for automotive applications will have to last for at least 5,000 h that is the equivalent of 150,000 driven miles. This target refers to the time before reaching 10% of voltage loss after cyclic operation; the durability status in 2011 was 2,500 h, while the target for 2017 is 5,000 h (the targets are the same for both entire fuel cell systems and stacks). Moreover, these systems will have to be able to operate properly over the full range of ambient temperatures, from -40°C to +40°C. Residential combined heat and power (CHP, 1-10 kWe) and distributed generation fuel cell systems operating on natural gas will need to operate for more than 40,000 h within 2015 and more than 60,000 within 2020. The performance degradation will have to be limited to 0.5% and 0.3% after 1000 h of cyclic operation; the status of 2011 was < 2%/1000h [3]. The platinum group metal (PGM) total content will have to be lower than 0.125 g/kW within 2017, a 35% reduction respect to the value reached in 2011 (0.19 g/kW).

An important metric that is annually tracked in the fuel cell sub-program is the projected high-volume manufacturing cost for automotive fuel cells. The estimate in 2012 was 47 $/kW, 36% and 83% less compared with the values of 2008 and 2002, respectively. The estimated cost of the fuel cell stack in 2012 was 20 $/kW. A significant part of the cost reduction between 2008 and 2012 is due to the reduction in platinum group metal (PGM) loading and increase in cell power density, allowing the design of smaller and cheaper stacks. It is important to notice that the reduction in PGM loading over the years have been carried out improving at the same time fuel cell durability. The typical PMG content decreases from 0.6 g/kW of 2007 to less than 0.18 g/kW in 2012 [91].

Table 11 lists the DOE technical targets for electrocatalysts and it is addressed to the evaluation progress of catalysts developers without testing full systems [91].

***Table 11**. U. S. DOE technical targets for electrocatalysts for transportation applications [3].*

Characteristic	Units	2011 (status)	2017	2020
Platinum group metal total content (both electrodes)	g/kW (rated)	0.19	0.125	0.125
Platinum group metal (PGM) total loading	$mg_{PGM}cm^{-2}$	0.15	0.125	0.125
Loss in initial catalytic activity	% loss	48	<40	<40
Electro catalyst support stability	% loss	<10	<10	<10
Mass activity	A/mg_{Pt} @ 900 $mV_{iR\text{-}free}$	0.24	0.44	0.44
Non-Pt catalyst activity per volume of supported catalyst	Acm^{-3} @ 800 $mV_{iR\text{-}free}$	60	300	300

The DOE targets for electrocatalysts presented in *Table 11* consider the 2011 status and are not currently updated to the last research advances. Mark Debe [48] presented the last improvements in electrocatalyst research for PEMFCs at the DOE's 2012 Annual Merit Review and Peer Evaluation Meetings (AMR) for the Hydrogen and Fuel Cells Program. The author reported a PGM total content of 0.14 - 0.18 g_{Pt}/kW for cell 0.6 < V < 0.65 at 80°C and 150 kPa to 250 kPa outlet, for Pt_3Ni_7 catalysts in a 50 cm^2 cell with a 0.15 mg/cm^2 total Pt loading. The 2012 status for mass activity (150 kPa H_2/O_2 80°C, 100% RH, 1050 s) was 0.43 A/mg_{Pt} @ 900 mV in 50 cm^2 with R2R Pt_3Ni_7. The specific activity (150 kPa H_2/O_2 at 80°C, 100% RH) was 2.7 - 3.0 $mAcm^{-2}{}_{Pt}$ @ 900 mV for R2R Pt_3Ni_7 at 0.125 mg_{Pt}/cm^2. Moreover, M. Debe reported the durability status of electrocatalysts subjected to different accelerated degradation tests and the targets for 2017, as shown in *Table 12*.

***Table 12**. 2012 status of the electrocatalyst performance under accelerated degradation tests [46].*

Durability test	Units	2017	2012 (status)
30,000 cycles between 0.6 and 1.0V, 50mVs^{-1}, 80°C, 100 kPa, H_2/N_2	mV at 0.8 Acm^{-2}	< 30	10 ± 7
	% ECSA loss (PtCoMn)	< 40	16 ± 2
	% mass activity loss	< 40	37 ± 2
1.2 V for 400 h at 80°C, H_2/N_2, 150 kPa, 100% RH	mV at 1.5 Acm^{-2}	< 30	10
	% ECSA loss	< 40	10
	% mass activity loss	< 40	10

The U. S. President's fiscal year (FY) 2013 budget request is approximately $38 million for the Fuel Cell sub-program, while the

FY 2012 funding was $45 million. Both in FY 2012 funding and FY 2013 request the largest part of the budget has been addressed to catalysts research and development ($12.8 and $15.5 million for FY 2012 funding and FY 2013 request, respectively). The budget reserved for catalysts improvements is 21% higher in FY 2013 request, also if the complex budget request for the Fuel Cells sub-program is lower [91]. This means that the development of novel electrocatalysts is still a priority for the U. S. DOE and it represent one of the main challenges for PEM fuel cells. The FY 2011 activities in the Fuel Cells sub-program addressed to the improvement of electrocatalysts and supports include the reduction in precious metal loading, the increase of activity, durability, stability and tolerance to reactants, the development of supports with reduced corrosion, lower cost and increased non-PGM catalyst loading, the development of anodes for fuel cells operating on non-hydrogen fuels [91].

A1.2 Japanese NEDO program

Japan's New Energy and Industrial Technology Development Organization (NEDO) promoted the national development of PEM fuel cells first in 2005, when a R&D road map for the technical development of stationary and automotive systems has been published. This document has been updated in 2008 and includes technical development themes and targets for each development stage [92]. NEDO agrees with DOE necessity to improve performance and durability of fuel cells systems for transport applications in order to meet the market needs. NEDO targets for 2015 are fuel cell durability higher than 5,000 h, efficiency for automotive systems higher than 60% (based on the LHV), durability for integrated stationary PEMFC power systems for home generation fuelled by reformate higher than 90,000 h, operating

temperatures higher than 90-100°C, and stack cost not larger than 10,000 Yen/kW. NEDO is not directly involved in the development of fuel cell systems for automotive applications, but it promotes the basic research of those systems and defines technological guidelines. A target indicated by NEDO for 2020 is a fuel cell operative temperature of about 100-120°C without humidifier, in order to promote waste heat removal. Another target for 2020 is the fuel cell operation at external temperatures down to -40°C [2].

A1.3 EU program

In 2003 the European Commission promoted the establishment of the European Hydrogen and Fuel Cell Technology Platform (HFP) in order to create a partnership with private enterprises for the development of hydrogen and fuel cell technologies. In 2005 the HFP adopted a research agenda for accelerating the development and market introduction of fuel cell and hydrogen technologies within the European Community [93]. The 2015 targets for transport applications include an efficiency higher than 40% on the NEDC (New European Drive Cycle, see *Paragraph A2.2.2* of *Appendix A2*), a cost lower than 100 €/kW, and a durability higher than 5,000 h and 10,000 for cars and buses, respectively [2,94]. The Fuel Cells and Hydrogen Joint Undertaken (FCH JU) is a public-private partnership launched in 2008 that supports research, technological development and demonstration activities in fuel cell and hydrogen energy technologies in Europe. The Fuel Cells and Hydrogen Joint Technology Initiative is a component of the Joint Technology Initiatives of the Seventh Framework Programme of the European Commission. The aim of FCH JU is to accelerate the market introduction of fuel cell technology. The three members of the FCH JU are the European Commission, fuel cell and hydrogen industries represented by the NEW Industry Grouping and the research

community represented by Research Grouping N.ERGHY. The continuation and further strengthening of the program (FCH 2 JU) has been proposed under Horizon 2020, the new innovation investment package for 2014-2020.

A2

Durability test protocols for PEMFC electrocatalysts

Polymer Electrolyte Membrane Fuel Cells (PEMFCs) are now very close to the first attempts of a widespread commercialization, especially in the automotive market. The main industrial companies interested in PEMFC applications increased their research on fuel cell lifetime due to the necessity to evaluate fuel cell durability in real operating conditions. Many studies have been recently focused on degradation mechanisms and durability of different components, for both stationary and mobile applications. Most of the long-term durability tests for stationary applications are carried out at a fixed set point or at a limited group of set points. Durability tests for applications in which the power demand vary with time need specific testing procedures that simulate the real operative conditions, since the degradation mechanisms that are induced during dynamic operation are different than the ones in static operation. Moreover, for both stationary and dynamic operation requirements, there is the necessity to reduce the testing time, since it is in the order of thousands of hours and that is often not compatible with the industrial timing. Testing time is thus another significant parameter to take into account. Especially during the development of single components and materials, short durability tests are required. Longer tests are preferred for the evaluation of cell and stack designs close to completion. According to Borup et al. [2] a final configuration of PEMFC components should be tested in a complete fuel cell for more than 10,000 h in total before its validation. 5,000 additional testing hours are then still necessary before being integrated with the system. Accelerated Stress Tests (ASTs) are specifically designed testing protocols that have the purpose to reproduce the same degrading effects of the normal operation of a specific system, but in a significantly shorter time. An additional advantage of ASTs is that it is possible to accelerate the stress of a singular component: this is a very useful feature for the testing of new components and materials. This procedure, however, in most of the cases is not able to completely isolate the effects of ageing of a singular component from the other components present

in the system, because the operative conditions have often a simultaneous effect on different components.

Many research groups developed specific procedures for the accelerated degradation of PEMFCs, but since most of the available data has been taken under different operative conditions, it is very difficult to compare different data sets. A standardization of AST protocols is thus necessary [2]. In the last ten years, interest on developing standardized accelerated degradation testing protocols has greatly increased. Standard protocols for durability evaluation and a diffuse information exchange are a very useful tool for the entire fuel cell community and could significantly help to boost the development towards a widespread fuel cell commercialization. Organizations such as the U. S. Department of Energy (DOE), the Fuel Cell Hydrogen Energy Association (FCHEA), the European Union (EU), and the International Electrotechnical Commission (IEC) have proposed and published many different methods to characterize performance and durability of PEMFCs. United States, European Union and Japan started some actions to standardize and harmonize these different methods. Projects such as FCTESTNET [95] and FCTESQA [96] investigated every aspect of single cell testing, including test plan preparation, operative conditions and diagnostics, and the resulting testing protocols were validated in a round-robin experiment in the EU and the US.

In this paragraph the main international protocols used to evaluate catalyst layer degradation are presented. In the first part (*Paragraph A2.1*) some testing protocols for electrocatalists and supports will be presented, while in *Paragraph A2.2* general testing protocols will be reported. The testing procedures presented in *Paragraph A2.2* are not specifically designed to investigate electrocatalysts and supports degradation, but since they are based on load cycling and start/stop, they can be effectively employed for this purpose.

A2.1 Test protocols for electrocatalists and supports

Electrocatalyst degradation is enhanced at high electrode potentials and dynamic operation, while support corrosion is accelerated at high electrode potentials, during start/stop cycles and during high temperature operation (>100°C) [2,97,98]. The accelerated stress protocols for electrocatalysts and supports are based on these assumptions and consist in the application of those degrading operative conditions. Electrocatalyst ASTs described in literature generally simulate a duty cycle that induces catalyst degradation by potential cycling from a lower potential, in the range of 0.1–0.7 V, to increased potential, such as OCV, 1.0, or 1.2 V [99]. The average value of the current over the cycle has a significant impact on the aging result [100,101]. In this paragraph, only durability protocols at single cell and stack level are considered and accelerated degradation procedures with different cell configurations are not presented.

A2.1.1 U. S. DOE test protocols

In 2006 the United States Department of Energy (U. S. DOE) published a program solicitation to industry and the national laboratories with the purpose to evaluate newly developed PEMFC components [102]. These protocols included an accelerated-test methodology based on potential cycling of electrocatalysts and a protocol to measure the corrosion of catalyst-support materials [2]. In 2007 the DOE cell component AST protocols for PEM fuel cells have been updated with a document that assesses performance and durability of fuel cell components intended for automotive propulsion applications [97,103]. The purpose of these tests was to gain a measure of component durability and performance of electrocatalysts, supports and membranes for comparison with DOE targets [104]. The data obtained from these tests has also been very

useful to model performance and degradation of the fuel cell under variable load conditions. These testing protocols had the purpose to establish a common approach for evaluating durability of PEM fuel cells components under simulated automotive drive conditions. Anyway, many critical issues in transport applications such as start/stop and freeze/thaw cycles have not been considered in this document. Moreover, the proposed cycles have not been fully correlated with data from stacks and systems operated under actual drive cycles [97,103]. The specific testing conditions are intended to isolate effects and failure modes, assuming the widely accepted degradation mechanisms. The electrocatalyst cycle is different from the support cycle because under different operation conditions they are subjected to different degradation mechanisms. Anyway, it is important to remark that electrocatalyst and support degradation are strongly related and it is thus indispensable to consider this aspect during both the component characterization and the data analysis. The 2007 U. S. DOE testing protocol for electrocatalysts is reported is *Table 13* and the corresponding load cycling profile is shown in *Figure 35*. The testing protocol for catalyst supports is reported is *Table 14*.

***Table 13**. 2007 U. S. DOE testing protocol for electrocatalyst degradation and metrics [55]. Catalytic activity should be measured in Amg^{-1} at 150 kPa abs backpressure at 900 mV iR-corrected on H_2/O_2, 100% RH and 80°C. Polarization curves should follow the procedure USFCC "Single Cell Test Protocol" [55].*

Fuel cell	single cell 25-50 cm^2
Cycle profile	step change: 30s at 0.7 V and 30s at 0.9 V.
Cycle number	30,000 cycles
Cycle time	60 s
Temperature	80°C
Relative humidity	anode/cathode 100%/100%
Fuel/oxidant	H_2/N_2
Pressure	150 kPA absolute

Metric	Frequency	Target
Catalytic activity	beginning and end of life	≤60% loss
Polarization curves from 0 to ≥1,500 mAcm^{-2}	after 0, 1k, 5k, 10k and 30k cycles	≤30 mV loss at 800 mAcm^{-2}
ECSA from cyclic voltammetry	after 1, 10, 30, 100, 300, 1,000, 3,000 cycles and every 5,000 cycles thereafter	≤40% loss

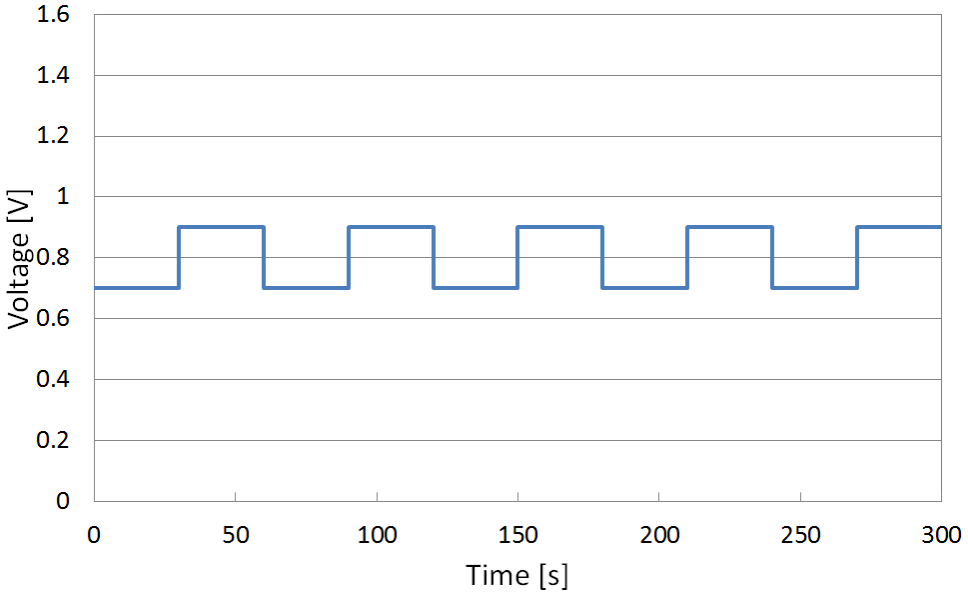

***Figure 35**. 2007 U. S. DOE testing protocol for electrocatalyst degradation* [97].

***Table 14**. 2007 U. S. DOE testing protocol for catalyst support and metrics [55]. Catalytic activity should be measured in Amg^{-1} at 150 kPa abs backpressure at 900 mV iR-corrected on H_2/O_2, 100% RH and 80°C. Polarization curves should follow the procedure USFCC "Single Cell Test Protocol" [55].*

Fuel cell	single cell 25-50 cm^2
Cycle profile	hold at 1.2 V for 24 h; run polarization curve and ECSA; repeat for total 200 h
Total time	continuous operation for 200 h
Diagnostic frequency	24 h

Temperature	95°C
Relative humidity	anode/cathode 80%/80%
Fuel/oxidant	H_2/N_2
Pressure	150 kPA absolute

Metric	**Frequency**	**Target**
CO_2 release	on-line	≤10% mass loss
Catalytic activity	every 24 h	≤60% loss
Polarization curve from 0 to ≥ 1,500 Acm^{-2}	every 24 h	≤30 mV loss at 1,500 $mAcm^{-2}$ or rated power
ECSA from cyclic voltammetry	every 24 h	≤40% loss

The stress protocol for electrocatalyst is based on a sudden potential change between 0.7 V and 0.9 V every 25 s, while in the protocol for the catalyst support the voltage is hold constant, but at a higher value (1.2 V) in order to accelerate the carbon corrosion. During both the tests the anode is fed with hydrogen and the cathode with nitrogen. In the electrocatalyst testing procedure both reactants are fully humidified, while in the catalyst support test the relative humidity of reactants is 80%. It is suggested to measure catalytic activity, polarization curves and cyclic voltammetry in both the protocols, but during the catalyst support test it is also suggested to detect the CO_2 release due to carbon corrosion. The frequency of the measurements is always constant during the catalyst support test, while it is more frequent at the beginning of the electrocatalyst test because most of the catalyst sintering and growth is expected during the first 100 h of cyclic operation [1].

The U. S. DOE cell component AST protocols for PEM fuel cells have been revised in 2009 [86,87]. The electrocatalyst test protocol of 2007 has been significantly modified in this document both in terms of load cycle profile and operating conditions. The DOE test protocol

revised in 2009 for the electrocatalyst is reported in *Table 15* and the load profile shown in *Figure 36*.

***Table 15**. U. S. DOE testing protocol for electrocatalyst revised in 2009* [86,87]. *Catalytic activity should be measured in Amg^{-1} at 150 kPa abs backpressure at 857 mV iR-corrected on 6% H_2 (bal N_2)/O_2, 100% RH, 80°C normalized to initial mass of catalyst and measured before and after test. Polarization curves should follow the procedure "Fuel Cell Tech Team Polarization Protocol"* [86]. *Cyclic voltammetry sweep from 0.05 to 0.6 V at 20mVs^{-1}, 80°C, 100% RH.*

Fuel cell	single cell 25-50 cm^2
Cycle profile	triangle sweep cycle: 50mVs^{-1} between 0.6 V and 1.0 V
Cycle number	30,000 cycles
Cycle time	16 s
Temperature	80°C
Relative humidity	anode/cathode 100%/100%
Fuel/oxidant	H_2/N_2 (H_2 at 200sccm and N_2 at 75sccm for a 50 cm^2 cell)
Pressure	atmospheric

Metric	**Frequency**	**Target**
Catalytic activity	at beginning and end of test, minimum	≤40% loss
Polarization curve from 0 to ≥ 1,500 Acm^{-2}	after 0, 1k, 5k, 10k and 10k cycles	≤30 mV loss at 800 mAcm^{-2} or rated power
ECSA from cyclic voltammetry	after 10, 100, 1k, 3k, 10k, 20k and 30k cycles	≤40% loss

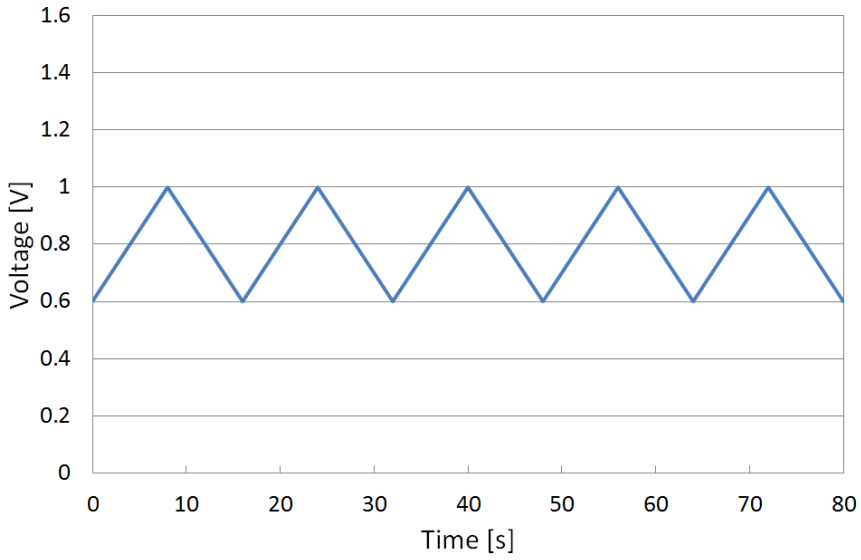

***Figure 36**. U. S. DOE testing protocol for electrocatalyst revised in 2009* [86,87].

The revised potential cycle profile is triangular instead of rectangular and also the potential range is increased (between 0.6 V and 1.0 V). The cycle period is reduced to 16 s, with a potential sweep rate of 50 mVs^{-1}. The suggested pressure is atmospheric, while in the 2007 version a 150 kPa absolute pressure was proposed. The suggested characterization techniques and the measurements frequencies are almost the same (except few point in the polarization curves). The DOE target for the catalytic mass activity is now ≤40% loss of initial catalytic activity, while polarization curve and the ECSA is the same of 2007. The test protocol for the catalyst support suggested by U. S. DOE has been proposed again in the revision of 2009 with the same testing parameters [86,87].

In 2013 the United States Driving Research and Innovation for Vehicle Efficiency (U. S. DRIVE) updated the previous U. S. DOE cell component accelerated stress test protocols for PEM fuel cells [7]. The test protocol for the electrocatalyst based on triangle sweep cycles modified in the DOE version of 2009 has been confirmed in this document. The DOE test protocol for the catalyst support

suggested in 2007 and proposed again in 2009 has been modified. The potential is no more hold constant at 1.2 V, but a triangular cycle between 1.0 V and 1.5 V is suggested. The cycle period is 2 s and the potential sweep rate is 500 mVs^{-1}. The total number of cycles suggested is 5,000, thus 400 h of operation. The changes of the previous test protocol for the catalyst support does not affect only the load profile, but also other operative parameters have been changed: the fuel cell operative temperature has been decreased from 95°C to 80°C, the relative humidity increased to 100% in both anode and cathode, the operative pressure hold at atmospheric conditions instead of 150 kPa absolute as suggested in 2007. The DOE test protocol revised in 2013 for the catalyst support is reported in *Table 16* and the load profile shown in *Figure 37*.

***Table 16**. U. S. DOE testing protocol for catalyst support revised in 2013 [7]. Catalytic activity should be measured in Amg^{-1} at 150 kPa abs backpressure at 857 mV iR-corrected on 6% H_2 (bal N_2)/O_2, 100% RH, 80°C normalized to initial mass of catalyst and measured before and after test. Polarization curves should follow the procedure "Fuel Cell Tech Team Polarization Protocol" [7]. Cyclic voltammetry sweep from 0.05 to 0.6 V at 20mVs^{-1}, 80°C, 100% RH.*

Fuel cell	single cell 25-50 cm^2
Cycle profile	triangle sweep cycle: 500 mVs^{-1} between 1.0 V and 1.5 V; run polarization curve and ECSA; repeat for total 400 h
Cycle number	5,000 cycles
Cycle time	2 s
Temperature	80°C
Relative humidity	anode/cathode 100%/100%
Fuel/oxidant	H_2/N_2
Pressure	atmospheric

Metric	**Frequency**	**Target**

Catalytic activity	at beginning and end of test, minimum	≤40% loss
Polarization curve from 0 to ≥ 1,500 Acm^{-2}	after 0, 10, 100, 200, 500, 1k, 2k, and 5k cycles	≤30 mV loss at 1,500 mAcm^{-2} or rated power
ECSA from cyclic voltammetry	after 0, 10, 100, 200, 500, 1k, 2k, and 5k cycles	≤40% loss

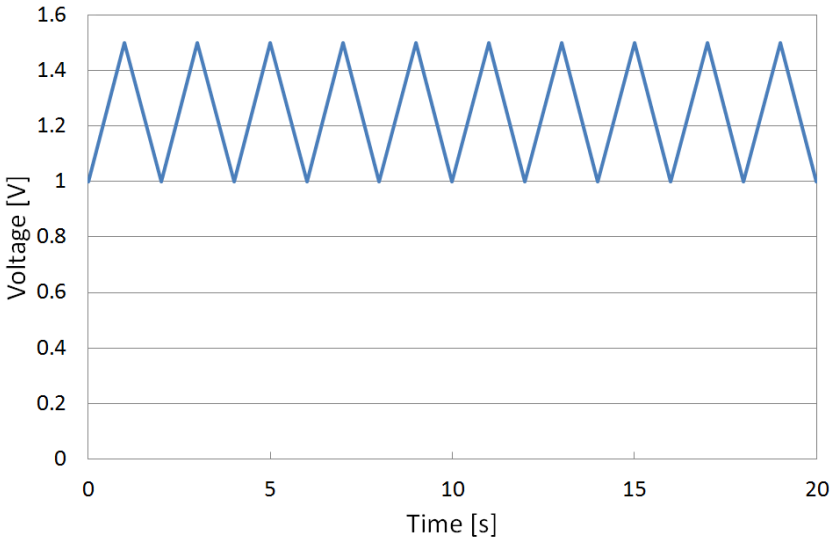

***Figure 37**. U. S. DOE testing protocol for supports revised in 2013 [7].*

In the 2013 revision also the suggested characterization procedure during the test has been modified. The CO_2 release is no more taken into account and both polarization curves and cyclic voltammetry measurements have been intensified at the beginning of the test as shown in *Table 16.*

A2.1.2 Literature review

Some reviews on accelerated stress tests for PEMFC have been published in the last years [105,106]. Frisk et al. [107] suggested an accelerated degradation protocol for PEMFC electrocatalyst based on the application of a fixed relative potential of 1.2 V, a cell operative temperature of 80°C and fully humidified reactants (N_2 at

the cathode and H_2 at the anode). More and Reeves [14] proposed a potential cycling test with a linear sweep from 0.1 V to 1.0 V (or 1.2 V) at 10 mVs^{-1}, 60°C (or 80°C) and 50% (or 100%) relative humidity of the reactants (N_2 at the cathode and H_2 at the anode). Borup et al. [40] suggested a potential cycling procedure as well, with a linear potential sweep from 0.1 V to an upper limit that varies from 0.8 V to 1.5 V at 10 mVs^{-1} in increments of 300 cycles. The operative cell temperature is 80°C, cathode is fed with N_2 with 226% RH and the anode with fully humidified H_2. Debe at al. [108] tested two new PEMFC catalyst durability test protocols using 3M's nanostructured thin film (NSTF) catalysts, which do not use carbon-supports or additional ionomer in the electrode layer (see *Paragraph 2.4*). In one test they used an automotive start/stop testing protocol provided by Nissan and compared the NSTF catalyst durability with the one of a conventional carbon supported dispersed Pt catalyst. In a second test they subjected the cell to high current density operation (over 1,600 scans between 0.1 and 2 Acm^{-2}) under totally dry H_2/O_2 conditions. Dillet et al. [38] developed a procedure to simulate the effects of start-ups and shutdowns separately. Then they investigated the effects of 700 start-up and shutdown cycles on performance degradation of PEMFCs with different Pt loadings. In the start-up aging protocol, hydrogen has been introduced in the air-filled anode compartment, whereas the shutdown effects were minimized by injecting high flow of nitrogen during each shutdown. In the shutdown aging protocol, air has been introduced in the hydrogen-filled anode compartment, whereas the fuel cell was started-up again only after carefully flushing the anode compartment with nitrogen, which minimized the start-up effects. In both the aging protocol, the fuel cell has been operated at a fixed current density of 0.67 Acm^{-2} for 5 min between two consecutive start-up or shutdown sequences in order to monitor the performance decrease. They found that start-ups are consistently more damaging than the shutdowns and this was evidenced by more

evolved CO_2 and charge exchanged, severe ECSA decrease, and higher performance losses.

In order to accelerate catalyst support degradation, Roen et al. [109] performed potential cycling from 0.04 V to 1.20 V (vs. RHE) at 2 mVs^{-1} with a cell operative temperature of 50°C and fully humidified 4% H_2/N_2 and He for anode and cathode, respectively. They concluded that platinum accelerated the corrosion rate of the carbon catalyst support. Makharia et al. [110] suggested idle and OCV condition as a suitable stressor to accelerate support degradation (idle at 0.9 V vs. RHE and OCV for 2,000 h at 80°C). They moreover recognized start/stop and local fuel starvation as an accelerating mechanism for carbon-support corrosion. Borup et al. [40] proposed load cycling operation also for the support accelerated ageing. They applied a potential sweep method to single cells to investigate the effect on electrocatalyst growth and its use as an accelerated testing technique. The dynamic test conditions simulated the US06 drive cycle. During potential sweeping, the anode was fed with hydrogen, while the cathode with nitrogen. The cathode potential was swept linearly with time from an initial voltage (usually 0.1 V) to an upper limit voltage, which was varied from 0.8 to 1.5, with increments of 300 cycles. Linse et al. [111] studied the effect of platinum on carbon corrosion in PEMFCs by means of single triangular potential sweeps with various upper and lower limits. For each investigated condition, the cell operated in H_2/N_2 or air/air mode was exposed to eight single triangular potential sweeps with a scan rate of 30 mVs^{-1}. The contribution of platinum catalysed carbon corrosion to total CO_2 evolution was found to decrease with increasing upper potential limit. Moreover, due to the high oxygen equilibrium potential of approximately 1 V, carbon corrosion in air/air mode has been found to be significantly influenced by platinum oxide formation.

A2.2 Other test protocols for PEMFCs

The test protocols presented in this paragraph are not specifically intended to accelerate the degradation of a specific component, such as electrocatalysts or supports. These procedures have instead the purpose to test the behaviour of the entire fuel cell during long-term operation. In some of these protocols the testing parameters are designed in order to simulate the fuel cell operative conditions in real applications. A significant part of the current research on fuel cells is promoted by automotive industry and dynamic testing is used simulate the real operation of a fuel cell stack in a car. Most of these durability tests are based on load cycling and start/stop operation. Dynamic operation, as discussed in *Paragraph 2.3.2*, is one of the main stressors for electrocatalyst degradation. Moreover, electrocatalyst durability is also considered the primary degradation issue in fuel cells systems for automotive applications. For these reasons, most of the durability testing protocols developed for fuel cell stacks are also particularly appropriate to investigate electrocatalyst degradation. Some of those protocols will be presented in this paragraph.

A2.2.1 European Commission JRC test protocols

In 2006 the Institute for Energy and Transport of the European Commission Joint Research Centre in collaboration with the Chemical Science and Engineering Division of the Argonne National Laboratory (USA) published an overview of international polymer-electrolyte fuel cell (PEMFC) test procedures. The purpose of this document was to be the first step in the global harmonization of testing methods, facilitate the understanding of test results and accelerate the commercialization of PEMFCs [112]. In 2006 the Research & Training Network (RTN) FCTESTNET (Fuel Cells Testing

& Standardisation NETwork) proposed two duty cycles shown in *Figure 38* and *Figure 39*.

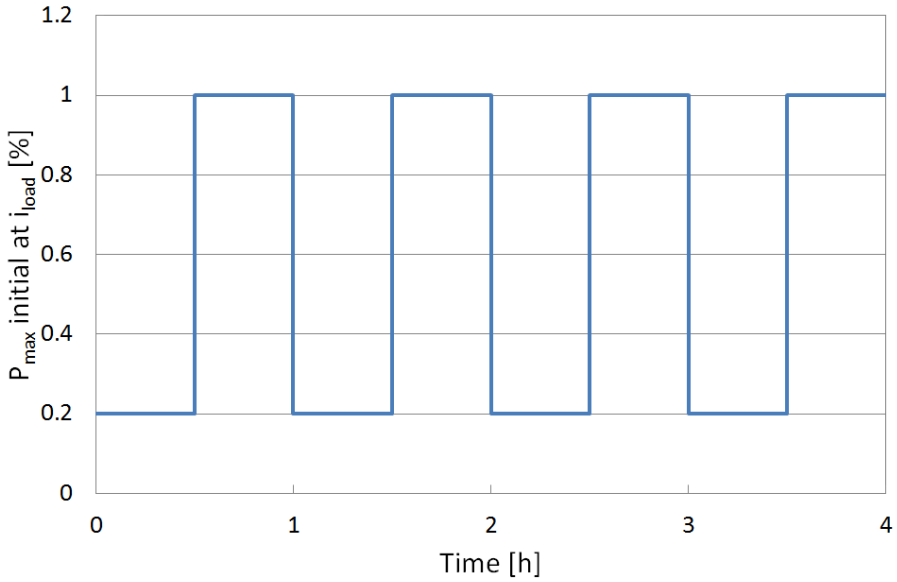

***Figure 38**. 2006 FCTESTNET testing protocol profile* [113].

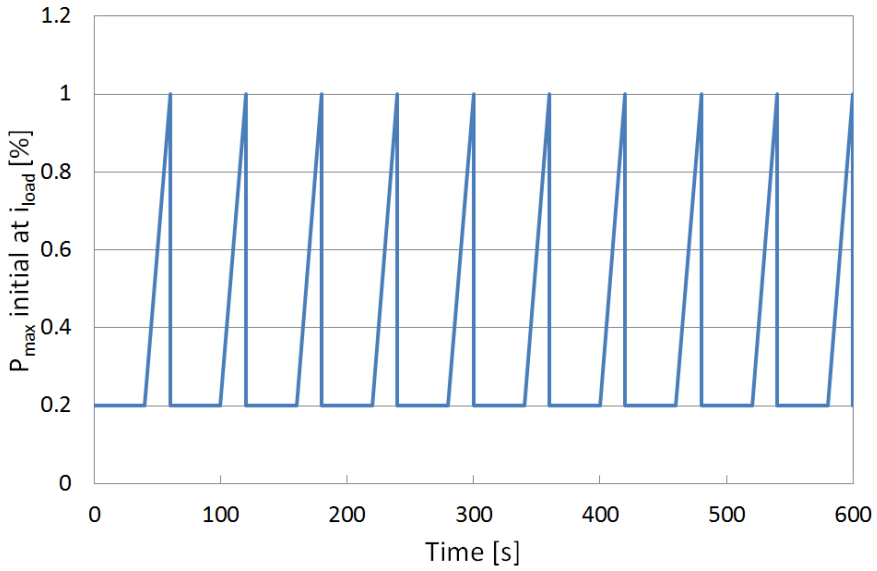

***Figure 39**. 2006 FCTESTNET testing protocol profile* [88].

These load cycling profiles has been proposed for both cell-level testing and stack testing. The purpose of these tests was to introduce different degrees of stress on the stack during the ageing process. IEC used these procedures as part of its Technical Specification on single cell testing. In the FCTESTNET report revised in 2010 [88] the load cycle profile showed in *Figure 38* has been proposed again. Even if this test module is specifically adapted for transportation applications, it can also be used to qualify the generic performance of a single cell or stack subjected to load cycling in order to characterize PEMFC components such as MEAs or sub-components of MEAs for research and development purposes [88]. The dynamic cycling of the ageing test consists in a current profile defined by a low power stationary phase of 40 s at a current equal to the 20% of the nominal one followed by a high power dynamic phase of 20 s with an increase of the current from the 20% to the 100% of the nominal value. It is suggested to measure 10 polarization curves at fixed equal intervals during the test. The maximum indicated duration of the test is between 500 and 10,000 hours depending on the operating conditions and on the application concerned. After the initial polarization curve, the current density should be fixed at the nominal value for a first high power phase of 10 minutes in order to stabilize the operating conditions before starting the dynamic cycling phase.

A2.2.2 Driving cycle protocols

In 2005 U. S. DOE released a first version of a recommended procedure for acquiring 2,000 h of stack-test data taken with variable loads [114]. The purpose was to assess the performance and durability of fuel cells for automotive applications and to compare cell and stack performance with U. S. DOE targets. This protocol simulates the automotive-type transients, but many issues such as the fuel cell behaviour under start/stop conditions are not taken into account [2]. In 2006 the US Fuel Cell Council (USFCC), in

2013 merged with National Hydrogen Association to form the Fuel Cell and Hydrogen Energy Association (FCHEA) [115], published a report on fuel cell component testing with the purpose to supply guidance to academia and the fuel cell industry on suggested dynamic testing profile for fuel cells [116]. In this report they suggested a dynamic testing profile based on the Federal Urban Schedule (FUDS) or the EPA Urban Dynamometer Driving Schedule [117]. In 1988 the DOE/EHP Battery Test Task Force (BTTF) developed a simplified version of the FUDS regime (SFUDS), originally derived for a specific vehicle, the Improved Dual Shaft Electric Propulsion (IDSEP). For driving-cycle testing of USABC batteries, the SFUDS profile was modified into the Dynamic Stress Test (DST) and was used in battery testing by the Argonne National Laboratory [116]. The profile developed by USFCC in the protocol of 2006 derived from the DST profile by eliminating the battery charging points and extending the higher power points. The resulting dynamic testing profile (DTP) cycle runs for 300 seconds and averages about 20% power. The load profile of the test is shown in *Figure 40.* The 100% power point has to be determined from the results of an initial power calibration curve and the limits of the fuel cell.

In Europe, a similar test protocol for automotive applications has been developed. The New European Driving Cycle (NEDC) is a driving cycle designed to simulate the typical usage of a car in Europe and assess emissions and fuel economy in passenger cars. It consists of four repeated ECE-15 urban driving cycles (UDC) and one Extra-Urban driving cycle (EUDC). The test protocol is defined in UNECE R101 [118] and maintained by the UNECE World Forum for Harmonization of Vehicle Regulations (WP.29) [119], today World Light Test Procedure (WLTP). Even if the protocol has been originally designed for petrol-based road vehicles, the driving cycle is currently also used to estimate electric power consumption, driving range and durability of Hybrid (HEV), Battery (BEV) and Fuel Cell (FCEV) Electric Vehicles [118]. The profile shown in *Figure*

41 was adapted from the original R15 cycle by relating speed to power and squaring the pulses [118].

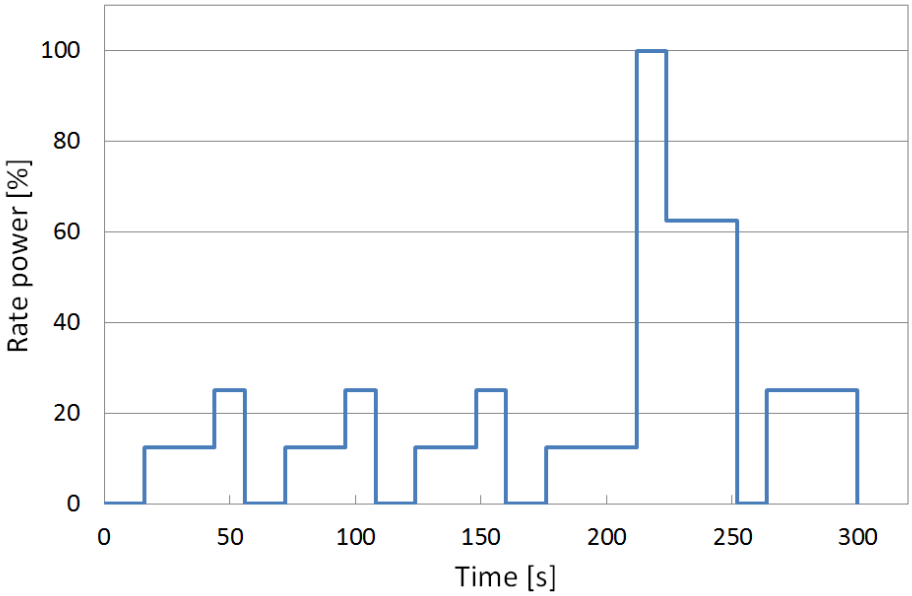

***Figure 40**. 2006 USFCC testing protocol profile [73].*

The dynamic load profile is defined by 35 steps, each with an individual dwell time and stack load value (in % of maximum load). The total duration of the cycle is 1,181 s. In 2014 Zentrum für Sonnenenergie- und Wasserstoff-Forschung Baden-Württemberg (ZSW) modified the NEDC dynamic load profile to investigate the degradation and lifetime of fuel cell components [120]. The load profile is shown in *Figure 42*.

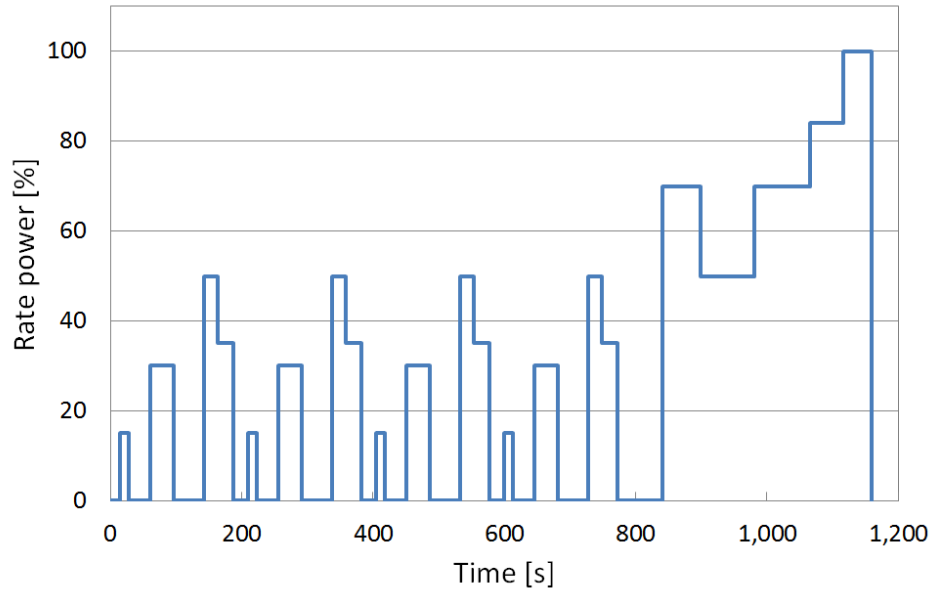

***Figure 41**. New European Driving Cycle (NEDC) adapted for fuel cell testing* [112].

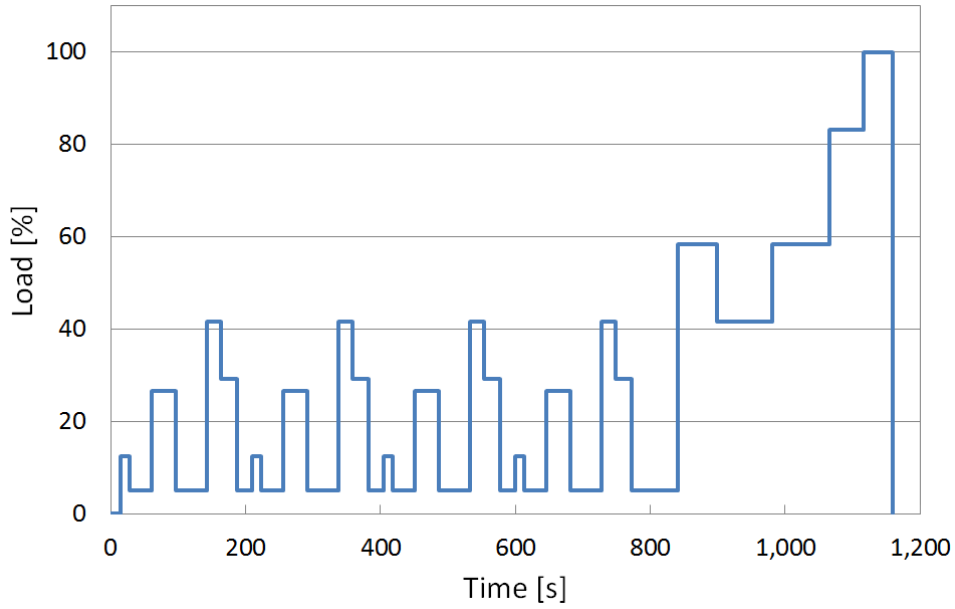

***Figure 42**. 2014 ZSW dynamic load profile derived from NEDC* [120].

A2.2.3 Literature review on LT-PEMFCs

Liu et al. [4] performed a long-term durability test based on load cycling and compared the results with the ones of steady-state operation. Each current aging cycle composed of 16 steps including open circuit, low current settings, intermediate current settings and the highest current setting, as shown in *Figure 43*. The duration of one cycle was 6 min. The MEA subjected to load cycling was aged for 10 aging periods, with 1,000 cycles or 100 h per period. Operation parameters have been measured after each 100 h aging period. Hydrogen crossover increased dramatically after 500 h of current cycling due to pinhole formation in the cyclically aged MEA, while it remained approximately constant during the steady-state test, where the major source of decreased performance were identified as due to mass transport limitations. This decrease in performance was partially reversible when cathode flooding was reduced by setting the cell at lower current densities.

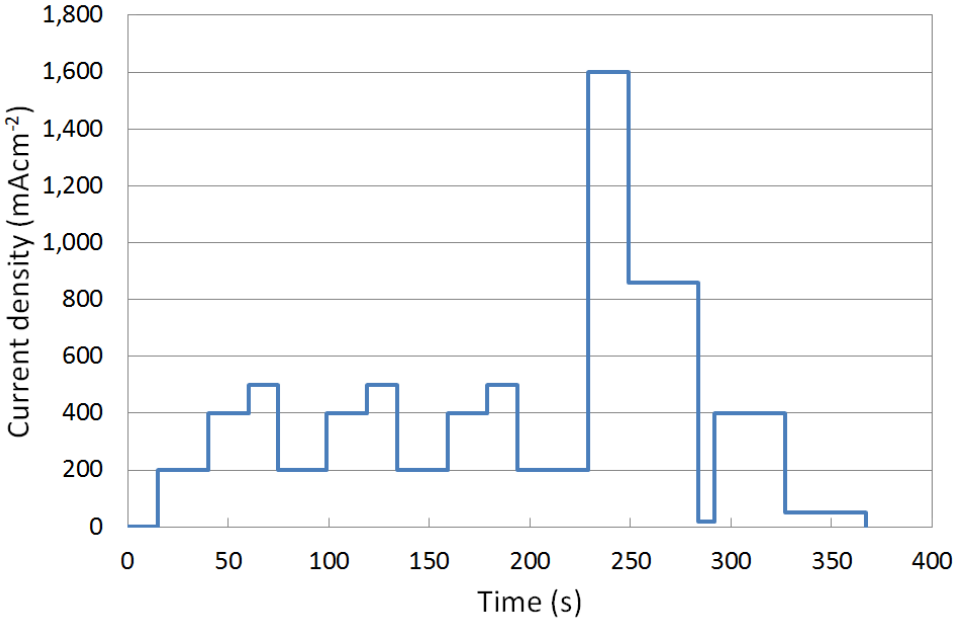

***Figure 43**. Load cycle profile developed by Liu et al. in 2006 [4].*

Borup et al. [121] tested a PEMFC in steady-state conditions and dynamic conditions using power cycling simulating a vehicle drive cycle and by accelerated testing methods. They observed a greater rate of particle growth in the test simulating automotive drive cycles than in the test in which the cell potential has been held constant. The loss of Pt ECSA has been shown to be due primarily to the growth in platinum particle size that appears to have multiple growth mechanisms. Moreover they observed the dependence of cathode particle size growth with temperature, relative humidity and potential. Wahdame et al. [100] carried out a 100 h steady-state test at 500 $mAcm^{-2}$ and a load cycling test based on transportation load profiles on two different 100 W stacks of 3 cells each. They observed that the average value of the load current over a cycle seems to have a very significant impact on the ageing process. Claude et al. [122] performed different accelerated stress tests in 12 fuel cells stack (on/off, back-up and base-load regimes) and compared the results with two on-site tests, a base load power application and a system coupled with photovoltaic panels operated in semi-base load mode. The on/off ageing test was performed during 500 h (around 6500 cycles) with a cycle of 2 min at OCV, followed by 10 s at 21 A and then 1 min 50 at 40 A. During the backup ageing test (1,800 h) the stack has been operated at 35 A for 4 h (T = 60°C, RH = 75% and λ = 2.5) and then it has been stored during 6 weeks in a climatic chamber at constant temperature and relative humidity before the next current solicitation. The base-load ageing test was performed at 45 A (T = 75°C, RH = 75% and λ = 2.5) for 500 h. The accelerated tests performed in laboratory did not reveal systematic MEA modifications during 500 h of operation while the 1500 h on-site system operation results in some MEA degradations. Scholta et al. [123] tested PEMFC stacks intended for long-term operation on reformate in domestic CHP systems. Since the performance decay strongly depends on gas composition, it has been investigated as close as possible to real operation conditions. The standard reformate used to feed the anode is a simulated

reformate containing hydrogen with additional 30 $\%_{mol}$ CO_2 and 5 $\%_{mol}$ CH_4. The tests have been performed in galvanostatic mode and a predefined 24 h load cycle was applied, as shown in *Figure 44*.

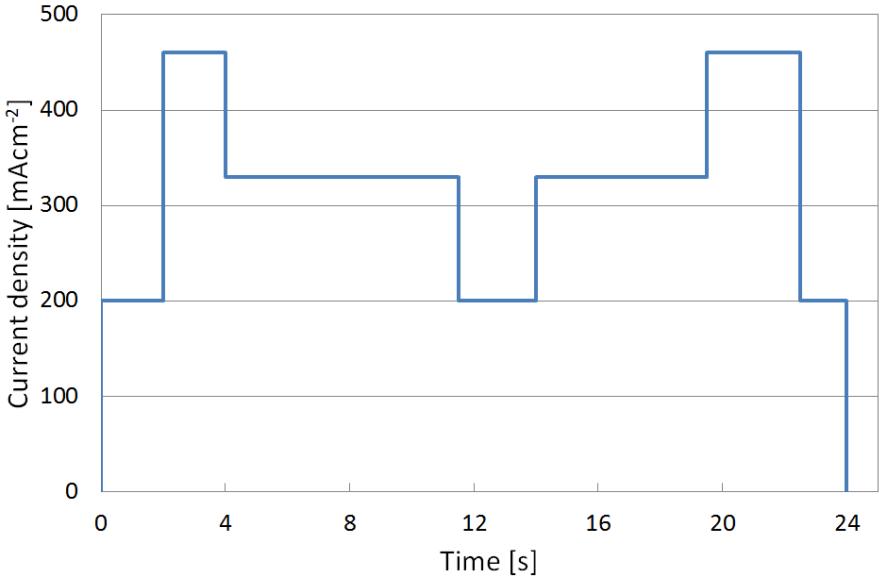

***Figure 44**. Load cycling profile used by Scholta et al. to simulate PEMFC long-term operation on reformate in domestic CHP systems* [123].

The load cycle profile simulates the load changes expected for a CHP house energy supply and included an OCV test under media flow. Every week, a current voltage curve and an OCV test under air shutdown were recorded. The total cumulated operation time of the stacks was more than 65,000 h, equivalent of almost 8 years of accumulated testing time. The degradation rates were higher during the first phase of the test (from 50 to 80 μVh^{-1}), while in the second one they significantly decreased (10.3 μVh^{-1} @0.46 Acm^{-2}). This result can be due to the change from H_2/N_2 mixtures to the use of simulated reformate gas. Wu et al. [45] performed accelerated stress tests to study the degradation mechanism of Nafion/PTFE composite membrane in PEM fuel cell with intensive RH cycling and load cycling. The cells were first aged at 0.6-0.7 V for more than 24 h under fully humidified conditions. The AST procedure consisted of

an alternation of 24 h of RH cycling (between dry and 100% RH conditions every 30 min) and 24 h of load cycling (between idle and heavy load conditions every 7 min and 3 min). They verified that the membrane has been chemically degraded by radicals attack due to the intensification of gas mutual permeation. Moreover, membrane thinning, Pt particles gathering along the interfaces and ionomer disappearing at cathode side has been observed from TEM and SEM results. Liu et al. [37] studied the long-term durability for of PEMFCs for vehicular applications using a drive cycle test protocol developed by Chinese NERC Fuel Cell & Hydrogen Technology and shown in *Figure 45*. The test has been performed on a 25 cm^2 single cell fed with H_2 and air at 70°C and consisted in four values of discharge current density (147 $mAcm^{-2}$, 500 $mAcm^{-2}$, 588 $mAcm^{-2}$ and 794 $mAcm^{-2}$) which simulate working conditions of starts/stops, idling and acceleration in real automobile application (loading step-up rate is 2.56 $mAcm^{-2}s^{-1}$ and loading step-down rate is 64 $mAcm^{-2}s^{-1}$).

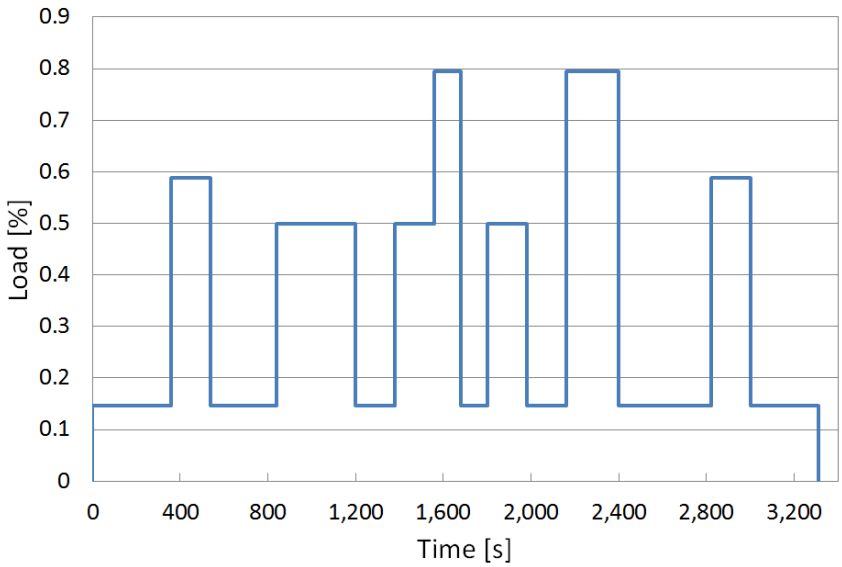

***Figure 45**. Drive cycle test protocol developed by Chinese NERC Fuel Cell & Hydrogen Technology and used by Liu et al. [37].*

After 900 h of load cycling the cell performance degraded at a rate of about 70 mVh^{-1} at current density of 500 $mAcm^{-2}$, 55% of the original cathode ECSA was lost and both electron and proton transfer resistances increased.

A2.2.4 Literature review on HT-PEMFCs

Some durability tests have been specifically developed for high temperature PEM fuel cells, in order to assess their behaviour during long-term operation. Yu et al. [124] performed long-term (10,000 h) tests of PBI-based PEMFC using protocols designed to simulate fuel cell operation in real applications. The test protocols included long-term operation at fixed conditions, load cycling, thermal cycling and start/stop cycling. All the tests were conducted using non humidified gases (H_2 and air) on single cells with an active area of 45.15 cm^2. The fuel cells were heated up by means of two heating pads and cooled down by an external fan. Thermal cycling tests were conducted by changing the fuel cell operative temperature and keeping constant the current density at 200 $mAcm^{-2}$. During the steady-state long-term test the current has been hold at 200 $mAcm^{-2}$ and the flow rates fixed with hydrogen (λ = 1.2, 75 $mLmin^{-1}$) as a fuel and air (λ = 2.0, 301 $mLmin^{-1}$) as an oxidant. Tests of 800-1,000 h have been conducted at different temperatures between 80°C and 190°C. The load cycling profile consisted in 2 min of OCV, 30 min at 200 $mAcm^{-2}$, 30 min at 600 $mAcm^{-2}$, and it has been repeated for 500 cycles. The thermal cycling test was based on two sets of temperature cycles: 100 high temperature cycles between 180°C and 120°C and 100 low temperature cycles between 120°C and 80°C. The fuel cells have been subjected to 100 h of break-in time (160°C and 200 $mAcm^{-2}$) before all the dynamic tests. The start/stop cycles were designed to simulate the fuel cell shutdown and restarting that is likely to occur in a real system operation. During the start-up the fuel cell has been heated to 120°C at OCV and then to 180°C at 10 $mAcm^{-2}$ with the minimum flow (Q_{H2}

= 50 $mLmin^{-1}$, Q_{air} = 83 $mLmin^{-1}$). The fuel cell has been operated for 3 h at 200 Acm^{-2} with hydrogen (λ = 1.2, 75 $mLmin^{-1}$) and air (λ = 2.0, 301 $mLmin^{-1}$). The shutdown procedure consisted in setting the load to OCV and reducing the gas flows to the minimum (Q_{H2} = 50 $mLmin^{-1}$, Q_{air} = 83 $mLmin^{-1}$) for 1 min in order to remove residual product water from the cell and then cooling down the fuel cell to 55°C without reactants. This cycle lasted about 6 h and it has been repeated for 100 times during the durability test. The voltage degradation during the steady-state operation at 160°C tests was low (4.9-6.3 μVh^{-1}). The phosphoric acid (PA) loss depended on the operative temperature: a significant increase in the PA loss rates has been observed at 180°C and 190°C. Moreover, the PA loss from the cathode was the major contributor to the overall PA loss rate form the MEA. During the dynamic durability tests the combination of high operative temperatures and high loads led to high water generation at the cathode and a steam distillation mechanism for PA removal from the MEA. Anyway, due to the abundance of PA in the membranes, PA loss does not seem to be a major factor of fuel cell failure under typical operating conditions. Moçotéguy et al. [125] tested a single cell and a 500 We 24-cells HT-PEMFC stack under accelerated typical annual μ-CHP profile. Both the single cell and the stack were assembled with BASF PEMEAS Celtec®-P 1000 MEAs and were operated at 160°C. The single cell active area was 49.5 cm^2 and the hardware designed for high temperature operation by BASF fuel cell. The stack has been designed and built by ZSW and assembled with 24 MEAs of 100 cm^2 active area. Both the single cell and the stack have been activated with a break-in procedure consisting of constant operation at 200 $mAcm^{-2}$, 160°C, atmospheric pressure and non-humidified reactants (hydrogen with λ = 1.2 and air with λ = 2.0). During all the ageing tests the single cell was operated with non-humidified H_2 containing 1% CO and air (λ_{H2} = 1.2, λ_{air} = 2.0), while the stack was operated with non-humidified synthetic reformate gas (70% H_2 + 29% CO_2 + 1% CO) and air (λ_{H2} = 1.4, λ_{O2} = 2.0). The test comprises 4 phases that have been defined according

to the demand characteristics of each season. The winter season has been simulated with 250 h of operation at 400 $mAcm^{-2}$ due to a high heat demand, the variation between various heat demand levels and continuous operation at intermediate power level that has been observed during spring has been simulated with 120 h daily cycling between 400 $mAcm^{-2}$ and 200 $mAcm^{-2}$ followed by 120 h of constant operation at 200 $mAcm^{-2}$, the low heat demand of summer has been simulated with 240 h daily start/stop cycling between 0 and 200 $mAcm^{-2}$, the variation between various heat demand levels and continuous operation at intermediate power level that has been observed in autumn has been simulated with 120 h daily cycling between 400 $mAcm^{-2}$ and 200 $mAcm^{-2}$ followed by 120 h of constant operation at 200 $mAcm^{-2}$. During the shutdown procedure, the single cell has been purged with N_2 at the cathode, while for the stack no N_2 purge was made. The total operation time was 1,000 h for the single cell and 674 for the stack. The cell performance during the single cell testing was very stable on voltage cycling over the two periods of 250 h, while the start-stop operation induced performance decline of about 1 mV per cycle over 10 cycles. At the stack level OCV was almost unaffected by ageing and performance losses remained negligible for the first 400 h of operation, including four start/stop cycles. Performance loss increased during the second period of constant operation at 200 $mAcm^{-2}$ with 3 additional start/stop cycles mainly due to some specific cells which exhibited a significantly higher degradation rate associated with lower OCV at beginning of life. The cell position has also been a determinant parameter in the voltage evolution during transient steps: the cells at stack dead end and the ones which exhibit the highest overall degradation rates showed a strong increase of the voltage undershoots. Hartnig et al. [126] performed simulated start/stop cycling in order to study the corrosion stability of supported catalysts employed in HT-PEMFCs. BASF PEMEAS Celtec®-P 1000 MEAs have been used in the tests. Degradation effects have been studied at different current densities with the purpose to

differentiate kinetic and mass transport effects. 150 simulated start/stop cycles were applied to three 50 cm^2 single cells with different cathodes (1 mg_{Pt}/cm^2 30% Pt/Vulcan XC-72, 0.75 mg_{Pt}/cm^2 30% Pt-alloy/Vulcan XC-72, 0.75 mg_{Pt}/cm^2 20% Pt/SC). The break-in procedure consisted in 15 h at 160°C and 200 $mAcm^{-2}$ with H_2 and air (λ_{H2} = 1.2, λ_{air} = 2.0) at ambient pressure. Then the cell temperature has been increased to 180°C and a first polarization curve has been measured in order to determine the beginning of life performance in two configurations of reactants: H_2/air (λ_{H2} = 1.2, λ_{air} = 2.0) and H_2/O_2 (λ_{H2} = 1.2, λ_{O2} = 9.5). The simulated start/stop cycles were performed keeping the fuel electrodes gas flows constant at 3.3 Nlh^{-1} and the air electrode constant at 20 Nlh^{-1}: the air electrode gas was air in all cases, while the fuel electrode gas was automatically switched every 90 s between pure hydrogen and air. The purpose of this procedure was to allow the H_2/air front to pass through the fuel electrode flow field at each cycle. The fuel cell was kept in OCV during the gas cycling and a polarization curve has been recorded every 50 cycles. The CO_2 content in the cathode exhaust gas was monitored online during the test with measurement intervals of 2 s. The accelerated aging test results have been then correlated with the ones of a more realistic durability test over 4,000 h and 157 start/stop cycles based on 16 h of operation at 200 $mAcm^{-2}$ and cool down to 25-30°C for 8 h. The cell was not purged during the stop period. The start-up procedure consisted in heating up the cell to 80°C, flow 3 Nlh^{-1} of hydrogen and 5 Nlh^{-1} of air and setting the load at 200 $mAcm^{-2}$ when 140°C were reached. The fuel cell outlets were kept open during the whole experiment. Comparing the simulated start/stop cycling test with the realistic one they found almost identical changes in MEA properties, demonstrating the validity of the proposed accelerated stress test for the simulation of start/stop cycling.

Bibliography

[1] J. Zhang, PEM Fuel Cell Electrocatalysts and Catalyst Layers, Springer London, 2008.

[2] R. Borup, J. Meyers, B. Pivovar, Y.S. Kim, R. Mukundan, N. Garland, et al., Scientific aspects of polymer electrolyte fuel cell durability and degradation., Chem. Rev. 107 (2007) 3904–51.

[3] U. S. Department of Energy, Fuel Cell Technologies Office Multi-Year Research, Development, and Demonstration (MYRD&D) Plan, 2012.

[4] D. Liu, S. Case, Durability study of proton exchange membrane fuel cells under dynamic testing conditions with cyclic current profile, J. Power Sources. 162 (2006) 521–531.

[5] W. Vielstich, H.A. Gasteiger, A. Lamm, Y. Harumi, Handbook of Fuel Cells - Fundamentals, Technology and Applications, 2010.

[6] H. Wang, H. Li, X.-Z. Yuan, PEM Fuel Cell Failure Mode Analysis, 2012.

[7] U. S. DRIVE, Fuel Cell Technical Team Roadmap, 2013.

[8] A. Chandan, M. Hattenberger, A. El-kharouf, S. Du, A. Dhir, V. Self, et al., High temperature (HT) polymer electrolyte membrane fuel cells (PEMFC) e A review, J. Power Sources. 231 (2013) 264–278.

[9] S.Z. Yi, F.F. Zhang, W. Li, C. Huang, H.N. Zhang, M. Pan, Anhydrous elevated-temperature polymer electrolyte membranes based on ionic liquids, J. Membr. Sci. 366 (2011) 349–355.

[10] P.J. Hamilton, B.G. Pollet, Polymer electrolyte membrane fuel cell (PEMFC) flow field plate: design, materials and characterisation, Fuel Cells. 10 (2010) 489–509.

[11] C. Hartnig, T.J. Schmidt, On a new degradation mode for high-temperature polymer electrolyte fuel cells: How bipolar plate degradation affects cell performance, Electrochim. Acta. 56 (2011) 4237–4242.

[12] P.J. Ferreira, G.J. la O', Y. Shao-Horn, D. Morgan, R. Makharia, S. Kocha, et al., Instability of Pt/C Electrocatalysts in Proton Exchange Membrane Fuel Cells, J. Electrochem. Soc. 152 (2005) A2256.

[13] P. Ascarelli, V. Contini, R. Giorgi, Formation process of nanocrystalline materials from x-ray diffraction profile analysis: Application to platinum catalysts, J. Appl. Phys. 91 (2002) 4556.

[14] K.L. More, K.S. Reeves, Microstructural Characterization Of PEM Fuel Cell MEAs, in: DOE Hydrog. Progr. Annu. Merit Rev. Proc., 2005.

[15] W. Bi, G.E. Gray, T.F. Fullera, PEM Fuel Cell Pt/C Dissolution and Deposition in Nafion Electrolyte, Electrochem. Solid-State Lett. 10 (2007) B101–B104.

[16] R.M. Darling, J.P. Meyers, Kinetic Model of Platinum Dissolution in PEMFCs, J. Electrochem. Soc. 150 (2003) A1523.

[17] J. Xie, D.L. Wood, K.L. More, P. Atanassov, R.L. Borup, Microstructural Changes of Membrane Electrode Assemblies during PEFC Durability Testing at High Humidity Conditions, J. Electrochem. Soc. 152 (2005) A1011.

[18] G.G. Paik, G. Saloka, Influence of Cyclic Operation on PEM Fuel Cell Catalyst Stability, Electrochem. Solid-State Lett. 10 (2007).

[19] F.A. Uribe, T.A. Zawodzinski, A study of polymer electrolyte fuel cell performance at high voltages. Dependence on cathode catalyst layer composition and on voltage conditioning, Electrochim. Acta. 47 (2002) 3799–3806.

[20] K. Kinoshita, Carbon: Electrochemical and Physicochemical Properties, J. Am. Chem. Soc. 110 (1988) 541.

[21] T.J. Schmidt, Durability and degradation in high-temperature polymer electrolyte fuel cells, ECS Trans. 1 (2006) 19–31.

[22] T.J. Schmidt, J. Baurmeister, Durability and Reliability in High-Temperature Reformed Hydrogen PEFCs, ECS Trans. 3 (2006) 861–869.

[23] K.U. K. Mitsuda, T. Murahashi, M. Matsumoto, Estimation of corrosion conditions of a phosphoric acid fuel celle, J. Appl. Electrochem. 23 (1993) 19–25.

[24] F. Wang, D. Yang, B. Li, H. Zhang, C. Hao, F. Chang, et al., Investigation of the recoverable degradation of PEM fuel cell operated under drive cycle and different humidities, Int. J. Hydrogen Energy. (2014) 1–7.

[25] T. Schmidt, F. Buechi, M. Inaba, High Temperature Polymer Electrolyte Fuel Cells: Durability Insights, Springer New York, 2009.

[26] U.S. Department of Energy, 2006 Annual Progress Report, DOE Hydrogen and Fuel Cells Program, 2006.

[27] Y. Shao, R. Kou, J. Wang, V. V. Viswanathan, J.H. Kwak, J. Liu, et al., The influence of the electrochemical stressing (potential step and potential-static holding) on the degradation of polymer electrolyte membrane fuel cell electrocatalysts, J. Power Sources. 185 (2008) 280–286.

[28] S. Zhang, X.-Z. Yuan, J.N.C. Hin, H. Wang, J. Wu, K.A. Friedrich, et al., Effects of open-circuit operation on membrane and catalyst layer degradation in proton exchange membrane fuel cells, J. Power Sources. 195 (2010) 1142–1148.

[29] Z. Qi, S. Buelte, Effect of open circuit voltage on performance and degradation of high temperature PBI–H3PO4 fuel cells, J. Power Sources. 161 (2006) 1126–1132.

[30] J. Wu, X.-Z. Yuan, J.J. Martin, H. Wang, D. Yang, J. Qiao, et al., Proton exchange membrane fuel cell degradation under close to open-circuit conditions, J. Power Sources. 195 (2010) 1171–1176.

[31] S.D. Knights, K.M. Colbow, J. St-Pierre, D.P. Wilkinson, Aging mechanisms and lifetime of PEFC and DMFC, J. Power Sources. 127 (2004) 127–134.

[32] Y.M. Akira Taniguchia, Tomoki Akitab, Kazuaki Yasudab, , Taniguchi, A.; Akita, T.; Yasuda, K.; Miyazaki, M. J. Power Sources 2004, 130, 42, J. Power Sources. 130 (2004) 42–49.

[33] N. Yousfi-Steiner, P. Moçotéguy, D. Candusso, D. Hissel, A review on polymer electrolyte membrane fuel cell catalyst degradation and starvation issues: Causes, consequences and diagnostic for mitigation, J. Power Sources. 194 (2009) 130–145.

[34] J. Wu, X.Z. Yuan, J.J. Martin, H. Wang, J. Zhang, J. Shen, et al., A review of PEM fuel cell durability: Degradation mechanisms and mitigation strategies, J. Power Sources. 184 (2008) 104–119.

[35] Y. Yu, H. Li, H. Wang, X.-Z. Yuan, G. Wang, M. Pan, A review on performance degradation of proton exchange membrane fuel cells during startup and shutdown processes: Causes, consequences, and mitigation strategies, J. Power Sources. 205 (2012) 10–23.

[36] Y.-C. Park, K. Kakinuma, M. Uchida, D. a. Tryk, T. Kamino, H. Uchida, et al., Investigation of the corrosion of carbon supports in polymer electrolyte fuel cells using simulated start-up/shutdown cycling, Electrochim. Acta. 91 (2013) 195–207.

[37] M. Liu, C. Wang, J. Zhang, J. Wang, Z. Hou, Z. Mao, Diagnosis of membrane electrode assembly degradation with drive cycle test technique, Int. J. Hydrogen Energy. (2014) 2–7.

[38] J. Dillet, D. Spernjak, a. Lamibrac, G. Maranzana, R. Mukundan, J. Fairweather, et al., Impact of flow rates and electrode specifications on degradations during repeated startups and shutdowns in polymer-electrolyte membrane fuel cells, J. Power Sources. 250 (2014) 68–79.

[39] T.J. Schmidt, J. Baurmeister, Properties of high-temperature PEFC Celtec®-P 1000 MEAs in start/stop operation mode, J. Power Sources. 176 (2008) 428–434.

[40] R.L. Borup, J.R. Davey, F.H. Garzon, D.L. Wood, M. a. Inbody, PEM fuel cell electrocatalyst durability measurements, J. Power Sources. 163 (2006) 76–81.

[41] M. Cai, M.S. Ruthkosky, B. Merzougui, S. Swathirajan, M.P. Balogh, S.H. Oh, Investigation of thermal and electrochemical degradation of fuel cell catalysts, J. Power Sources. 160 (2006) 977–986.

[42] D.A. Stevens, J.R. Dahn, Thermal degradation of the support in carbon-supported platinum electrocatalysts for PEM fuel cells, Carbon N. Y. 43 (2005) 179–188.

[43] Y. Oono, T. Fukuda, A. Sounai, M. Hori, Influence of operating temperature on cell performance and endurance of high temperature proton exchange membrane fuel cells, J. Power Sources. 195 (2010) 1007–1014.

[44] S. Vengatesan, M.W. Fowler, X.-Z. Yuan, H. Wang, Diagnosis of MEA degradation under accelerated relative humidity cycling, J. Power Sources. 196 (2011) 5045–5052.

[45] B. Wu, M. Zhao, W. Shi, W. Liu, J. Liu, D. Xing, et al., The degradation study of Nafion/PTFE composite membrane in PEM fuel cell under accelerated stress tests, Int. J. Hydrogen Energy. (2014) 1–10.

[46] M.K. Debe, Electrocatalyst approaches and challenges for automotive fuel cells, Nature. 486 (2012) 43–51.

[47] Y. Shao, G. Yin, Y. Gao, Understanding and approaches for the durability issues of Pt-based catalysts for PEM fuel cell, J. Power Sources. 171 (2007) 558–566.

[48] M.K. Debe, Advanced Cathode Catalysts and Supports from PEM Fuel Cells, 2012.

[49] H. Wang, X. Yuan, H. Li, PEM fuel cell diagnostic tools, CRC Press, 2011.

[50] J. Wu, X. Yuan, H. Wang, M. Blanco, J. Martin, J. Zhang, Diagnostic tools in PEM fuel cell research: Part I Electrochemical techniques, Int. J. Hydrogen Energy. 33 (2008) 1735–1746.

[51] European Commission, FCTESTNET TM PEFC SC 5-2, V1.2, Testing the voltage-power as function of the current density, V. 1.2, 2006.

[52] M.M. Mench, Fuel Cell Engines, 2008.

[53] European Commission, PEFC power stack performance testing procedure, Measuring voltage and power as function of current density Polarisation curve test method, Test Module PEFC ST 5-3, 2009.

[54] S. Aricò, A. Stassi, E. Modica, R. Ornelas, I. Gatto, E. Passalacqua, et al., Performance and degradation of high temperature polymer electrolyte fuel cell catalysts, J. Power Sources. 178 (2008) 525–536.

[55] J. Hu, H. Zhang, Y. Zhai, G. Liu, B. Yi, 500h Continuous aging life test on PBI/H3PO4 high-temperature PEMFC, Int. J. Hydrogen Energy. 31 (2006) 1855–1862.

[56] B.K. Matsutani, K. Hayakawa, T. Tada, Platinum-Cobalt Catalysts on Stability Against Load Cycling, (2010) 223–232.

[57] H. Kumpulainen, T. Peltonen, In situ voltammetric characterization of PEM fuel cell catalyst layers, 2002.

[58] A. Pozio, M. De Francesco, A. Cemmi, F. Cardellini, L. Giorgi, Comparison of high surface Pt / C catalysts by cyclic voltammetry, 105 (2002) 13–19.

[59] L.D. A. M. Chaparro, A. J. Martín, M. A. Folgado, B. Gallardo, Comparative analysis of the electroactive area of Pt/C PEMFC electrodes in liquid and solid polymer contact by underpotential hydrogen adsorption/desorption, Int. J. Hydrogen Energy. (2009) 4838–4846.

[60] N.M.Z. A. D. Modestov, M. R. Tarasevich, V. Ya Filimonov, Degradation of high temperature MEA with PBI-H3PO4 membrane in a life test, Electrochim. Acta. 54 (2009) 7121–7127.

[61] S. Galbiati, A. Baricci, A. Casalegno, R. Marchesi, Degradation in phosphoric acid doped polymer fuel cells: A 6000 h parametric investigation, Int. J. Hydrogen Energy. 38 (2013) 6469–6480.

[62] B.R. Pauw, How to do a perfect SAXS measurement, Everything SAXS. (2011).

[63] O. Glatter, O. Kratky, Small angle X-ray scattering, Acad. Press. (1982).

[64] D. Svergun, L. Feigin, G. Taylor, Structure analysis by small angle X-ray and neutron scattering, (1987).

[65] Y. Shao-Horn, W.C. Sheng, S. Chen, P.J. Ferreira, E.F. Holby, D. Morgan, Instability of Supported Platinum Nanoparticles in Low-Temperature Fuel Cells, Top. Catal. 46 (2007) 285–305.

[66] W. Bi, T. Fuller, Temperature Effects on PEM Fuel Cells Pt/C Catalyst Degradation, ECS Trans. 11 (2007) 1235–1246.

[67] Y. Zhai, H. Zhang, D. Xing, Z.-G. Shao, The stability of Pt/C catalyst in H3PO4/PBI PEMFC during high temperature life test, J. Power Sources. 164 (2007) 126–133.

[68] C. Wannek, B. Kohnen, H.-F. Oetjen, H. Lippert, J. Mergel, Durability of ABPBI-based MEAs for High Temperature PEMFCs at Different Operating Conditions, Fuel Cells. 8 (2008) 87–95.

[69] C.-I. Hong, H.-Y. Kang, H.P. Wang, W.-K. Lin, U.-S. Jeng, C.-H. Su, Cu–ZnO@C nanoreactors studied by in situ synchrotron SAXS spectroscopy, J. Electron Spectros. Relat. Phenomena. 184 (2011) 301–303.

[70] D.A. Stevens, S. Zhang, Z. Chen, J.R. Dahn, On the determination of platinum particle size in carbon-supported platinum electrocatalysts for fuel cell applications, Carbon N. Y. 41 (2003) 2769–2777.

[71] C.S. Tsao, C.Y. Chen, Small-angle X-ray scattering of carbon-supported Pt nanoparticles for fuel cell, Phys. B Condens. Matter. 353 (2004) 217–222.

[72] J. Speder, A. Zana, I. Spanos, J.J.K. Kirkensgaard, K. Mortensen, M. Arenz, On the influence of the Pt to carbon ratio on the degradation of high surface area carbon supported PEM fuel cell electrocatalysts, Electrochem. Commun. 34 (2013) 153–156.

[73] M.C. Smith, J. a Gilbert, J.R. Mawdsley, S. Seifert, D.J. Myers, In situ small-angle X-ray scattering observation of Pt catalyst particle growth during potential cycling., J. Am. Chem. Soc. 130 (2008) 8112–3.

[74] B. Ruiz-Camacho, M. a. Valenzuela, R.G. González-Huerta, K. Suarez-Alcantara, S.E. Canton, F. Pola-Albores, Electrochemical and XAS investigation of oxygen reduction reaction on Pt-TiO2-C catalysts, Int. J. Hydrogen Energy. 8 (2013) 0–8.

[75] G. Liu, H. Zhang, J. Hu, Y. Zhai, D. Xu, Z. Shao, Studies of performance degradation of a high temperature PEMFC based on H3PO4-doped PBI, J. Power Sources. 162 (2006) 547–552.

[76] Y. Oono, A. Sounai, M. Hori, Long-term cell degradation mechanism in high-temperature proton exchange membrane fuel cells, J. Power Sources. 210 (2012) 366–373.

[77] BASF Fuel Cell, Celtec-P 1000 Membrane Electrode Assembly, Technical Information Brochure, (1997).

[78] Zahner, Thales Zennium-CV-software, (2011).

[79] H. Amenitsch, S. Bernstorff, M. Kriechbaum, D. Lombardo, H. Mio, M. Rappolt, et al., Performance and First Results of the ELETTRA High-Flux Beamline for Small-Angle X-ray Scattering, J. Appl. Crystallogr. 30 (1997) 872–876.

[80] A. Hammersley, ERSP International Report, ESRF98-HA01T, FIT2D V9, 129 Reference Manual V3.1, 1998.

[81] D. Pontoni, S. Finet, T. Narayanan, a. R. Rennie, Interactions and kinetic arrest in an adhesive hard-sphere colloidal system, J. Chem. Phys. 119 (2003) 6157.

[82] T.C. Huang, H. Toraya, T.N. Blanton, Y. Wu, X-ray powder diffraction analysis of silver behenate, a possible low-angle diffraction standard, J. Appl. Crystallogr. 26 (1993) 180–184.

[83] F. Valle, B. Marmiroli, H. Amenitsch, R. Taccani, Electron microscopy and small-angle X-ray scattering analysis of the catalyst layer degradation in PBI-based HT-PEM fuel cells, in: Convegno Naz. Assoc. Termotec. Ital., Trieste, 2012.

[84] S. Basu, Recent Trends in Fuel Cell Science and Technology, Springer Science & Business Media, 2007.

[85] BASF Fuel Cell, Cell Building and Testing Instructions, (n.d.).

[86] USCAR, USCAR Fuel Cell Tech Team Cell Component Accelerated Stress Test Protocols for PEM Fuel Cells, 2010.

[87] U.S. Department of Energy, DOE Solicitation DE-PS36-06GO96017, 2009.

[88] European Commission, FCTESTNET PEFC TM ST5-7, Measuring voltage and power as function of current density following a dynamic profile versus time. Dynamic load cycling aging profile, 2006.

[89] J.J. Hu, H. Zhang, Y. Zhai, G. Liu, B. Yi, Performance degradation studies on PBI/H3PO4 high temperature PEMFC and one-dimensional numerical analysis, Electrochim. Acta. 52 (2006) 394–401.

[90] U. S. Federal Government, ImageJ, (2004).

[91] U. S. Department of Energy, 2012 Annual Progress Report, DOE Hydrogen and Fuel Cells Program, 2012.

[92] NEDO, Outline of NEDO New Energy and Industrial Technology Development Organization, (2008) 80–86.

[93] Wikipedia, Fuel Cells and Hydrogen Joint Technology Initiative, (2014).

[94] European Hydrogen and Fuel Cell Technology Platform, Strategic Research Agenda, 2005.

[95] 2020-horizon.com, The fuel cell testing and standardization network(FCTESTNET), (2003).

[96] European Commission, Fuel Cell Systems Testing, Safety & Quality Assurance (FCTESQA), (2014).

[97] U. S. Department of Energy, DOE CELL COMPONENT ACCELERATED STRESS TEST PROTOCOLS FOR PEM FUEL CELLS, 2007.

[98] S. Zhang, X. Yuan, H. Wang, W. Merida, H. Zhu, J. Shen, et al., A review of accelerated stress tests of MEA durability in PEM fuel cells, Int. J. Hydrogen Energy. 34 (2009) 388–404.

[99] X.-Z. Yuan, H. Li, S. Zhang, J. Martin, H. Wang, A review of polymer electrolyte membrane fuel cell durability test protocols, J. Power Sources. 196 (2011) 9107–9116.

[100] B. Wahdame, D. Candusso, X. Francois, F. Harel, M. Pera, D. Hissel, et al., Comparison between two PEM fuel cell durability tests performed at constant current and under solicitations linked to transport mission profile, Int. J. Hydrogen Energy. 32 (2007) 4523–4536.

[101] N. Garland, Electrode Stability, excerpt from DOE Hydrogen Program 2006 Progress Report, (2006) 920–922.

[102] U. S. Department of Energy, Solicitation announcement DE-PS36-06GO96018, (2006).

[103] T.B. and J.K. Nancy Garland, DOE Fuel Cell Program: Durability Technical Targets and Testing Protocols, ECS Trans. 11 (2007) 923–931.

[104] U. S. Department of Energy, Hydrogen, Fuel Cells & Infrastructure Technologies Program Multi-Year Research, Development and Demonstration Plan, 2006.

[105] S. Zhang, X. Yuan, H. Wang, W. Merida, H. Zhu, J. Shen, et al., A review of accelerated stress tests of MEA durability in PEM fuel cells, Int. J. Hydrogen Energy. 34 (2009) 388–404.

[106] X. Yuan, H. Li, S. Zhang, J. Martin, H. Wang, A review of polymer electrolyte membrane fuel cell durability test protocols, J. Power Sources. 196 (2011) 9107–9116.

[107] A.S. J. Frisk, W. Boand, M. Hicks, M. Kurkowski, R. Atanasoski, MEA Component Durability, in: 2004 Fuel Cell Semin., San Antonio, TX, USA, 2004.

[108] M.K. Debe, A.J. Steinbach, K. Noda, Stop-Start and High-Current Durability Testing of Nanostructured Thin Film Catalysts for PEM Fuel Cells, ECS Trans. 3 (2006) 835–853.

[109] T.D.J. L.M. Roen, C.H. Paik, Electrocatalytic Corrosion of Carbon Support in PEMFC Cathodes, Electrochem. Solid-State Lett. 7 (2004) A19–A22.

[110] H.A.G. R. Makharia, S.S. Kocha, P.T. Yu, M.A. Sweikart, W.B. Gu, F.T. Wagner, Durable PEM Fuel Cell Electrode Materials: Requirements and Benchmarking Methodologies, ECS Trans. 1 (2006) 3–18.

[111] N. Linse, L. Gubler, G.G. Scherer, A. Wokaun, The effect of platinum on carbon corrosion behavior in polymer electrolyte fuel cells, Electrochim. Acta. 56 (2011) 7541–7549.

[112] G.D. Ira Bloom, John K. Basco, Lee K. Walker, Thomas Malkow, and G. Saturnio, Antonio Tsotridis, Fuel Cell Testing Protocols: An International Perspective, 2013.

[113] European Commission, FCTESTNET PEFC TM SC5-4, Accelerated aging procedure for single cell, V. 1.2, 2006.

[114] U. S. Department of Energy, Durability test Protocols for PEM Fuel Cells, 2005.

[115] Fuel Cell and Hydrogen Energy Association (FCHEA), (2014).

[116] FCHEA, Protocol on Fuel Cell Component Testing, Suggested Dynamic Testing Protocol (DTP), (2006).

[117] U. S. Environmental Protection Agency, EPA Urban Dynamometer Driving Schedule (UDDS), (2012).

[118] UNITED NATIONS, E/ECE/324/Rev.2/Add.100/Rev.3, 2013.

[119] The United Nations Economic Commission for Europe (UNECE), World Forum for Harmonization of Vehicle Regulations (WP.29), n.d.

[120] J.H. Alexander Kabza, Development of PEM Fuel Cell Stack Reference Test Procedures for Industry, 2014.

[121] R.L. Borup, J.R. Davey, F.H. Garzon, D.L. Wood, P.M. Welch, K. More, PEM Fuel Cell Durability With Transportation Transient Operation, (2008) 2014.

[122] E. Claude, G. De Moor, C. Bas, F. Lesage, A.S. Dane, E. Rossinot, et al., Understanding the Degradation of MEA in PEMFC : Definition of Structural Markers and Comparison Between Laboratory and On-Site Ageing, (n.d.).

[123] J. Scholta, J. Pawlik, N. Chmielewski, L. Jörissen, Longevity test results for reformate polymer electrolyte membrane fuel cell stacks, J. Power Sources. 196 (2011) 5264–5271.

[124] S. Yu, L. Xiao, B.C. Benicewicz, Durability Studies of PBI-based High Temperature PEMFCs, Fuel Cells. 8 (2008) 165–174.

[125] P. Moçotéguy, B. Ludwig, J. Scholta, R. Barrera, S. Ginocchio, Long Term Testing in Continuous Mode of HT-PEMFC Based H 3 PO 4 /PBI Celtec-P MEAs for µ-CHP Applications, Fuel Cells. 9 (2009) 325–348.

[126] C. Hartnig, T.J. Schmidt, Simulated start – stop as a rapid aging tool for polymer electrolyte fuel cell electrodes, J. Power Sources. 196 (2011) 5564–5572.

Curriculum vitae

Contact

Name:	Francesco Valle
Address:	via Genova Cavalleria 35, 33041 Aiello del Friuli, Italy
Landline:	+39 0431 998889
Mobile:	+39 328 1920912
Email:	fvalle@units.it / valle.phd@gmail.com

Education

2012 - 2014	Ph.D. in µCHP Energy Systems Università degli Studi di Trieste, Italy
2012	Professional qualification of Industrial Engineer Università degli Studi di Trieste, Italy
2012	Certificate of health and safety manager (RSPP) Università degli Studi di Trieste, Italy
2009 - 2012	M.Sc. in Mechanical Engineering (110/110) Università degli Studi di Trieste, Italy
2010 - 2011	Erasmus program during the M.Sc. University of Manchester, United Kingdom

2006 - 2009	Bachelor in Industrial Engineering (100/110) Università degli Studi di Trieste, Italy

Conferences, workshops and seminars

11-14/09/2012	Convegno Nazionale ATI Trieste, Italy
22-23/11/2012	Primo workshop italiano su celle a combustibile Perugia, Italy
14/12/2012	2nd Small Angle Xmas Workshop at Elettra Trieste, Italy
27/02/2013	National Instruments Days 2013 Milano, Italy
16-18/04/2013	Fundamentals and Development of Fuel Cells Karlsruhe, Germany
19/07/2013	Lubelski Park Naukowo Technologiczny conference Lublin, Poland
07-09/10/2013	1st FVG PhD Symposium Grado, Italy
11-13/12/2013	EERA and H_2FC workshop Roma, Italy
11-13/12/2013	European Fuel Cell, Piero Lunghi Conference Roma, Italy
31/03/2014	Fuel Cells @ ChemE at TU Delft Delft, The Netherlands
03-04/04/2014	Fuel Cell Science and Technology Amsterdam, The Netherlands
19-23/05/2014	ICTP Workshop on Material Challenges in Devices for Fuel Solar Production and Employment Trieste, Italy

Schools and courses

02-06/07/2012	Second Joint Summer School on Nanotechnology Università degli Studi di Udine

14-18/01/2013	Bath Electrochemistry Winter School University of Bath
10-16/03/2013	8th European NESY Winter-School Leoben University
02-07/2013	Electrode Systems, Prof Claudio Tavagnacco Università degli Studi di Trieste
02-07/2013	LabVIEW CLAE course, Prof Giuseppe Cautero Elettra
11/2013-03/2014	Programma Formazione e Innovazione FixO Università degli Studi di Trieste
22-28/06/2014	European Technical School on Hydrogen and Fuel Cells University of Ulster

Experience and internships

Internship at Zentrum für Sonnenenergie- und Wasserstoff-Forschung (ZSW) in Ulm, Germany, between November 2013 and November 2014. The research activities carried out during the internship are:

- performance tests on a 3-cells MT-DMFC stack
- optimization of a 10-cells HT-PEMFC stack system
- long-term durability tests on a 3-cells HT-PEMFC stack
- synchrotron *in situ* radiography and tomography study of the water management in PEMFCs (Bessy, Helmholtz Zentrum Berlin)

Position as Academic Assistant at Zentrum für Sonnenenergie- und Wasserstoff-Forschung (ZSW) in Ulm, Germany, between February 2015 and April 2015. The research activities carried out in this period are:

- study of the water management in PEMFCs by means of in situ laboratory radiography and tomography, a master student has been followed during this activity
- determination of the heat conductivity of PEM fuel cell materials: design of experiment

Expertise

- Testing and characterization of polymeric fuel cells (PEMFCs)
- Electrochemical diagnostic techniques (I-V curves, HFR, CV, LSV, EIS)
- Experience at synchrotron beamlines (SAXS, radiography, tomography)
- Electron microscopy (SEM, TEM)
- Health and safety (RSPP certificate)

Software:

- MS Office (ECDL certificate)
- Matlab
- LabVIEW
- Igor Pro
- AutoCAD
- Thales Zennium-CV-software
- Image J

Scholarships and awards

- PhD scholarship, Università degli Studi di Trieste, Trieste
- Scholarship for Fuel Cell Science and Technology Grove Conference 2014
- Scholarship for European Technical School on Hydrogen and Fuel Cells 2014
- Best Poster Award, Fuel Cell Science and Technology Grove Conference 2014

Languages

Italian:	mother tongue
English:	fluent (C1 level)

Publication list

Articles

1. F. Valle, B. Marmiroli, H. Amenitsch, R. Taccani, “Electron microscopy and small-angle X-ray scattering analysis of the catalyst layer degradation in PBI-based HT-PEM fuel cells”, Convegno nazionale Associazione Termotecnica Italiana, Trieste, 2012.
2. N. Zuliani, F. Valle, R. Taccani, “Degrado accelerato di celle a combustibile polimeriche: sistema di acquisizione dati e controllo”, National Instruments Days, Milano, 2013.
3. F. Valle, B. Marmiroli, H. Amenitsch, R. Taccani, “Experimental analysis of catalyst degradation in High Temperature PEM Fuel Cells subjected to accelerated ageing tests”, 5th International Conference FDFC 2013, Karlsruhe, 2013.
4. F. Valle, N. Zuliani, B. Marmiroli, H. Amenitsh, R. Taccani, “SAXS analysis of catalyst degradation in High Temperature PEM Fuel Cells subjected to accelerated ageing tests”, Fuel Cells, 2014.

Conference talks

1. F. Valle, B. Marmiroli, H. Amenitsch, R. Taccani, “Electron Microscopy and Small-angle X-ray Scattering Analysis of the Catalyst Layer Degradation in PBI-based HT-PEM Fuel Cells”, 67° Congresso Nazionale ATI, 2012, Trieste, Italy
2. F. Valle, N. Zuliani, “SAXS Analysis of the Catalyst Layer Degradation in PBI-based HT-PEM Fuel Cells”, Primo workshop italiano su celle a combustibile, 2012, Perugia, Italy

3. F. Valle, B. Marmiroli, H. Amenitsch, R. Taccani, “SAXS Analysis of the Catalyst Layer Degradation in Fuel Cells”, 2nd Small Angle XmaS workshop, 2012, Trieste, Italy
4. F. Valle, B. Marmiroli, H. Amenitsch, R. Taccani, “SAXS Analysis of the Catalyst Layer Degradation in Fuel Cells”, 8th European NESY Winter-School & Symposium on Neutrons and Synchrotron Radiation, 2012, Planneralm, Austria
5. F. Valle, N. Zuliani, B. Marmiroli, H. Amenitsch, R. Taccani, “Nanomorphological characterization of the catalyst degradation in HT-PEM fuel cells”, 5th Interntional Conference Fundamentals & Development of Fuel Cells, 2013, Karlsruhe, Germany
6. F. Valle, N. Zuliani, B. Marmiroli, H. Amenitsch, R. Taccani, “Nanomorphological characterization of the catalyst degradation in HT-PEM fuel cells”, Lubelski Park Naukowo Technologiczny conference, 2013, Lublin, Poland
7. F. Valle, N. Zuliani, B. Marmiroli, H. Amenitsch, R. Taccani, “Synchrotron SAXS and GISAXS characterization of HT-PEMFC catalyst degradation”, European Fuel Cell Technology & Applications, 2013, Rome, Italy

Conference posters

1. F. Valle, B. Marmiroli, H. Amenitsch, R. Taccani , “SAXS characterization of the catalyst layer of a HT-PEM fuel cell”, Second Joint Doctorate Summer School on Nanotechnology, 2012, Udine, Italy
2. N. Zuliani, F. Valle, R. Taccani, “Performance degradation study on polybenzimidazole fuel cells subjected to different ageing tests”, European Fuel Cell Technology & Applications, 2013, Rome, Italy
3. F. Valle, B. Marmiroli, H. Amenitsch, R. Taccani, “PEM Fuel Cells degradation study through catalyst layer SAXS nano-morphology mapping”, Fuel Cells Science & Technology, 2014, Amsterdam, The Netherlands
4. F. Valle, B. Marmiroli, H. Amenitsch, R. Taccani, “PEM fuel cells degradation study through catalyst layer SAXS nano-morphology mapping”, Workshop on Material Challenges in Devices for Fuel Solar Production and Employment, 2014, Trieste, Italy

5. F. Valle, B. Marmiroli, H. Amenitsch, R. Taccani, “PEM fuel cells degradation study through catalyst layer SAXS nano-morphology mapping”, European Technical School on Hydrogen and Fuel Cells, 2014, Rethymnon, Greece